UNIVERSITÀ
DEGLI STUDI
DI PADOVA

Sede Amministrativa: Università degli Studi di Padova

Dipartimento di Biologia

SCUOLA DI DOTTORATO DI RICERCA IN: BIOSCIENZE E BIOTECNOLOGIE

INDIRIZZO: BIOCHIMICA E BIOFISICA

CICLO XXVII

The Role of the Prion Protein in Neurodegenerative Disorders

Direttore della Scuola: Ch.mo Prof. Giuseppe Zanotti

Coordinatore d'indirizzo: Ch.mo Prof. Fabio Di Lisa

Supervisore: Ch.mo Prof. Maria Catia Sorgato

Dottorando: Agnese De Mario

INDEX

ABBREVIATIONS

$[Ca^{2+}]_{cyt}$	cytosolic free Ca^{2+} concentration
$[Ca^{2+}]_{er}$	ER Ca^{2+} concentration
$[Ca^{2+}]_{mit}$	mitochondrial free Ca^{2+} concentration
Ab	antibody
Abeta	amyloid beta protein
ACPD	aminocyclopentane-1,3- dicarboxylic acid
AD	Alzheimer's disease
AEQ	Aequorin
AEQ_{cyt}	AEQ targeted to the cytosol
AEQ_{er}	AEQ targeted to the ER lumen
AEQ_{mit}	AEQ targeted to the mitochondrial matrix
AEQ_{pm}	AEQ targeted to the cytosolic domains proximal to the PM
AFM	atomic force microscopy
AICD	APP intracellular domain
AMPA	α-amino-3-hydroxy-5-methyl-4-isoxazole propionic acid
AMPA-R	AMPA-receptor
APP	amyloid precursor protein
$A\beta_{1-40}$	Abeta 40
$A\beta_{1-42}$	Abeta 42
BSA	bovine serum albumin
CGN	cerebellar granule neurons
CICR	Ca^{2+} induced-Ca^{2+} release
CNS	central nervous system
DEPC	diethylpyrocarbonate
DHPG	3,5-dihydroxyphenylglycine
DMSO	dimethylsulfoxide
ER	endoplasmic reticulum
ERK1/2	extracellular regulated kinases 1/2
FCCP	trifluorocarbonylcyanide phenylhydrazone

GluRs	glutamate receptors
GPI	glycosilphosphatidylinositol
HA	hemagglutinin
iGluRs	ionotropic glutamate receptors
IP_3	inositol-1,4,5-trisphosphate
IP_3R	IP_3-sensitive receptor
kainate-R	kainate receptor
KO	knock-out
KRB	Krebs-Ringer buffer
LTP	long-term potentiation
m	monoclonal
MCU	mitochondrial Ca^{2+} uniporter
mGluRs	metabotropic glutamate receptors
mRFP	monomeric red fluorescent protein
NCX	Na+/Ca^{2+} exchanger
NMDA	N-methyl-D-aspartate
NMDA-R	NMDA-receptor
OR	octarepeats
p	polyclonal
PBS	phosphate buffer saline
PD	Parkinson's disease
PM	plasma membrane
PMCA	plasma membrane Ca^{2+} pump
Prnp	the gene encoding PrP^C
PrP^C	cellular prion protein
PrP-KO	PrP knock-out
PrP^{Sc}	scrapie prion protein
PrP-Tg	PrP transgenic
PSD	postsynaptic density
PTP	permeability transition pore
PVDF	polyvinylidene fluoride

ROS	reactive oxygen species
RyR	ryanodine receptor
s	soluble
SDH	succinate dehydrogenase
SDS	sodium dodecyl-sulphate
SERCA	sarco-endoplasmic reticulum Ca^{2+} pump
SFK	Src family of tyrosine kinases
SOCC	store-operated Ca^{2+} channels
SOCE	store-operated Ca^{2+} entry
SOD	superoxide dismutase
STIM	stromal interaction molecules
TBS	Tris-buffered saline
TBS-T	Tris-buffered saline added with Tween-20
Tg	transgenic
TMRM	tetramethylrhodamine methyl ester probe
TSE	transmissible spongiform encephalopaties
VGCC	voltage-gated Ca^{2+} channels
WB	Western blot
WT	wild type
$\Delta\psi m$	mitochondrial membrane potential

SUMMARY

The cellular prion protein (PrP^C) is a cell surface glycoprotein predominantly expressed in the central nervous system. A modification of the mainly α-helical PrP^C into an isoform enriched in β-strands generates the prion, the infectious particle at the basis of fatal prion diseases. In spite of PrP^C's intimate involvement in prion propagation, its physiological function remains enigmatic. Past observations have supported the possibility that PrP^C regulates Ca^{2+} homeostasis, a notion that has been recently reinforced by the demonstration that PrP^C controls Ca^{2+} fluxes in domains close to the neuronal plasma membrane, and interacts physically with a ionotropic glutamate receptor, thus protecting from glutamate excitotoxicity. Recently, however, it has been proposed that PrP^C serves as a high-affinity receptor for soluble amyloid-β (Aβ) oligomers implicated in Alzheimer's disease (AD), and this interaction could thus be crucial for AD-related synaptic dysfunctions.

In light of this background, using genetically-encoded Ca^{2+} probes targeting different cell domains of cerebellar granule neurons expressing, or not, PrP^C, this work focused on whether PrP^C regulates local Ca^{2+} fluxes arising from the activation of store-operated Ca^{2+} entry (SOCE), and/or of glutamate receptors. We found that, with respect to PrP^C-expressing neurons, the absence of PrP^C caused alterations of several local Ca^{2+} fluxes, indicating that PrP^C could act as a key component of the system(s) controlling neuronal Ca^{2+} homeostasis. As to the molecular mechanism enabling PrP^C to exert such control, the results showed the implication of Fyn tyrosine kinase and of the Ca^{2+}-induced-Ca^{2+}-release from the ryanodine receptor.

The study has also analyzed whether soluble Aβ oligomers could affect the PrP^C-dependent regulation of Ca^{2+} homeostasis. Obtained results have shown that the acute treatment of neurons with Aβ oligomers abrogates the control of PrP^C over Fyn and SOCE, and alters mitochondrial Ca^{2+} uptake after stimulation of ionotropic glutamate receptors. This data thus suggests a PrP^C-dependent mechanism for Aβ-induced neuronal Ca^{2+} dyshomeostasis.

RIASSUNTO

La proteina prionica (PrP^C) è una glicoproteina di membrana espressa maggiormente nel sistema nervoso centrale. A seguito di una modificazione in un'isoforma ricca di foglietti β, essa genera il prione, la particella infettiva responsabile delle malattie da prioni. Sebbene la sua implicazione nelle malattie da prioni sia ormai acclarata, la funzione di PrP^C nelle cellule deve essere ancora chiarita. Osservazioni passate hanno evidenziato che PrP^C possa essere implicata nell'omeostasi del Ca^{2+}. Successivamente, tale possibilità è stata supportata anche dalla dimostrazione che essa regola i flussi di Ca^{2+} in domini prossimi alla membrana plasmatica dei neuroni e dal fatto che interagisca direttamente con un recettore ionotropico del glutammato, prevenendo in tal modo l'eccitotossicità indotta dal glutammato. Recentemente, è stato anche proposto che la PrP^C funga da recettore ad alta affinità per gli oligomeri solubili del peptide amiloide β (Aβ) implicati nella malattia di Alzheimer (AD) e che l'interazione PrP^C- Aβ sia cruciale per la disfunzione neuronale osservata nella malattia.

Alla luce di queste nozioni, questa tesi ha analizzato se la PrP^C regoli l'ingresso di Ca^{2+} indotto dalla deplezione dei depositi intracellulari (SOCE) o dalla stimolazione dei recettori del glutammato, utilizzando a tal fine neuroni granulari di cervelletto isolati da topi esprimenti, o no, la PrP^C e sonde sensibili al Ca^{2+} indirizzate a specifici compartimenti neuronali.

Questo studio ha dimostrato che, rispetto ai neuroni con la PrP^C, l'assenza di PrP^C causa alterazioni in molti flussi locali di Ca^{2+}, a indicare come la PrP^C possa essere implicata nei complessi sistemi adibiti al controllo dell'omeostasi neuronale del Ca^{2+}. Abbiamo inoltre trovato come ciò passi attraverso la modulazione della tirosin chinasi Fyn e del rilascio del Ca^{2+}-indotto dal Ca^{2+} da parte del recettore rianodinico.

Il lavoro ha inoltre analizzato se gli oligomeri solubili del peptide Aβ alterino il controllo esercitato dalla PrP^C sull'omeostasi del Ca^{2+}. I risultati ottenuti hanno evidenziato che il trattamento acuto dei neuroni con tali oligomeri altera la regolazione della PrP^C sul SOCE e su Fyn e l'ingresso di Ca^{2+} nel mitocondrio a seguito dell'attivazione dei recettori ionotropici del glutammato. Questi dati suggeriscono pertanto l'esistenza di un meccanismo PrP^C-dipendente che causa dis-omeostasi neuronale del Ca^{2+} indotta dal peptide Aβ.

1 INTRODUCTION

1.1 PRIONS AND PRION DISEASES

Prion diseases, also known as transmissible spongiform encephalopaties (TSE), are a group of fatal neurodegenerative disorders that include Creutzfeldt-Jacob disease, fatal familial insomnia, kuru and Gerstmann-Straussler-Scheinker in humans, bovine spongiform encephalopaty in cattle, and scrapie in sheep and goats. TSE are typically characterized by neuronal loss, astrogliosis, vacuolization, and a variable degree of cerebral accumulation of amyloid plaques that closely resemble those observed in other neurodegenerative disorders, e.g., Alzheimer's and Parkinson's disease (AD and PD).

TSE's etiology is diverse, spanning from familial to infectious, although for the most part is sporadic. In the past century, scrapie was the first TSE to be thoroughly studied. Its unusual infectious mode of transmission finally led J.S. Griffith (1967) to propose the hypothesis for scrapie transmission - incredibly unortodox for those times but also for many subsequent years - the so called "protein only" hypothesis, which dictates that only a protein, i.e., with no aid from nucleic acids, was capable to "replicate" and, thus, to spread biological information in another organism. After decades of skepticism, S. Prusiner and coworkers (1984) eventually provided the experimental proof for the validity of Griffith's hypothesis, coining the term prion (the acronym for 'proteinaceous and infectious particle') for this unconventional infectious agent. Specifically, they established that TSE pathogenesis is not determined by common infectious bacteria or viruses, but by a conformational conversion of a normal protein (the cellular prion protein, PrP^{C}) into an aberrant (PrP^{Sc}) isoform. PrP^{Sc} is the major component of the prion, which possesses physico-chemical and biological properties different from PrP^{C}, such as resistance to proteases, neurotoxic features and, most remarkably, the capacity to self-propagate into host organisms through an auto-catalytic mechanism in which pre-formed PrP^{Sc} promote the PrP^{C}-PrP^{Sc} conversion.

Much data has been accumulated over the years to support the "protein only" hypothesis, including other "unorthodox" prion aspects. One of these is the observation that PrP^{Sc} can give rise to different disease phenotypes that are faithfully propagated (Bruce and Fraser, 1991), which suggests the existence of prion strains distinguishable by hystopathological features, biochemical and physico-chemical properties, and by the incubation period of the disease. Recently, it was demonstrated

the capacity of prions to "adapt" to the environment, thereby providing an explanation for the long incubation time needed for prions of an animal species to trigger morbidity in another animal species (Li *et al*., 2010).

However, despite the now recognized implication of PrP^C in the onset and transmission of prion diseases, the mechanism of prion-associated neurodegeneration and the physiological function of PrP^C are still unclear after decades of intensive research. At large, it is now accepted that both these issues are intimately related, and that knowledge of the physiology of PrP^C could be crucial for the understanding of the process of neurodegeneration and, hence, for the design of effective therapeutic interventions.

1.2 THE CELLULAR PRION PROTEIN

1.2.1 Structural and molecular biology of PrP^C

PrP^C is a highly conserved sialoglycoprotein of about 250 aminoacids (aa) in its mature form, attached to the outer surface of the plasma membrane (PM) via a C-terminal glycosilphosphatidylinositol (GPI) anchor (Stahl *et al*., 1990) (Fig. 1). PrP^C, which is expressed in almost all tissues of vertebrates, is particularly rich in postsynaptic density (PSD) of the central nervous system (CNS) (Um *et al*., 2012).

The gene that codes for PrP^C (*Prnp)* is well conserved among species and contains either three (in rat, mouse, bovine and sheep), or two (in hamster and humans) exons, of which a single one encodes PrP^C. In humans, *Prnp* is located in the short arm of chromosome 20 (Sparkes *et al*., 1986), and the two exons are separated by one intron: exon one contains the promoter and termination site, while exon two harbours the open reading frame (Lee *et al*., 1998). The control of *Prnp* expression has been attributed to sequences within the 5'-flanking region of the first intron, and to 3'-untranslated sequences. In spite of the high *Prnp* conservation, mice devoid of PrP^C (PrP-KO) develop normally and apparently show only minor abnormalities, including some deficits in spatial learning, increased excitability of hippocampal neurons and modification in the circadian sleep rhythm (Collinge *et al*., 1994; Sakaguchi *et al*., 1996). The polypeptide coded by *Prnp* is subjected to several post-translational modifications: removal of the N-terminal signal peptide (aa 1-22), and of approximately 20 aa at the C-terminus (aa 231-253) to allow the GPI attachement (Stahl *et al*., 1990); the N-glycosilation at two asparagine residues (Asn181, 197) in the endoplasmic reticulum (ER); removal of mannose residues and addition of complex oligosaccharidic chains in the Golgi apparatus (Fig. 2).

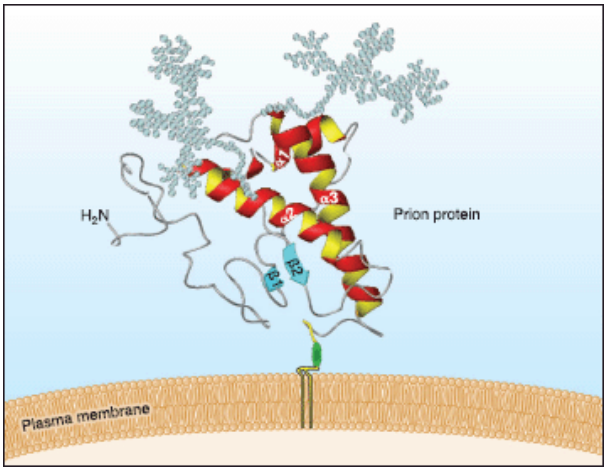

Figure 1. Location of PrP in cells. *PrP^C secondary structure is fully explained further on and in Fig. 4 (forms.asm.org).*

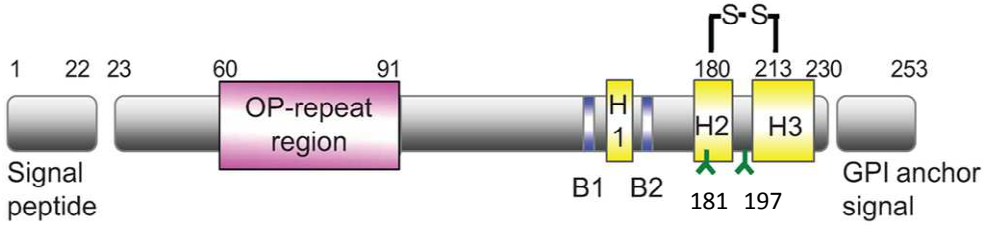

Figure 2. Schematic representation of the mature human PrP^C. *Mature PrP^C is the product of many post-translational modifications. The following domains are highlighted: the signal peptide (1-22) for ER import, and the C-end sequence (231-253), both of which are removed during PrP^C maturation; the conserved octapeptide repeats (OP-repeat region) (in violet) (60-91); B1 (128-131), and B2 (161-164) β-strands (blue boxes); the α-helical region composed of helices H1 (144-154), H2 (173-194), and H3 (200-220) (yellow boxes); Asn181 and 197 for the attachment of glycans; the disulfide bridge (S-S) between Cys180 and 213; the attachment of the GPI moiety (GPI-anchored signal) at residue 230 (modified from Kojima et al., 2014).*

NMR and biochemical studies of recombinant PrP have established that the mature protein consists of a flexible N-terminal (of approximately 100 aa) and of a globular domain (of about 100 aa) arranged in three helices and two antiparallel β sheets (Fig. 3), which is further stabilized by a single disulfide bond (Riek *et al.,* 1996; Zahn *et al*., 2000). The N-terminal contains five repetitions of eight aa (PHGGGWGQ) (octarepeats, OR) that can coordinate up-to six Cu^{2+} (Brown *et al*., 1997). A hydrophobic region, located between the OR and the first α-helix (aa 106-126) is considered a possible trans-membrane domain, and exerts neurotoxic functions (Forloni *et al*., 1993).

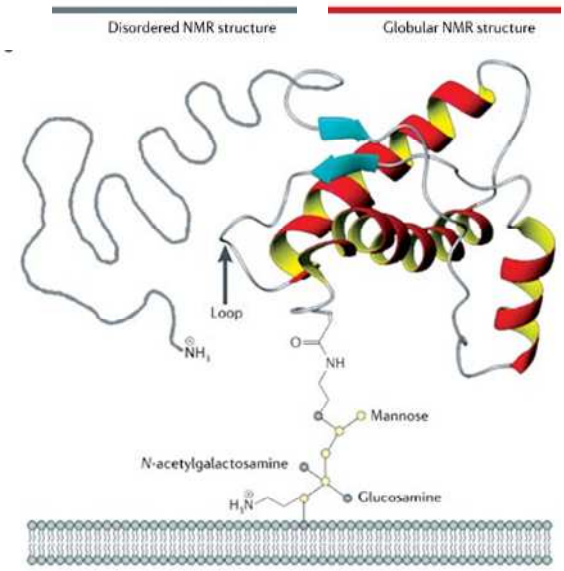

Figure 3. NMR structure of PrP^C. *The figure shows the two principal domains, the unstructured N-terminus (in blue) and the globular C-terminus (in red) of PrP^C (modified from Aguzzi and Heikenwalder, 2006).*

The globular half of PrP^C is highly conserved among mammals, and is found in non-, mono-, or diglycosylated isoforms, corresponding to the variable occupancy of residues Asn-181 and Asn-197 (Haraguchi *et al*., 1989). The role of PrP^C glycosylation has been investigated both for the susceptibility to conformational conversions, and for TSE diverse forms. According to molecular dynamics simulations (Lawson *et al*., 2005), attached *N*-glycans may modulate PrP^C stability, and/or could affect other aspects of PrP^C biology, such as the intracellular trafficking and the binding to ligands.

After the maturation process, the protein moves along the secretory pathway to eventually reach, and bind to, the external leaflet of the PM exploiting the GPI moiety. Like other GPI-anchored proteins, PrP^C is located to sphingolipid- and cholesterol-abundant microdomains, known as detergent-resistant patches, or lipid rafts (Simons and Toomre, 2000), which many studies indicate as putative centres for signal transduction events. It remains to be tested whether the GPI-anchoring modulates other biological properties of PrP^C, as shown for the fibroblast GPI-growth factor (Kohl *et al*., 2002).

1.2.2 *From PrP^C to PrP^{Sc}*

As mentioned, aberrant PrP^{Sc} isoforms originate solely from a conformational conversion of PrP^C. Accordingly, PrP^C and PrP^{Sc} share the primary sequence and post-translational modifications, but have a different secondary structure. In particular, atomic force microscopy (AFM) studies have shown that, whereas in PrP^C the α-helix and β-strand content accounts for 30% and 3%, respectively, the conversion of different PrP^C segments to β-strands increases the β-sheet percentage of PrP^{Sc} up to 40% (Fig. 4) (Pan *et al*., 1993; Safar *et al*., 1993). Such a conformational switch is responsible for the above-reported novel biological properties. Notably, detectability of a proteinase K-resistant PrP form is taken as proof for the presence of PrP^{Sc}, and thus of prion infection. Investigation of the steps required for prion propagation, carried out mainly in transgenic (Tg) mice expressing chimeric mouse–hamster–mouse or mouse–human–mouse PrP transgenes, has indicated that residues 90-140 could play a key role in the PrP^C-PrP^{Sc} interaction and conformational transition (Scott *et al*., 1993; Telling *et al*., 1995).

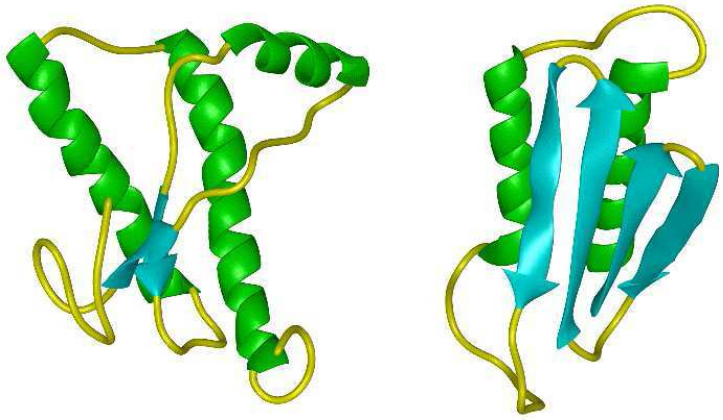

Figure 4. Models for the structure of PrP^C (left) and PrP^{Sc}(right). *The α-helical and β-strand regions are shown in green and blue, respectively. It is to be noted the PrP^{Sc} enrichement in the β-sheet content (www.bio.davidson.edu).*

Starting from the necessary presence of PrP^C (PrP-KO mice are not susceptible to prion invasion), the mechanism of PrP^C-PrP^{Sc} conversion is not yet fully established. Along the years, the refolding and the seeding models have been proposed to explain PrP^{Sc} formation and aggregation that proceed in an exponential manner. According to the refolding model, monomeric (or low level oligomeric) PrP^{Sc} converts single PrP^C molecules into the thermodynamically more stable PrP^{Sc} conformation, possibly with

the aid of a chaperone (protein X) (Eigen, 1996; Caughey *et al*., 1995; Kocisko *et al*., 1994). This model assumes that aggregated forms are not essential, i.e., fibrils would be only a side product, in agreement with the observation that many TSE present no amyloid aggregates. In contrast, the seeding model proposes a fast equilibrium between the two PrP isoforms, in which, however, PrP^{C} is highly favoured thermodynamically. Thus, only in the presence of a stable nucleus of PrP^{Sc} aggregates, PrP^{C} can be trapped in the unfavourable (PrP^{Sc}) conformation and be removed from equilibrium. In addition, once reaching a high mass, the breaking off of the aggregates would amplify the PrP^{C}-PrP^{Sc} conversion.

The mechanisms of prion-induced neurodegeneration are unclear. Different hypothesis has been postulated. One suggests that neuronal damage is linked to the direct toxicity of aggregated PrP^{Sc} (*gain of function hypothesis*). Alternatively, a loss of PrP^{C} function (*loss of function hypothesis*) is indicated as the cause of neurodegeneration. Neither of them has been conclusively proved, despite the fact that the systematic examination of the brain of deceased patients has revealed no spatial correlation between neuronal apoptosis and PrP^{Sc} deposition (Chretien *et al*., 1999; Dorandeu *et al*., 1998).

A third possibility, somehow referring to the *loss of function hypothesis*, recently proposed that PrP^{C} acts as high affinity surface binding partner for misfolded β sheet-enriched aggregates, including PrP^{Sc} oligomers (Lauren *et al*., 2009; Resenberger *et al*., 2011). In this way, PrP^{C} would transduce the neurotoxic signal of oligomers into neurons, loosing, in parallel, its native role. In this context, it is good to mention the demonstration that in prion-infected Tg mice the absence of membrane-bound PrP^{C} renders impossible PrP^{Sc}-induced synaptic dysfunction and clinical syntoms (Chesebro *et al*., 2005), indicating the strict requirement of an integral PrP^{C} to mediate PrP^{Sc} toxicity.

1.2.3 The physiology of PrP^{C}

The function played by PrP^{C} in cells is still elusive, in spite of the multiple roles ascribed so far to the protein. These include involvement in: (i), defence mechanisms against oxidative stress and apoptotic processes; (ii), Cu^{2+} uptake and metabolism; (iii), cell adhesion, differentiation, proliferation and migration, which PrP^{C} would accomplish after interacting with extracellular partners, or by taking part in multi-component signaling complexes at the cell surface. A summary of the major putative

functions of PrP^C will now be reported (for comprehensive reviews see Aguzzi *et al*., 2008; Linden *et al*., 2008).

1- Implication of PrP^C in cell protection and in other neuronal aspects

One major feature emerging from the vast array of the proposed roles is that PrP^C is neuroprotective, particularly against internal, or environmental, stress that could initiate an apoptotic program. One of the clearest examples, obtained from comparing wild type (WT) and PrP-KO neurons, is the protection exerted by PrP^C in cultured human fetal neurons triggered to apoptosis (by the pro-apoptotic protein Bax) (Roucou *et al*., 2004). Among other examples, it is good to recall that PrP^C is up-regulated after cerebral ischemia, and that PrP^C amounts inversely correlate with damage severity induced in rat brains by *in vivo* focal ischemia (Weise *et al*., 2004; Shyu *et al*., 2005). Other lines of evidence suggest that PrP^C acts against oxidative stress. A support to this possibility is that isolated PrP-KO neurons are more susceptible to treatment with agents inducing reactive oxygen species (ROS), i.e., H_2O_2, xanthine oxidase and Cu^{2+} (Brown *et al*., 1997; Brown *et al*., 2002), and have decreased levels of anti-oxidant enzymes, such as Cu^{2+}/Zn^{2+} superoxide dismutase (SOD), catalase and glutathione reductase. As to SOD, it was proposed that PrP^C influences its activity also by promoting Cu^{2+} internalization into cells possibly by binding Cu^{2+} at the OR region (Brown *et al*., 1997; Brown and Besinger, 1998). Along this line, it was suggested that PrP^C binds and internalizes also Fe^{3+} (Singh *et al*., 2009), in light of the altered Fe^{3+} homeostasis detected in prion-infected cells.

Following interaction with cell adhesion molecules, and/or through the interaction with laminin, PrP^C has been implicated in cell adhesion, recognition and differentiation (Graner *et al*., 2000). Further, interactions with the mature 67 kDa-receptor (and its 37 kDa-precursor) for laminin, and with glycosamminoglycans, has led to the hypothesis that PrP^C acts in neuronal differentiation and axon growth (Caughey *et al*., 1994; Rieger *et al*., 1997; Gauczynski *et al*., 2001; Hundt *et al*., 2001; Pan *et al*., 2002), and that PrP^C binding with the secreted cochaperone stress-inducible protein 1 promotes neuritogenesis (Lopes *et al*., 2005). Several observations suggest that PrP^C could play a role also in synaptic structure and function and, consequently, in learning and memory consolidation (Hansen *et al*., 2008), in accord with the synaptic pathology that characterizes prion diseases (Jeffrey *et al*., 2000).

To properly localize PrP^C, light and electron microscopy immunocytochemical studies, together with the use of PrP–EGFP, have indicated that PrP^C is concentrated

along axons and in pre-synaptic terminals (Laine *et al*., 2001), although other studies suggest that it preferentially localizes to PSD (Collins *et al*., 2006; Um *et al*., 2012). In addition, PrP^C is subjected to anterograde and retrograde axonal transport (Moya *et al*., 2000; Borchelt *et al*., 1994) while PrP–EGFP fusion proteins were visualized in what appeared to be axonally-transported synaptic vesicles.

Consistent with a synaptic localization and function, it was found that addition of recombinant PrP to cultured neurons induced rapid elaboration of axons and dendrites, increased number of synaptic contacts, as well as potentiation of acetylcholine release at the neuromuscular junction (Re *et al*., 2006).

2- PrP^C and signal transduction

In front of such a multifaceted behavior, the most sensible possibility is that PrP^C participates in signal transduction centres, as already suggested for other GPI-anchored proteins (Simons and Ikonen, 1997). Accordingly, several putative partners of PrP^C (for details see Linden *et al*., 2008) and different intracellular effectors have been proposed, including Fyn, a member of the Src family of tyrosine kinases (SFK), mitogen-activated kinases, extracellular regulated kinases 1/2 (ERK1/2), Akt, and PKA. For example, perturbation of the ERK1/2 signalling pathways has been reported following ischemic challenge in PrP-KO brains with respect to the WT counterparts, with increased post-ischemic caspase-3 activation, and exacerbation of neuronal damage (Spudich *et al*., 2005; Weise *et al*., 2006).

However, multiple are the indications that focus on Fyn tyrosine kinase (highly expressed in neurons) as the preferential downstream effector of PrP^C in the regulation of key processes, ranging from embryogenesis and neuritogenesis to, at large, neuroprotective signaling. One example is the antibody-mediated cross-linking of PrP^C (in 1C11 cell line) that, converging to ERK1/2 through Fyn signaling, finally modulates cell survival (Mouillet-Richard *et al*., 2000). Using the same experimental cell model, antibody ligation of PrP^C also resulted in the Fyn-dependent activation of NADPH oxidase (Schneider *et al*., 2003), ultimately generating ROS-mediated downstream signalling (Pradines *et al*., 2009). Likewise, a PrP^C-dependent activation of Fyn (Kanaani *et al*., 2005; Santuccione *et al*., 2005), and ERK1/2 (but also PKA) (Chen *et al*., 2003), was documented in other neuronal paradigms (Toni *et al*., 2006) and non-neuronal cells (Jurkat and T cells; Stuermer *et al*., 2004).

1.3 INTRACELLULAR CALCIUM HOMEOSTASIS

Because the present Ph.D. thesis is intimately releted to Ca^{2+} signals, the PrP^{C}-Ca^{2+} connection is now preceded by a brief overview of how Ca^{2+} homeostasis is governed in neurons.

1.3.1 Calcium homeostasis and signaling

Ca^{2+} is the most important carrier of biological signals in cells, capable to convey messages to a wide range of key processes, which span from the survival to the death of the cell once the control of Ca^{2+} homeostasis is disrupted. At resting condition (Fig. 5), the cytosolic free Ca^{2+} concentration ($[Ca^{2+}]_{cyt}$) is about 10^{-7} M, which is about ten thousand times less than the extracellular concentration of the ion. Elevation of $[Ca^{2+}]_{cyt}$ (>100 nM) - achieved by activating external Ca^{2+} entry or by discharging Ca^{2+} stores as illustrated in Fig. 5 - represents therefore a powerful signal that can control both short term (contractile, secretory, or metabolic responses) and long term (regulation of transcription, growth, and cell division) processes (Berridge *et al*., 2003). However, by exploiting different means (pumps and carriers, see Fig. 5) the cell immediately removes Ca^{2+} signals and restores basal $[Ca^{2+}]_{cyt}$. Thus, at any moment in time, the level of $[Ca^{2+}]_{cyt}$ is tightly and finely tuned.

In neurons, external Ca^{2+} entry is mediated by PM channels named voltage (VGCC)-, or ligand (e.g., glutamate)–gated, or store-operated (SOCC), Ca^{2+} channels. Also, stimulation of G protein-coupled receptors (e.g., metabotropic glutamate receptors, mGluRs) leads to increased $[Ca^{2+}]_{cyt}$ by generating inositol-1,4,5- trisphosphate (IP_3) that binds to the IP_3-sensitive receptor (IP_3R) of the ER membrane to release the stored Ca^{2+}. Instead, the ryanodine receptor (RyR), which is Ca^{2+}-sensitive, serves to amplify Ca^{2+} signals arising from the IP_3R, or the extracellular pool, through a mechanism termed Ca^{2+} induced-Ca^{2+} release (CICR) (Berridge, 1998). Cytosolic Ca^{2+} can also enter into mitochondria, thereby activating Ca^{2+}-dependent enzymes (dehydrogenases and phosphatases) and ATP production (Duchen, 2000) (Fig. 5).

During the course of a typical Ca^{2+} transient, the reaction that cause an increase in $[Ca^{2+}]_{cyt}$ are counteracted by the reactions that cause a decrease in $[Ca^{2+}]_{cyt}$, during which time various pumps and exchanger remove Ca^{2+} from cytosol. While sarco-endoplasmic reticulum Ca^{2+} pump (SERCA) can accumulate Ca^{2+} in the ER lumen, there are two main mechanisms that extrude Ca^{2+} out off the cells, the plasma membrane Ca^{2+} pump (PMCA) and the Na^{+}/Ca^{2+} exchanger (NCX). The diverse PMCA, SERCA and

NCX molecular toolkit, enables cells to select the combination of off reactions that exactly meats their Ca^{2+}-signalling requirements (Berridge *et al*., 2003).

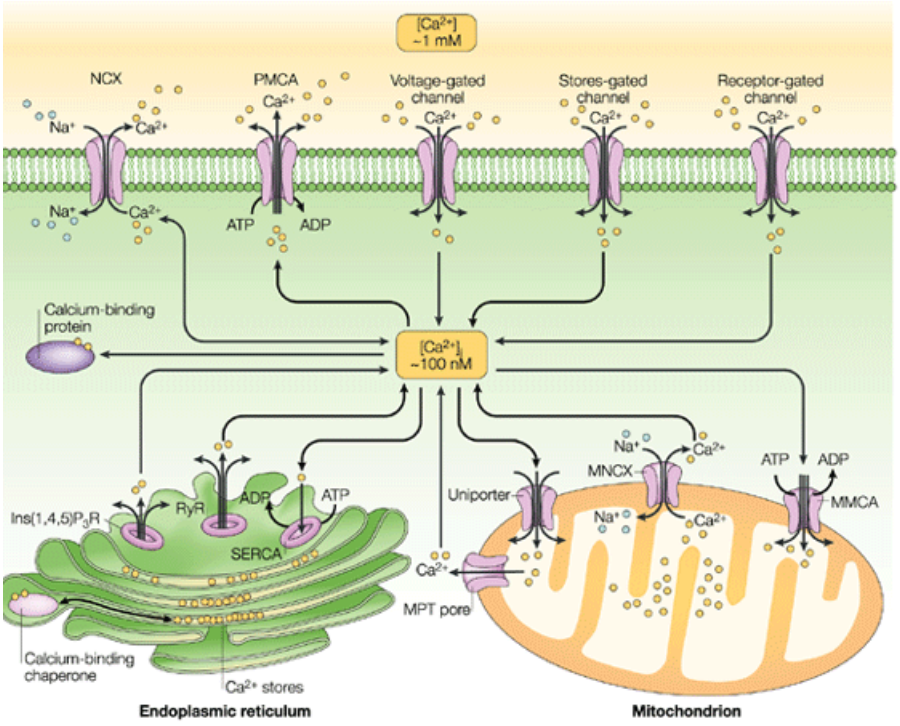

Figure 5. Ca^{2+} homeostasis. *Cytosolic Ca^{2+} elevation is induced by a range of stimuli that activate external Ca^{2+} entry through various types of channels (voltage-, receptor- or store-gated), or that discharge intracellular stores, after formation of the appropriate second messenger activating the ER inositol-1,4,5-trisphosphate-sensitive receptor (IP_3R) or the ryanodine receptor (RyR). Counterbalancing mechanisms then reduce cytosolic Ca^{2+}, i.e., plasma membrane and sarco-endoplasmic reticulum (SERCA) Ca^{2+} pumps, and the Na^{+}/Ca^{2+} exchanger (NCX). Mitochondria can take up Ca^{2+} using the Ca^{2+} uniporter (MCU), while Ca^{2+} release is accomplished through the mitochondrial NCX and, in the case of Ca^{2+} overload, through the opening of the permeability transition pore (PTP) (Syntichaki and Tavernarakis, 2003).*

Clearly, a multifaced picture arises from all above-described Ca^{2+} fluxes, which comprehends the modulation of membrane excitability and enzyme activity, gene expression, mitochondrial functions, production of reactive oxygen and nitrogen species, and apoptosis in the case of free mitochondrial Ca^{2+} concentration $[Ca^{2+}]_{mit}$ overload (Berridge *et al*., 2000).

1.3.2 Store-operated calcium entry

Store-operated Ca^{2+} entry (SOCE) has been discovered well after the external Ca^{2+} entry through classical voltage– or ligand- gated channels. Yet, is presently a well established mechanism through which depletion of intracellular Ca^{2+} stores leads to the opening of SOCC, allowing external Ca^{2+} entry and replenishment of the ER-Ca^{2+} store. This "new" type of channel was first described in non-neuronal cells (e.g., limphocytes), but its importance is now increasingly recognized also in neurons.

The first model of this process (previously defined capacitative Ca^{2+} entry) was proposed by Putney *et al*. (1993) after observing that SERCA inhibitors (e.g., thapsigargin) were inducing external Ca^{2+} entry without involving the typical cell surface channel-receptors. After as much as 20 years, SOCE mechanistic details were finally unveiled, through the identification (using RNA-interference screens) of two protein families: that of ER *stromal interaction molecules* (STIM) (with STIM1 and STIM2 isoforms), and that of the PM Orai proteins (with Orai1-3 isoforms).

STIM1 and STIM2 are expressed in primary lymphocytes, e.g., T and B-cells, at lower levels in many organs, and at appreciable levels also in the central and the peripheral nervous system (Williams *et al*., 2001; Wissenbach *et al*., 2007; Dziadek and Johnstone, 2007). Extensive Nothern blot analyses suggest an ubiquitous expression of also Orai1 and Orai3 proteins, and that Orai2 is predominantly expressed in the brain (Gwack *et al*., 2007; Wissenbach *et al*., 2007). Because of the presence of a single EF-hand Ca^{2+}-binding motif, STIM1 and 2 sense luminal Ca^{2+} changes albeit with different sensitivity, entailing a role in, and/or a different contribution to, SOCE activation by the two isoforms. Regarding STIM1, whose EF-hand binds Ca^{2+} with low affinity (ideal to sense substantial changes of ER Ca^{2+} concentration, $[Ca^{2+}]_{er}$), the protein is likely uniformly distributed in the ER membrane at resting conditions (Fig. 6, left panel), whereas it oligomerizes upon Ca^{2+} depletion in membrane punctae iuxtaposed to the PM. Eventually, this membrane apposition leads to the Orai-pore opening, possibly through a protein-protein interaction (Fig. 6, right panel) (Liou *et al*., 2005; Zhang *et al*., 2005). Instead, the EF hand of STIM2 is sensitive to mild reductions of $[Ca^{2+}]_{er}$, so that STIM2 could form "punctae" already at resting $[Ca^{2+}]_{er.}$

Given the mentioned wide expression of STIM and Orai proteins, SOCE is a process probably occurring in all cells, although its relevance in neurons has been disputed in light of the redundant VGCC presence in these cells. However, it has been proposed that, once activated, STIM1 could inhibit VGCC (Wang *et al*., 2010; Park *et al*., 2010) nullifying, in this way, the unnecessary promotion of two parallel means of

external Ca^{2+} entry. A corollary information regarding SOCE machinery is the recent proposition by Lalonde and coworkers (2014) that, in addition to mantaining filled ER-Ca^{2+} stores, active neuronal STIM regulates also gene transcription.

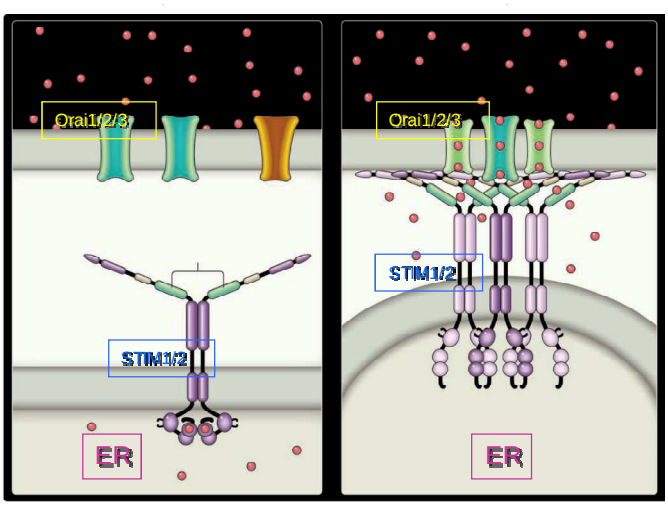

Figure 6. Molecular coupling between STIM and Orai in the "SOCE machinery". *At resting conditions (left panel), STIM proteins are uniformely distributed in the ER membrane, whereas, upon ER Ca^{2+} depletion (right panel), they oligomerize into punctae in domains very close to the PM, where they activate Orai proteins, representing the pore of the channel. In this way Ca^{2+} (violet circles) enters into the cell through SOCC to replenish ER-Ca^{2+} stores (modified from Cahalan, 2010).*

The mechanism of SOCE is under the tight control of post-translational modifications of its machinery components. In particular, the function of STIM1 has been reported to be influenced by glycosylation and phosphorylation processes. In fact, STIM1 harbours several potential target residues for different kinases in its cytosolic C-terminus domain (Olsen *et al*., 2006). Accordingly, Guisado and coworkers (2010) have demonstrated the phosphorylation of Ser519, 575 and 628 by ERK1/2 (in HEK 293T cells), and Lopez *et al*. (2012) the phosphorylation of Tyrosines (Tyr) by SFK members occurring upon Ca^{2+} store depletion. The latter partecipation was confirmed by others who demonstrated a reduction of SOCE by the tyrosine kinase inhibitors genistein, or PP2, suggesting that the activity of tyrosine kinases on STIM1 positively regulates SOCE (Zuo *et al*., 2011).

1.3.3 *Glutamate-mediated calcium fluxes*

The impact of glutamate in the mammalian brain and spinal cord has been known since the 1950s (Hayashi 1954; Curtis and Watkins 1960), within the notion that glutamate is the principal excitatory transmitter of the vertebrates' nervous system. It follows that the level of extracellular glutamate must be tightly regulated, and indeed there are multiple processes regulating its release into, and re-uptake from, the synaptic cleft. In presynaptic terminals, Ca^{2+} influx (thorugh VGCC) triggers the release of glutamate stored in vescicles, allowing the binding of glutamate to postsynaptic receptors and the generation of excitatory postsynaptic potentials.

Although glutamate is crucial for neurons to communicate, the overactivation of glutamate receptors (GluRs) - and the consequent Ca^{2+} overload - exerts dangerous effects that may provoke neuronal damage (Rothman *et al*., 1987). Understandibly, glutamate could be implicated in acute and chronic CNS-degenerative disorders, as suggested (Berridge, 2014).

Mammalian GluRs are classified on the basis of their action, and can be divided into two broad categories: ionotropic (iGluRs) and metabotropic (mGluRs). iGluRs are non selective cationic channels that open following a conformational change subsequent to glutamate binding. Pharmacological studies have documented that iGluRs can be discriminated upon the response to the following agonists: N-methyl-D-aspartate (NMDA), α-amino-3-hydroxy-5-methyl-4-isoxazole propionic acid (AMPA), and kainate. Conversely, mGluRs belong to the G protein-coupled receptor family, which activate, or inhibit, the formation of second messengers (Fig. 7).

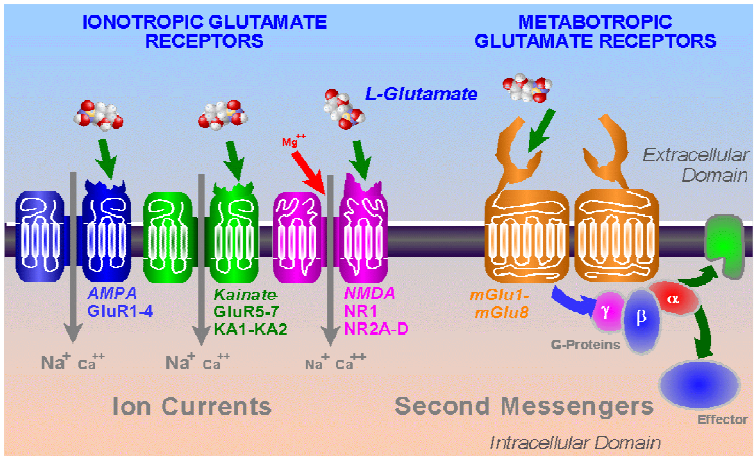

Figure 7. Glutamate receptors. *Once bound to glutamate, iGluRs (in blue, green and violet) move cations (Ca^{2+}, Na^{+}) into cells, whereas mGluRs (in orange) activate the formation of second messengers (modified from Tom Salt's Lab home page).*

The NMDA-receptor (NMDA-R) has a relatively higher permeability and affinity (EC_{50}, 1 μM) to Ca^{2+}than the other iGluRs, although it is also permeable to Na^{+}. It can be antagonised by a growing number of competitive and non-competitive inhibitors, it is blocked by Mg^{2+} in a voltage-dependent manner (Johnson and Ascher, 1990), and requires glycine as co-agonist. It has also modulatory sites for polyamines, reducing agents, Zn^{2+} and H^{+} (Niciu *et al*., 2012). Molecular biology techniques have revealed that NMDA-Rs are composed of two obligatory NR1 subunits that coassemble with two NR2 subunits into a tetrameric complex. Four different genes coding for NR2 subunit (NR2A-D) are present in the mammalian brain. It is thought that neonatal NMDA-Rs comprise mainly the B-type subunit, while adult synapses preferentially harbour the A-type subunit (Cull-Candy and Lezskiewicz, 2004), likely reflecting the functional properties of the NMDA-R at different times of development. Also, the presence of the NR2D subunit impacts slower kinetic properties to the channel than the other subunits (Cull-Candy and Lezskiewicz, 2004), while the NR2C subunit reduces the sensitivity to Mg^{2+}(Candy *et al*., 2001).

As to AMPA-(AMPA-R) and kainate-(kainate-R) receptors, originally classified by their activation by quisqualate and kainate, four subunits (GluR1-4) belong to the former, and five (GluR5-7 and KA1-2) to the latter, receptor. Both these subunit groups can form homomeric or heteromeric assemblies (with other members of the groups). The most notable modification in the function of AMPA-R is provided by the Ca^{2+}-impermeable GluR2 subunit (Dingledine *et al*., 1999).

As expected, iGluRs are tightly controlled by kinases (Wang *et al*., 1994a; Wang *et al*., 1994b; Knapp *et al*., 1990) whose action has important consequences for neuronal functions. For example, the phosphorylation at Ser845 of the GluR1 subunit of AMPA-R increases the channel open probability (Knapp *et al*., 1990), while the action of CAMKII and PKC is implicated in long-term potentiation (LTP). Also the properties of NMDA-Rs are controlled by phosphorylation. While the effect of PKA and CAMKII is not completely understood, the tyrosine phosphorylation by SFK members, in particular by Fyn, is known to play a role in LTP induction and to enhance synaptic excitatory postsynaptic currents (Lu *et al*., 1998).

mGluRs are divided into three groups according to the sensitivity to agonist molecules and to the coupling to signal transduction mechanisms. Group I comprises mGluR1 and mGluR5, which are coupled to the phosphoinositide hydrolysis and are selectively activated by 3,5-dihydroxyphenylglycine (DHPG); group II comprises mGluR2 and mGluR3, which inhibit adenylate cyclase and activated by 1-aminocyclopentane-1,3-dicarboxylic acid (ACPD); group III consists of mGluR4 and

mGluR6-8, which are also negatively coupled to adenylate cyclase and are activated by 2-amino-4-phosphobutyrate (Ferraguti and Shigemoto, 2006).

1.3.4 PrP^C and calcium

To possibly explain the multiple roles attributed to PrP^C, it has been proposed that PrP^C controls Ca^{2+} homeostasis (Sorgato and Bertoli, 2009). In fact, like PrP^C, Ca^{2+} controls a plethora of cell functions, and is both beneficial and detrimental to the cell life.

Many past studies have addressed the connection of PrP^C/PrP^{Sc} to Ca^{2+} dyshomeostasis. For example, Prusiner and coworkers reported a marked reduction of bradikynin-induced Ca^{2+} responses in neuronal cell lines chronically infected with prions, which was linked to the downregulation of a VGCC sub-type (Kristensson *et al*., 1993; Wong *et al*., 1996). Other studies have highlited the alteration of Ca^{2+} homeostasis in animal and cell models of prion infection, with impairment of Ca^{2+}-dependent neuronal excitability, LTP and synaptic plasticity (reviewed in Peggion *et al*., 2011).

Similar disturbances were reported to occur in PrP-KO hippocampal slices, e.g., the significantly weakened LTP and reduced slow after hyperpolarization [with respect to wild type (WT) neurons] (Mallucci *et al*., 2002; Powell *et al*., 2008), probably arising from compromised iGluRs and Ca^{2+}-activated K^+ channels, respectively, with respect to the WT counterpart. Instead, Zamponi and coworkers (2008) have demonstrated that PrP^C downregulates the activity of the NMDA-R by physically interacting with the 2D regulatory subunit (Fig. 8). Thus, in the absence of PrP^C, the large influx of Ca^{2+} and Na^+ would account not only for the augmented excitability of PrP-KO neurons, but also explain the increased vulnerability of PrP-KO mice to NMDA- and kainate-induced excitotoxicity (Khosravani *et al*., 2008; Rangel *et al*., 2007), epileptic seizures (Walz *et al*., 1999) and ischemic brain injury (Spudich *et al*., 2005).

The PrP^C-dependent modulation of Ca^{2+} homeostasis have been investigated also in our laboratory, using a Ca^{2+}-sensitive probe targeted to specific domains of WT and PrP-KO primary cerebellar granule neurons (CGN). In particular, it was found that, after SOCE, PrP-KO CGN displayed a dramatic increased Ca^{2+} transients near the PM and a reduced steady-state ER Ca^{2+} levels with respect to WT neurons and that the latter event could be likely attributed to the decreased expression of PMCA and SERCA pumps (Lazzari *et al*., 2011).

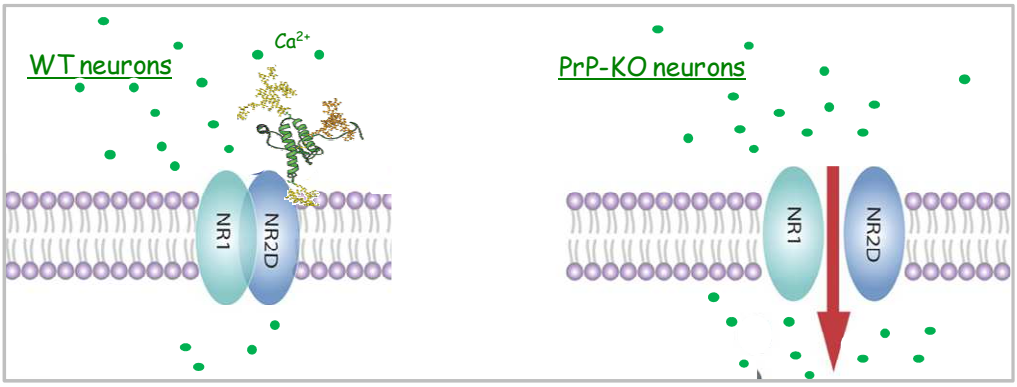

Figure 8. NMDA-R inhibition by PrP^C. *In WT neurons (left) PrP^C silences the NR2D subunit of the NMDA-R preventing Ca^{2+} entry, while in PrP-KO neurons (right) the NMDA-R opens more readily leading to massive Ca^{2+} entry under conditions of excessive glutamate presence (modified from JCB.rupress.org).*

1.4 ALZHEIMER'S DISEASE

AD is a progressive neurodegenerative disorder characterized by an age-dependent loss of memory and cognitive impairment. It can be classified into two forms: sporadic, which accounts for the vast majority of cases (with aging representing the main risk factor), and familial, caused by autosomal dominant gene mutations. Both types of AD share clinical and neuropathological features, including neuritic alterations, reactive gliosis and the presence of two distinct structures, the intracellular "tangles" and the extracellular amyloid plaques (Eckert *et al*., 2001). Tangles are abnormal fibres composed by the hyperphosphorylated tau protein, while amyloid plaques are composed primarily by the amyloid beta protein (Abeta), which is a predominantly 40-42 aa-long peptide derived from the proteolytic processing of the amyloid precursor protein (APP).

1.4.1 Generation of Abeta fragments

Abeta is generated by the cleveage of APP, a glycoprotein ubiquitously present in human tissues and localized to the PM and to the membrane of organelles, such as the ER and the Golgi apparatus. Curiously, APP was also reported in the outer (Anandatheerthavarada *et al*., 2003; Devi *et al*., 2006) and the inner (Manczac *et al*., 2006) mitochondrial membranes.

APP can undergo two proteolytic paths, named non-amyloidogenic and amyloidogenic. In the former, the first cut is catalized by an α-secretase (belonging to the ADAM family of disintegrin and metelloprotease), which, by cleaving APP within

the Abeta aa sequence, forms the small membrane-anchored C83 fragment and the soluble (s) sAPPα. The C83 fragment is subsequently cleaved by the γ-secretase, a multimeric complex made of (PS1 and PS2) presenilin proteins and nicastrin (Edbauer *et al*., 2003), to form the P3 fragment and the APP intracellular domain (AICD). In the amyloidogenic pathway, first the activity of the β-secretase and then of the γ-secretase generate the so-called Abeta fragments. The β-secretase acts at APP's N-terminus forming the 99 aa fragment C99 and sAPPβ. C99 is subsequently cleaved by the γ-secretase, finally yielding the Abeta fragment and AICD (Selkoe, 2000) (Fig. 9).

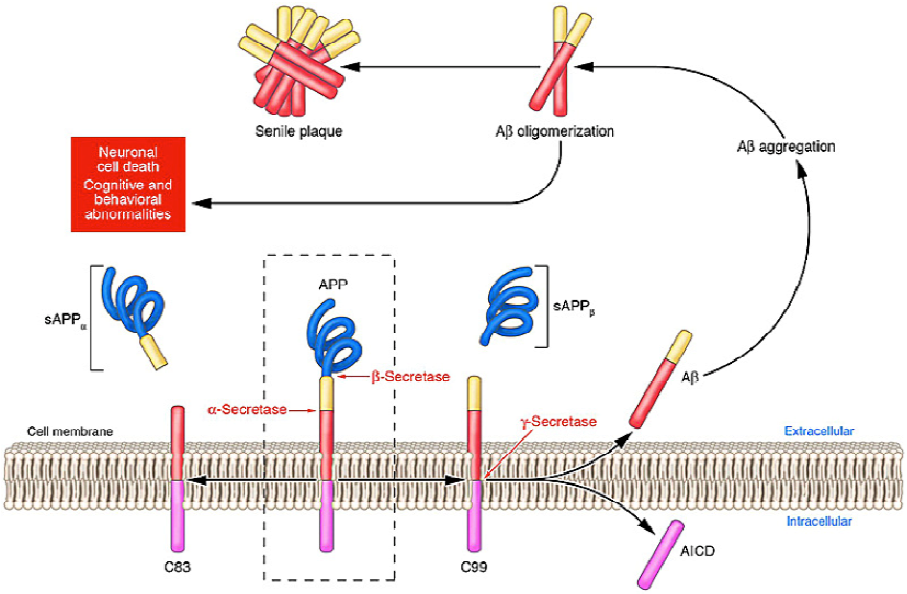

Figure 9. The non-amyloidogenic and amyloidogenic pathways of APP processing. *APP is firstly cleaved by either α- or β-secretase. Cleavage by α-secretase generates sAPPα and C83 (on the left), while cleavage by β-secretase generates sAPPβ and C99 (on the right). C83 and C99 are then cleaved by the γ-secretase generating AICD and Abeta, or the P3 fragment, involved in the amyloidogenic and non-amyloidogenic pathway respectively (American Society for Clinical investigation).*

The amyloidogenic cleveage of APP results in several Abeta isoforms. Of these, Abeta 40 ($A\beta_{1-40}$) and Abeta 42 ($A\beta_{1-42}$) are the most commonly found. $A\beta_{1-42}$ is the fragment that aggregates more rapidly - in fact is the one predominantly found in the amyloid plaques - given its random coil-rich structure prone to form β sheet-rich oligomers of increasing mass (El-Agnaf *et al*., 2000; Walsh and Selkoe, 2007; Klein, 2002). However, recent analyses using size-exclusion chromatography, gel electrophoresis, and AFM have demonstrated that there are several stable types of soluble oligomers: naturally occurring soluble dimers or trimers, Abeta-derived diffusible ligands, Abeta globulomers, and protofibrils (Yu *et al*., 2009). Increasing

evidence suggests that, instead of amyloid deposits, the soluble oligomers are the true cause to synaptic dysfunction and neuronal degeneration (Walsh and Selkoe, 2007). Accordingly, it was reported that the naturally secreted sodium dodecyl-sulphate (SDS)-stable low mass oligomers (dimers, trimers, or tetramers), but not Abeta monomers or larger aggregates, inhibit LTP and cause loss of dendritic spines and synapses (Sivanesan *et al*., 2013). In addition, each low mass oligomer could act at different times and bring differential consequences on neuronal survival, by affecting, for example, kinases and phosphatases already recognised as intracellular effectors of Abeta (Zhu *et al*., 2003). Consequent to this hypothesis, Abeta oligomers isolated directly from human AD brains were found to exert equal toxicity as syntethic Abeta forms (Shankar *et al*., 2008).

Apparently, Abeta oligomers may greatly increase vulnerability to oxidative and metabolic stress. Indeed, neurons from AD patients exhibit abnormally high amounts of oxidized proteins, lipids and DNA (Butterfield *et al*., 2001), which - one or the other - impair the function of several proteins, e.g., ion-motive ATPases, glucose and glutamate transporters, but may also impair G-binding proteins (Mattson, 1997). By disturbing cellular ion homeostasis and energy metabolism, Abeta oligomers can also render neurons vulnerable to excitotoxicity and apoptosis (Mattson, 2004; Li *et al*., 2009).

As to the physiological role of these fragments that - it is good to remind - are generated by a double enzymatic action, there is emerging evidence that they are involved in the regulation of neuronal (Ca^{2+} and K^{+}) channels (Ramsden *et al*., 2001; Plant *et al*., 2006). These findings, therefore, suggest that Abetas become toxic only when their level abnormally increases in the extracellular space, possibly as a result of an imbalance between production and clearance.

1.4.2 Abeta and calcium

It has been claimed that Abeta impinges, directly or indirectly, on Ca^{2+} signaling through (at least) three different mechanisms: (i), formation of PM pores; (ii), disruption of the membrane lipid integrity; (iii), a direct action on ion channels. The pore-forming mechanism for Abeta has been supported by studies employing AFM (Lin *et al*., 2001), electron microscopy (Lashuel *et al*., 2002; Lashuel *et al*., 2003), and high resolution transmission electron microscopy, which have detected Abeta pores distributed in the cell membrane of post-mortem neurons of AD patients (Inoue, 2008). Concerning the second mechanism, electron microscopy techniques have

shown that Abeta oligomers interact with several types of membrane lipids (Decout *et al*., 1998; Terzi *et al*., 1997; Avdulov *et al*., 1997), while fluorescence spectroscopy has revealed that Abeta induced substantial changes in synaptic membrane fluidity by affecting both the bulk lipid milieu and the overall lipid architecture. As to the third mechanism, it is supposed to represent one of the earliest and primary Abeta-caused adverse events. Already in 1989, Khachaturian has proposed that substantial changes in Ca^{2+} homeostasis could provide the common pathway for aging and AD-associated neuropathological changes.

Recently, memantine has been approved by the FDA for treating patients with moderate-to-severe AD. Because memantine antagonizes the NMDA-R, its approved application illustrates the potential involvement of altered Ca^{2+} signalling in AD clinical manifestations. More precisely, Abeta oligomers apparently interact with various Ca^{2+}-permeable channels, including most VGCC, nicotinic acetilcholine channels, iGluRs, dopamine and serotonin receptors and intracellular IP_3Rs (Rovira *et al*., 2002; Stutzmann, 2005). More subtle interactions of Abeta with Ca^{2+}-regulating G protein-coupled receptors have also been uncovered, given that incubation with Abeta oligomers enhances both the expression of mGluR5, and the Ca^{2+} response to DHPG (Casley *et al*., 2009).

1.4.3 Abeta and PrP^C

An intringuing connection between PrP^C and AD is the proposition that PrP^C acts as a high affinity receptor for $A\beta_{1\text{-}42}$ soluble oligomers and mediates their neurotoxic effects into neurons (Fig. 10). This link was found by Strittmatter and coworkers (Lauren *et al*., 2009), demonstrating that $A\beta_{1\text{-}42}$ oligomers bind to PrP^C with nanomolar affinity and that this docking (which accounts for approximately 50% of the membrane-bound Abeta) inhibits LTP in murine hippocampal slices. This phenotype, which is absent in PrP-KO slices, can be rescued by adding, for example, a monoclonal antibody (6D11) against PrP^C residues 93-109, the putative $A\beta_{1\text{-}42}$ binding site (Lauren *et al*., 2009). Interestingly, it was also found that PrP^C binds others oligomers made of misfolded, β-enriched proteins (Fig. 10) (Resenberger *et al*., 2011), thus placing PrP^C at the center of different neurodegenerative disorders.

Others have confirmed that $A\beta_{1\text{-}42}$ oligomers bind to the central region of PrP^C with high affinity (Balducci *et al*., 2010; Calella *et al*., 2010), but the notion that PrP^C is required for Abeta-mediated cognitive impairment and cell death has been strongly questioned, with reports favouring (Chen *et al*., 2010; Chung *et al*., 2010; Gimbel *et al*.,

2010), or denying (Kessels *et al*., 2010; Balducci *et al*., 2010), this hypothesis. A likely explanation for the different observations may reside in the used cell/animal AD model, and in administred Abeta preparations (Yu *et al*., 2009).

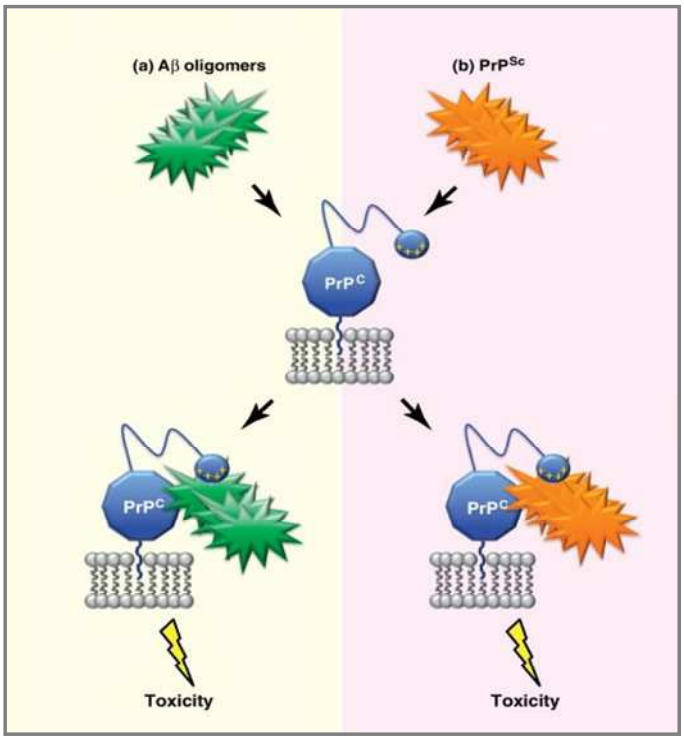

Figure 10. PrP^C as a receptor for Abeta oligomers and PrP^{Sc}. *PrP^C is proposed to act as a high affinity surface binding partner for Abeta (on the left) and PrP^{Sc} (on the right) oligomers, thereby transducing their toxic signal into neurons (modified from www.sciencedirect.com).*

Fyn has been recognized as an important partner in the neuronal impairment induced by PrP^C-Abeta complexes. Indeed, Um *et al*. (2012) have demonstrated that soluble Abeta assemblies, synthetic or derived from AD brains, interact with PrP^C to activate Fyn that, in turn, phosphorylates the NR2B subunit of the NMDA-R. Eventually this causes the displacement of the NMDA-R from the PM, provokes loss of dendritic spines and alters the Ca^{2+} signaling (Um *et al*., 2012)(Fig. 11).

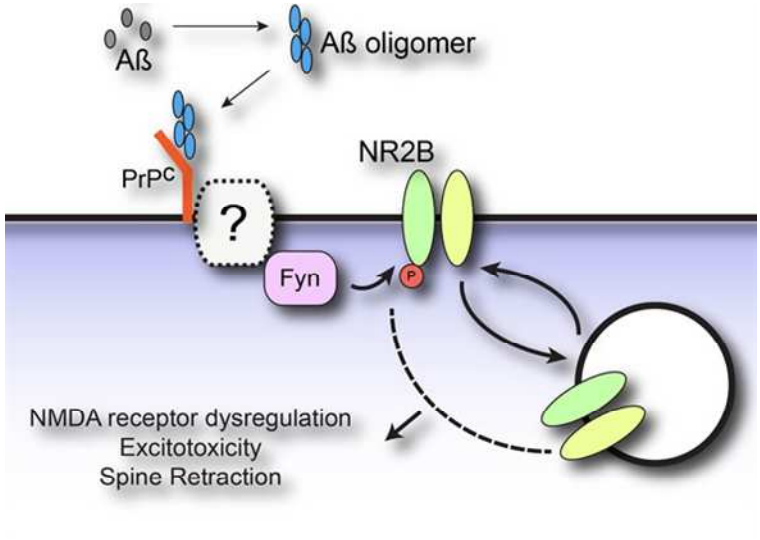

Figure 11. Model for Abeta oligomer-induced synaptic dysfunctions. *The binding between PrP^C and Abeta leads to the activation of Fyn and to the consequent NMDA-R redistribution, Ca^{2+} signaling alterations, spine loss and death in neurons, and AD pathology in mice (modified from medicine.yale.edu).*

The location of PrP^C and Fyn to the opposite sides of the PM impedes that the two proteins interact directly. Indeed, proteomic analysis of PSD, which is enriched in both PrP^C and Fyn, and immunoprecipitation assays, have identified mGluR5 as the structural and functional link between PrP^C and Fyn (Um *et al*., 2013).

2 AIM OF THE STUDY

The issue at the center of the present Ph.D. thesis has dealt with the role exerted by PrP^C in neurons. In spite of long standing efforts and the proposed plethora of functions, what PrP^C effectively does in cells is still largely undefined.

The work focused on the possible control of Ca^{2+} homeostasis by PrP^C, using primary neuronal cultures expressing, or not PrP^C, and Ca^{2+}-sensitive probes targeted to specific cell domains. In particular, the first part of the study dealt with local Ca^{2+} fluxes originating from SOCE, while the second part has analyzed Ca^{2+} movements triggered by the opening of iGluRs. In addition, effort was given to identifying proteins downhill of PrP^C that could aid PrP^C in the control of Ca^{2+} homeostasis.

In light of the proposition that PrP^C acts as a binding partner for misfolded aggregates, both the first and the second part of the thesis have analyzed whether soluble $A\beta_{1\text{-}42}$ oligomers were capable to impair the putative control of PrP^C over neuronal Ca^{2+} fluxes.

3 MATERIALS AND METHODS

3.1 ANIMALS

We used transgenic (Tg46, have indicated with PrP-Tg) and PrP-KO (line F10) mice, kindly provided by the M.R.C. Prion Unit, London, UK. The F10 PrP-KO mice was generated by crossing $PrP^{0/0}$ mice of the Zurich I line with WT FVB mice, after which $PrP^{+/-}$ were crossed with each other to obtain a PrP-KO progeny with an almost pure (>99%) FVB genotype. Instead of WT FVB mice, in this thesis the PrP-Tg line was used as control, given that these mice were obtained by reintroducing the PrP transgene into the PrP-KO genotype.

All aspects of animal care and experimentation were performed in compliance with European and Italian (D.L. 116/92) laws concerning the care and use of laboratory animals. The authors' Institution has been acknowledged by the Italian Ministry of Health, and by the Ethical Committee of the University of Padova, for the use of mice for experimental purposes.

3.2 PRIMARY CULTURES OF CEREBELLAR GRANULE NEURONS

Each culture was prepared by combining cerebella obtained from 7 day-old mice, killed by decapitation after anesthesia with methoxyflurane. Cerebella, deprived from meningeal layers and blood vessels, were minced in an ice-cold buffer [124 mM NaCl, 5.4 mM KCl, 1 mM NaH_2PO_4, 0.5 mM $MgSO_4$, 3.6 mM dextrose, 0.3% (w/v) bovine serum albumin (BSA), 25 mM HEPES/KOH (pH 7.4)], and were then added with trypsin (0.8 mg/mL) and DNAse, whose activity was stopped by adding in two steps suitable inhibitors (trypsin inhibitor, Sigma; deoxy-ribonuclease I, Roche Corporation). After sedimenting the cell debris, the dissociated CGN-containing supernatant was added with an equal volume of the above buffer (containing also 1.2 mM $MgSO_4$ and 1.4 mM $CaCl_2$) and centrifuged (180 g, 10 min). Finally, the pellet was gently resuspended in the Minimum Essential Medium Eagle (Sigma), supplemented with 10% heat-inactivated foetal bovine serum (FBS; Euroclone), 2 mM L-glutamine (Gibco), 0.1 mg/mL gentamycin (Gibco), and KCl (25 mM).

After seeding cells at a density of: (i), 9×10^5 (onto poly-L-lysine-coated 13-mm coverslips) for luminometer assays; (ii), 6×10^5 (onto poly-L-lysine-coated 13-mm coverslips) for immunofluorescence assays; (iii), 3×10^6 (onto 35-mm poly-L-lysine-coated plates) for biochemical assays; (iv), 1.2×10^6 (onto 35-mm poly-L-lysine-coated plates) for fluorescence and transmission electron microscopy assays, CGN were

cultured at 37 °C and 5% CO_2 atmosphere. Lentiviral particles (see below) were added to cells 24 h after plating, and after additional 24 h cytosine arabinoside (0.04 mM, Sigma) was added to impede proliferation of non-neural cells. After further 48 h, CGN were used for experiments at (at least) >97% purity, as proved by the immunocytochemical test for the presence of astrocytes (Lazzari *et al*., 2011).

3.3 CONSTRUCTION OF LENTIVIRAL VECTORS AND CELL INFECTION

To follow Ca^{2+} fluctuations in specific CGN compartments, we exploited a lentiviral expression system to transduce cells with chimeric constructs encoding the Ca^{2+}-probe aequorin (AEQ) tagged with the influenza virus hemagglutinin (HA) epitope, and linked to sequences addressing the protein to the cytosolic domains proximal to the PM (AEQpm, Marsault *et al*., 1997), the cytosol (AEQcyt, Brini *et al*., 1995), the ER lumen (AEQer, Montero *et al*., 1995), and the mitochondrial matrix (AEQmit, Rizzuto *et al*., 1992). Lentiviral vectors for AEQpm, AEQer and AEQmit were generated as described (Lim *et al*., 2008; Lazzari *et al*., 2011), using an AEQ mutant with reduced Ca^{2+} affinity that allows measurements of $[Ca^{2+}]$ >10 μM (Kendall *et al*., 1992).

Conversely, to detect variations of cytosolic $[Ca^{2+}]$, a chimeric construct of WT AEQ fused to the monomeric red fluorescent protein (mRFP) was used. To generate the AEQcyt lentiviral vector, two PCR reactions were performed. In the first PCR, the mRFP sequence was amplified without the stop codon using the pCDNA3-mRFP plasmid (Clontech) as template, and the following primers:

XbaI-mRFP (forward, CGTCTAGAATGGCCTCCTCCGAGGAC)

mRFP-BglII (reverse, GAGGCGCCGGTGGAGTGGAGATCTCG)

In the second PCR, the HA-AEQ cassette was amplified using the pCDNA1-AEQcyt plasmid (Brini *et al*., 1995) as template, and the following primers:

BglII-AEQ (forward, CGAGATCTCGAGCTCAAGCTTTATGA)

AEQ-SalI (reverse, GGTATCGATAAGCTTGATGTCGACGC).

PCR products were digested with XbaI and BglII for mRFP and with BglII and SalI for HA-AEQ, and the resulting fragments were assembled into the XbaI- and SalI-digested backbone of the lentiviral vector pRRLsin.PPTs.hCMV.GFP.pre, in a three-step ligation reaction.

Lentiviral particles were produced as described in Follenzi and Naldini (2002). Briefly, HEK293T packaging cells (15 x 10^6 cells in 150 mm culture plates), cultured in Dulbecco's modified Eagle's medium (Sigma) supplemented with 10% FBS, 2 mM L-glutamine, 40 lg/mL penicillin/streptomycin (Euroclone), were co-transfected (24 h after plating) with plasmids pMDLg/pRRE, pMD2.VSVG, pRSV-Rev and the desidered pLV-AEQ construct, by means of the calcium-phosphate transfection method. After 10 h, the transfection medium was replaced with fresh culture medium, and cells were grown for 72 h, after which the culture medium was collected. Viral particles were harvested by ultracentrifugation (50,000 g, 2 h), resuspended in 0.2 mL of phosphate buffer saline (PBS), and stored at -80 °C until use.

3.4 AEQUORIN-BASED CALCIUM MEASUREMENTS

AEQ (isolated from the luminescent jellyfish *Aequorea Victoria)* is a 189 aa-long protein containing three high affinity Ca^{2+} binding sites (EF-hand type) and a binding site for its prostetic group, coelenterazine. Upon Ca^{2+} binding, the protein undergoes a conformational change that triggers the oxidation of coelenterazine to coelenteramide with emission of light (λ_{max} = 469nm). In our experiments, apo-AEQs were reconstituted into the active forms by adding coelenterazine just before Ca^{2+} measurements.

All experiments were performed by means of a computer-assisted luminometer equipped with a perfusion system. Depending on the type of measurement, neurons were treated as described below. All experiments ended by lysing cells with digitonin (100 · M, Sigma) in a hypotonic Ca^{2+}-rich solution (10 mM $CaCl_2$ in H_2O) to discharge the remaining AEQ pool. The light signal was digitalized and stored for subsequent analyses. Luminescence data were calibrated off-line into [Ca^{2+}] values, using a computer algorithm based on the Ca^{2+} response curve of AEQ (Brini *et al.,* 1995).

3.4.1 Calcium transients after activation of SOCE or VGCC

To measuring Ca^{2+} movements elicited by SOCE with AEQpm, AEQcyt and AEQmit, CGN were incubated (1 h, 37 °C, 5% CO_2) in a modified Krebs-Ringer buffer [(KRB, 125 mM NaCl, 5 mM KCl, 1 mM Na_3PO_4, 1 mM $MgSO_4$, 5.5 mM glucose, 20 mM HEPES (pH 7.4)] supplemented with EGTA (100 µM, to deplete Ca^{2+} from cells), and coelenterazine (5 µM, Santa Cruz). After transferring the cell-containing coverslip to the thermostatted chamber of the luminometer, experiments started by perfusing cells with KRB, first containing EGTA (100 µM), then $CaCl_2$ (1 mM). To monitor Ca^{2+} fluxes

elicited by VGCC, CGN were perfused with different [K^+]-containing KRB buffers (see text) (keeping the final total [K^+ plus Na^+] at 130 mM) and $CaCl_2$ (1 mM). If needed, VGCC inhibitors [nifedipine (10 µM in 0.1% dimethylsulfoxide (DMSO), Sigma) or $NiCl_2$ (50 µM or 1 mM, Sigma)], or the SFK inhibitor PP2 (10 µM in 0.04% DMSO, Tocris Bioscience), were added before activating VGCC and/or SOCE. When measuring $[Ca^{2+}]_{er}$, CGN were washed three times with KRB supplemented with EGTA (1 mM), left 10 min at 37 °C (5% CO_2), and incubated (1 h, 4 °C) in KRB supplemented with ionomycin (5 µM, Sigma), EGTA (500 µM) and a modified coelenterazine (coelenterazine n, 5 µM, Sigma), whose reduced Ca^{2+} affinity allows detection of high $[Ca^{2+}]_{er}$. After transferring the coverslip to the luminometer chamber, experiments started by perfusing cells with KRB containing (in sequence): EGTA (500 µM), (2 min); 2% (w/v) BSA and EGTA (1 mM) (3 min); EGTA (500 µM) (2 min); $CaCl_2$ (1 mM). It is to be noted that, despite few different steps, the procedure to deplete ER Ca^{2+} store ensured that CGN were subjected to similar conditions to those employed when measuring $[Ca^{2+}]$ in the other tested domains before SOCE.

3.4.2 Calcium transients after stimulating GluRs

To measuring Ca^{2+} transients elicited by active iGluRs, or mGluRs, CGN were incubated (1 h, 37 °C, 5% CO_2) in KRB supplemented with EGTA (100 µM) and coelenterazine (5 µM). After transferring the coverslips to the thermostatted chamber of the luminometer, experiments started by perfusing cells with KRB, first containing EGTA (100 µM), then $CaCl_2$ (1 mM), and finally with Mg^{2+}-free KRB containing $CaCl_2$ (1 mM), glutamate (100 µM, Sigma) and glycine (10 µM, Sigma), or NMDA (50 µM, Sigma) plus glycine, to activate all glutamate receptors, or only the NMDA-R, respectively. To stimulate specifically AMPA/kainate/mGluRs, CGN were first perfused with KRB containing $CaCl_2$ (1 mM) and then with KRB containing $CaCl_2$ (1 mM), AMPA (100 µM, Tocris Bioscience) kainate (30 µM, Tocris Bioscience), or the mGluR1,5 agonist DHPG (100 µM, Tocris Bioscience), respectively. In some experiments AEQcyt and AEQmit were reconstituted in KRB containing $CaCl_2$ (1 mM) but no difference was observed in Ca^{2+} transients with respect to when the protocol to reconstitute AEQpm in EGTA-containing KRB was used. To inhibit RyR, ryanodine (50 µM in 0.2% DMSO, Tocris Bioscience) was added before (during the perfusion step with the Mg^{2+}-free, and $CaCl_2$ 1 mM-containing KRB) and during glutamate addition.

3.5 ABETA PEPTIDES

3.5.1 Preparation and characterization of $A\beta_{1-42}$ peptides

Chemically synthetized human $A\beta_{1-42}$ peptides (Keck Laboratories, U.S.A.) were dissolved (1 mg/mL), and incubated (1 h, RT), in 1,1,1,3,3,3-hexafluoro-2-propanol. The suspension was divided into solvent-free (by evaporation) aliquots (each with about 50 · g of peptide) and stored (at -80 °C). Just before use, peptides were dissolved in 50 · L of 20 mM NaOH, sonicated (15 min on ice in a bath sonicator), diluted (with PBS to a final volume of 250 · L), and centrifuged (14,000 g, 5 min) to remove insoluble aggregates. After determining their concentration spectrophotometrically (at 214 nm), $A\beta_{1-42}$ peptides were aged to form oligomers (1 h, 37 °C), and then administered to CGN during the AEQ reconstitution step (see above) at a final concentration of 5 · M of monomer equivalent.

To characterize $A\beta_{1-42}$ oligomerised state by Western blot (WB), ~300 ng samples, collected both before and after each oligomerization process, were diluted in a sample buffer containing 12% SDS (w/v), 6% mercaptoethanol (v/v), 30% glycerol (w/v), 0.05% Coomassie blue, 150 mM Tris/HCl (pH 7.0), and run in a (6M) urea-containing tricine gel (16% (w/v) acrylamide) (Schägger, 2006). Proteins were then electro-blotted onto polyvinylidene fluoride (PVDF) membranes (0.22 μm pore size, Millipore Corporation, Bedford, MA, USA), and membranes were incubated first (1 h, RT) with a blocking solution containing non-fat dry milk (5% (w/v) (Bio-Rad Laboratories, Hercules, CA, USA) diluted in Tris-buffered saline (TBS) added with 0.02% (w/v) Tween-20 (TBS-T 0.02%), and then (over-night, 4 °C) with a monoclonal (m) antibody (Ab), see below) to $A\beta_{1-42}$. After three 10 min-washes with TBS-T 0.02%, membranes were treated (1 h, RT) with a horseradish peroxidase-conjugated anti-mouse IgG secondary polyclonal (p) Ab. Immunoreactive bands were visualized and digitalized by means of a digital Kodak Image Station, using an enhanced chemiluminescence reagent kit (Millipore Corporation). For densitometric analysis, band intensities were evaluated by the Kodak 1D image analysis software.

3.6 FLUORESCENCE MICROSCOPY

3.6.1 Measurement of mitochondrial membrane potential

The membrane potential of CGN mitochondria ($\Delta_{\psi m}$) was measured using the (PM-permeable) cationic tetramethylrhodamine methyl ester probe (TMRM, λ_{exc} = 548 nm, λ_{em} = 574 nm), which accumulates electrophoretically into the mitochondrial matrix.

To analze $\Delta_{\psi m}$ under the conditions experienced by CGN immediately before activation of external Ca^{2+} entry, CGN were first incubated (1 h, 37 °C, 5% CO_2) with KRB containing $CaCl_2$ (1 mM), and then (30 min, 37°C, 5% CO_2) with TMRM (10nM, Molecular Probes) in KRB containing $CaCl_2$ (1 mM) and finally in Mg^{2+} free-KRB. Coverslip images were collected with an inverted microscope (Olympus IMT-2) equipped with a (75W) xenon lamp to provide fluorescence light, a 16 bit digital cooled CCD camera (provided with a cooling system Miromax, Princeton Instruments), a 40 x oil objective, and appropriate excitation and emission filters. Several fields were acquired from each coverslip before and after addition of trifluorocarbonylcyanide phenylhydrazone (FCCP) (5 µM, Sigma) that, by collapsing the $\Delta_{\psi m}$, releases the probe from mitochondria.

Images were analyzed using the Image J software. Fluorescence intensity was measured in regions rich in mitochondria. For each analyzed coverslip, the TMRM fluorescence intensity was calculated as the difference between the mean fluorescence intensity before and after of FCCP addition.

3.6.2 Immunofluorescence

The number of mitochondria in CGN was analyzed under the condition used to stimulate glutamate/NMDA-Rs and using the mitochondrial protein TOM20 as marker. CGN were first incubated (1 h, 37°C, 5% CO2) in KRB containing CaCl2 (1 mM), then fixed with paraformaldehyde 4% (20 min, RT) and permeabilized with ice cold Triton 0.1% (w/v) in PBS (10 min, 4°C). Then CGN were incubated (overnight, 4 °C) with a pAb against TOM20 (Santa Cruz Biotechnology) diluted in BSA [1% (w/v) in PBS]. After 3x10 min washes (with PBS), cells were incubated (30 min, RT) with the secondary anti-rabbit Ab Alexa Fluor 555 (Molecular probes) [(1:100 in BSA 1% (w/v in PBS)], and washed again (3x10 min with PBS). Finally, coverslips were mounted onto glass slides using moviol reagent (Sigma), and images were collected using a confocal microscope (Leica SP5) provided with a 63x oil objective and appropriate emission filters.

Images were analyzed using the Image J software. Given that CGN have a tiny neuronal dendrite network, the fluorescence of TOM20 was analyzed only in regions of the cell soma. Acquired fluorescence was then diminished to the corresponding number of pixels (contained in the analyzed area), and the result subtracted by the normalized fluorescence intensity of the background, i.e., belonging to an unspecific fluorescent region.

3.7 TRANSMISSION ELECTRON MICROSCOPY

To evaluate the number and distance of mitochondria from the PM, CGN were fixed in glutaraldehyde (3.9% w/v in a sodium cacodylate buffer, pH 7.4), and embedded in Epon 812 resin. Semi-thin (1 µm) and ultra-thin (80 nm) cross-sections were cut with an ultra-microtome (Ultratome V, LKB). The semi-thin sections were stained with toluidine blue, and pictures were taken at a light microscope (5000B, Leica) equipped with a digital photocamera (DFC 480, Leica). Ultra-thin sections were mounted on copper grids, contrasted with uranyl acetate (1%) and lead citrate (1%), and examined at a transmission electron microscope (Tecnai G2, FEI) operating at 100 kV. Images were acquired using a digital camera (F114, Tvips) and a dedicated software (TIA, FEI).

Images were analyzed using the Image J software. The number of mitochondria was analyzed in the soma and in the dendrites normalized to the corresponding area, and the distance of mitochondria from the nearest rim of the PM was evaluated.

3.8 SEMI-QUANTITATIVE PCR

3.8.1 RNA extraction and cDNA synthesis

Total RNA extraction from CGN was performed using the Trizol reagent (Invitrogen), a monophasic solution of phenol and guanidine isothiocyanate, according to the manufacturer instructions. Briefly, cells were lysed directly in the 3.5 mm culture dish by adding 1 ml of Trizol and by passing the lysate several times through a pipette. Homogenized samples were incubated (5 min, RT) to permit the complete dissociation of nucleoprotein complexes. After the addition of 0.2 ml of chloroform, RNA-containing tubes were shaken vigorously and incubated (3 min, RT), and samples centrifuged at (12,000 g, 15 min, 4 °C) to separate the different phases of the mixture. Of these, the upper aqueous phase was transferred into a new tube. RNAs were precipitated by adding 0.5 ml of isopropyl alcohol. After incubation (10 min, RT), samples were centrifuged again (12,000 g, 15 min, 4 °C) and the supernatant was

discarded. RNA precipitate was washed with 70% ethanol and dissolved in 40 µl of RNase-free DEPC (diethylpyrocarbonate)-treated water (Amersham).

Reverse transcription reactions were performed using 1 µg of total RNA pretreated with DNAse I (Invitrogen), to eliminate the contaminating DNA. After addition of dNTP and oligo dT to prime the first strand cDNA synthesis, RNA was denatured (5 min 65 °C) and then placed on ice. Reverse transcriptase III (Invitrogen) was then added and the mixture incubated to synthesize cDNA (5 min, 25 °C; 1 h 50 °C; 15 min 70 °C).

3.8.2 PCR

Each PCR reaction was run in a 20 µl volume by combining 1 µl of cDNA, 1 µM of forward and reverse primers (Sigma Genosys), 0.25 µM of each dNTP (Euroclone), 2 mM $MgCl_2$, and 0.025U/µl Taq polimerase (Euroclone) in a buffer containing 150 mM TRIS/HCl, 500 mM KCl, 0.1% v/v Tween 20 (Euroclone). Amplification steps (using Applied Biosystems thermal cycler) were as follows: starting: 95 °C 5 min; denaturing: 95 °C 45 sec; annealing: 64 °C 30 sec x 35 cycles; extending: 72 °C 60 sec; completing the amplicons: 72 °C 10 min; finalling: 4 °C.

The sequence of forward and reverse primers used for mGluR1, mGluR5 and GAPDH were as follows:

mGluR1 F: 5'GGTCCCTTCTGACACTTTGC 3'; R: 5'CATTCCACTCTGCCGTAAT 3'

mGluR5 F: 5'GCCATGGTAGACATAGTGAAG3'; R: 5'TAAGAGTGGGCGATGCAAAT3'

GAPDH F: 5'CAAGGTCATCCATGACAACTT3'; R: 5'GGGCCATCCACAGTCTTCTG3'

To visualize PCR products, amplified DNA was run on agarose gel in the presence of ethidium bromide. Briefly, the loading buffer was added to the samples loaded on a 2% agarose gel in 1x TAE buffer (40mM Tris/acetate, 1mM EDTA), in the presence of 0.25 µg/mL ethidium bromide. The gel was immersed in the running buffer (TAE 1x) and subjected to an electric field (100 V, 20 min). Bands were visualized with a fluorescence reader (Euroclone) and images analyzed using the Image J software.

3.9 WESTERN BLOT ANALYSIS

3.9.1 Sample preparation

CGN, incubated (1h, 37 °C, 5% CO_2) in KRB supplemented with $CaCl_2$ (1 mM), were homogenized in a buffer containing 10% glycerol (w/v), 2% (w/v) SDS, 62.5 mM Tris/HCl (pH 6.8), 1.8 M urea, 5 mM $NaVO_4$, protease and phosphatase inhibitor cocktails (Roche), and boiled (5 min). The total protein content was determined by the Lowry method (Total Protein Kit, Micro Lowry, Peterson's Modification, Sigma), using BSA as standard. Dithiothreitol (50 mM) and bromophenol-blue (0.004% (w/v)) were added to samples just before gel loading.

3.9.2 SDS-polyacrylamide gel electrophoresis (SDS-Page) and immunoblot

Electrophoresis was performed on polyacrylamide gels (prepared in 1-mm thick glass slabs) with 10% acrylamide in the separating gel and 5% acrylamide in the stacking gel. The following solutions were used for the preparation of gels and the electrophoresis: acrylamide/bisacrylamide: 30% acrylamide and 0.8% bisacrylamide; lower Tris-HCl: 1.5 M Tris-HCl and 0.4% SDS, pH 8.8; upper Tris-HCl: 0.5 M Tris-HCl and 0.4% SDS, pH 6.8; running buffer: 0.1 M Tris-HCl, 0.77 M glycine and 0.4% SDS, pH 8.3.

Polymerization was obtained by adding TEMED (Sigma) and ammonium persulfate 0.1 mg/ml (Sigma). Samples (20 μg of proteins in each lane) were run on the gel using an Electrophoresis Power Supply (BioRad), providing a constant voltage of 150 V in the stacking gel and 200 V in the separating gel.

Proteins were then electro-blotted onto PVDF membranes (0.22 μm pore size, Bio-Rad), which were subsequently Coomassie blue-stained to verify equal loading and transfer. Membranes were incubated (1 h, RT) with a blocking solution (TBS-T), and 5% (w/v) non-fat dry milk, or 3% (w/v) BSA, followed by addition of the appropriate primary antibody (see below) (4 °C, over-night). After three 10 min-washes (with TBS-T), membranes were incubated (1 h, RT) with a horseradish peroxidase-conjugated anti-rabbit or anti-mouse IgG secondary antibody (Santa Cruz Biotechnology, cat. n. sc-2004 and sc-2005, respectively).

Used antibodies were (dilution in parentheses): anti-Fyn pAb (1:1000; Cell Signaling Technology, cat. n. 4023); anti-phosphorylated (p-) SFK pAb (recognizing p-Y416, 1:1000; Cell Signaling Technology, cat. n. 2101); anti phospho Tyrosine (p-Tyr) mAb (1:1000; Millipore cat. n. 05-947); anti-Aβ mAb 6E10 (1:1000; Covance, cat. n.

SIG-39320), anti SDH (subunit A) pAb (1.1000; Sigma, cat. n. SAB1100429); anti MCU pAb (1.1000; Sigma cat.n. HPA016480).

Immunoreactive bands were visualized and digitalized by means of a digital Kodak Image Station, using an enhanced chemiluminescence reagent kit (Millipore Corporation). For densitometric analyses, band intensities were normalized to the optical density of the corresponding lane stained with Coomassie blue.

3.10 STATISTICAL ANALYSIS

Values will be reported as mean ± SEM. Data analysis was performed as described in Lazzari et al. (2011). Statistics was based on two-sample Student's t-test, with a p-value <0.05 being considered statistically significant (*p<0.05, **p<0.01, ***p<0.001, ****p<10^{-5})

4 RESULTS –PART 1

4.1 PrP^C CONTROLS LOCAL CALCIUM FLUXES FOLLOWING SOCE

4.1.1 PrP^C attenuates SOCE and SOCE-induced mitochondrial Ca^{2+} uptake

We have previously observed that the presence of PrP^C attenuates SOCE in CGN (Lazzari *et al*., 2011). In particular, using the AEQpm probe, we found that PrP-KO CGN had larger and more persistent Ca^{2+} elevations in PM micro-domains compared to CGN derived from WT (FVB) mice. In this work, the study was extended to monitor whether PrP^C was also controlling cytosolic and mitochondrial Ca^{2+} transients after SOCE. To exclude potential interference by the different (<1%) genetic background between WT (FVB) and PrP-KO mice, another variance of this work was that the isogenic line PrP-Tg, provided the control, given that in this line the expression of normal amounts of PrP^C was rescued over the PrP-KO genotype.

To activate SOCE, after depletion of Ca^{2+} stores (with EGTA 100 µM), CGN were perfused with 1 mM $CaCl_2$. Fig. 12 reports Ca^{2+} fluctuations in PM micro-domains (A), in the cytosol (B) and in the mitochondrial matrix (C), as detected by AEQpm, AEQcyt and AEQmit, respectively. The rise of $[Ca^{2+}]_{pm}$ had a significantly higher (30%) peak value in PrP-KO CGN (black) than in PrP-Tg CGN (grey) (Fig. 12A), confirming that the absence of PrP^C leads to a higher Ca^{2+}replenishment of PM micro-domains. Similarly, PrP-KO CGN exhibited higher Ca^{2+} transients also in the cytosol (Fig. 12B) and in the mitochondrial matrix (Fig. 12C), possibly due to both the increased Ca^{2+} entry through SOCC (Fig. 12A) and to the lower buffer capacity of the ER. In fact, the PrP-KO ER accumulated approximately 20% less Ca^{2+} than the PrP-Tg ER (Fig. 13).

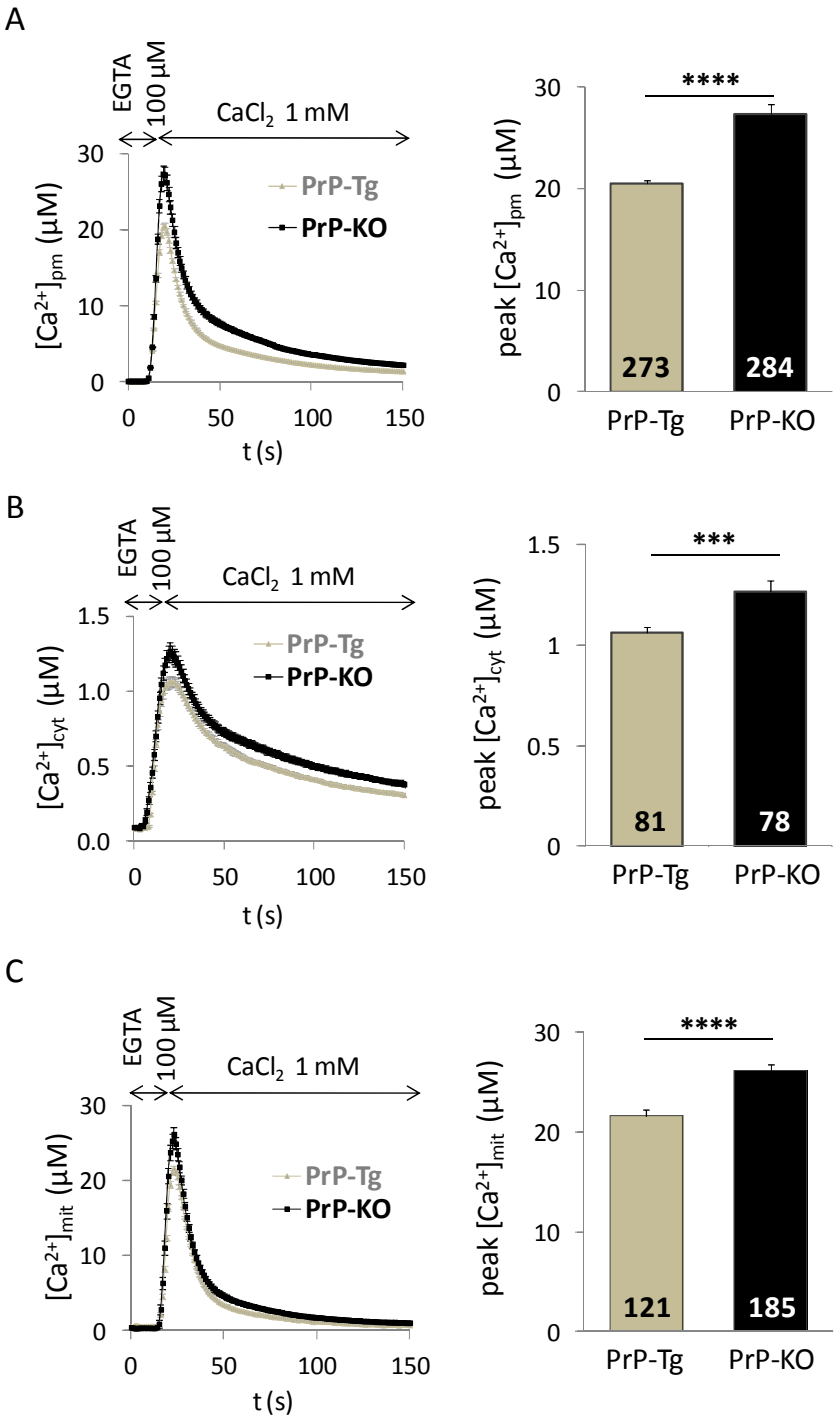

Figure 12. Ca^{2+} transients in CGN domains after SOCE. *CGN were first incubated with EGTA (100 µM) and then perfused with $CaCl_2$ (1 mM). Both the mean of the recorded traces (left panels), and the bar diagrams reporting the mean peak values of Ca^{2+} transients (right panels), indicate that PrP-KO (black) have higher Ca^{2+} fluxes than control PrP-Tg CGN (grey) near the PM (A), in the cytosol (B), and in the mitochondrial matrix (C). Here and after reported values are mean ± SEM, numbers inside bars indicate number of replicates. Peak values: in PM microdomains, 20.45 ± 0.41 µM in PrP-Tg CGN; 27.33 ± 1.04 µM*

*in PrP-KO CGN; in the cytosol, 1.06 ± 0.03 in PrP-Tg CGN; 1.27 ± 0.06 µM in PrP-KO CGN; in mitochondria, 21.63 ± 0.67 µM in PrP-Tg CGN; 26.15 ± 0.67 µM in PrP-KO CGN. ***p<0.001; ****p<10^{-5} Student's t-test.*

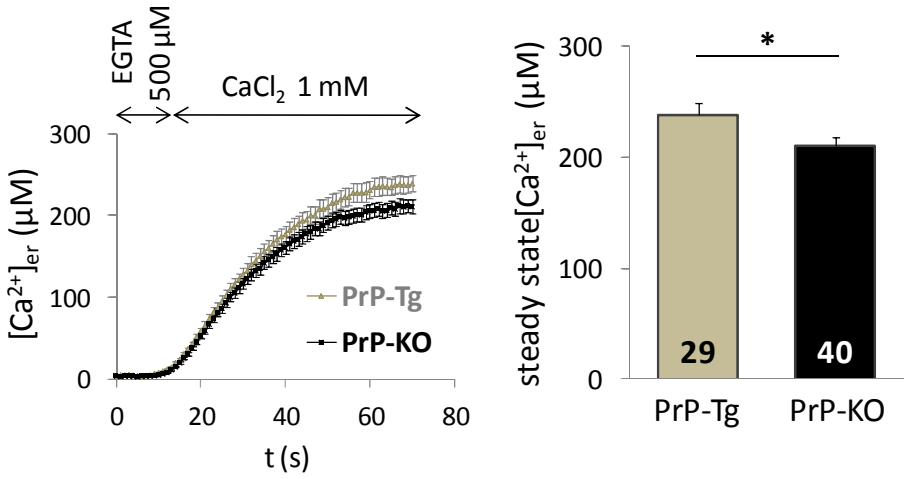

Figure 13. Steady state Ca^{2+} levels in the lumen of the ER after SOCE. *CGN were first incubated with EGTA (500 µM) and the Ca^{2+} ionophore ionomycin (5 µM), after which ER Ca^{2+} refilling was achieved by perfusing CGN with $CaCl_2$ (1 mM). Both the mean of the recorded traces (left panel), and the bar diagram reporting the mean steady state ER Ca^{2+} level (right panel), indicate that $[Ca^{2+}]_{er}$ is lower in PrP-KO CGN (black). Peak values: 238.42 ± 10.71 µM in PrP-Tg CGN; 210.47 ± 8.30 µM in PrP-KO CGN. *p<0.05 Student's t-test.*

4.1.2 VGCC do not contribute to the observed Ca^{2+} transients

To prove that Ca^{2+} replenishment of PM micro-domains could be imputed only to SOCE, we performed a set of controls to exclude that SOCC-mediated Ca^{2+} entry provoked a (local) membrane depolarization leading to the activation of VGCC. VGCC exist in several subtypes that can be broadly divided into two groups upon their activation by voltage: the group (T-type VGCC) activated by mild, and that activated by large, membrane depolarization (L/P/R-type VGCC) (Connor *et al*., 1987; Catterall *et al*., 2005). These conditions were experimentally mimicked using a perfusion solution containing 25 mM and 125 mM K^+, respectively. We found no AEQpm-detectable Ca^{2+} transients in both CGN genotypes using 25 mM K^+ (data not shown). Instead, perfusion with 125 mM K^+ induced a similar (albeit smaller than with SOCE, ~ 3 µM) Ca^{2+} peak in both CGN genotypes (Fig. 14), implying that PrP^C was not involved in controlling L/P/R type-VGCC in our cell paradigms, contrary to previous suggestions (Herms *et al*., 2000; Korte *et al*., 2003).

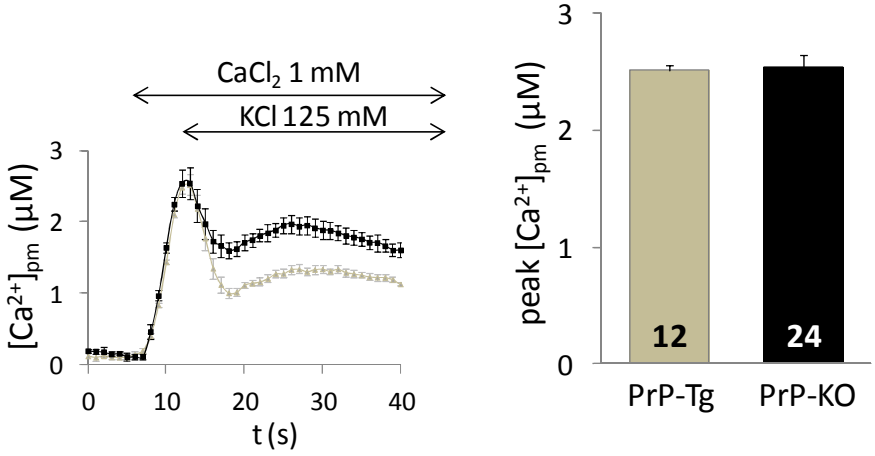

Figure 14. $[Ca^{2+}]_{pm}$ transients after perfusing CGN with the 125 mM K^+ depolarizing solution. *Both the mean of the recorded traces (left panel), and the bar diagram (right panel) reporting the mean $[Ca^{2+}]_{pm}$ peak values, indicate that the 125 mM K^+-depolarizing protocol elicits $[Ca^{2+}]_{pm}$ peaks of similar amplitude in both types of neurons, although with values much smaller compared to those measured after SOCE. Peak values: 2.51 ± 0.17 µM in PrP-Tg CGN; 2.54 ± 0.22 µM in PrP-KO CGN.*

To block VGCC, we used nifedipine (10 µM), a specific inhibitor of the L type-VGCC, or $NiCl_2$ (50 µM or 1 mM), which inhibits all high voltage-activated VGCC. The obtained results demonstrate that both inhibitors had a similar effect, independently of the CGN genotype, i.e., approx. 20% inhibition by nifedipine and 95% inhibition by 1 mM $NiCl_2$ (Fig. 15A). However, when the inhibitors were added to neurons under the specific conditions employed to activate SOCE, we found that in both control and PrP-KO CGN they induced no statistically significant diminution of the Ca^{2+} transients observed in their absence (Fig. 15B). Altogether, these results clearly indicate that the contribution of VGCC to the PM-Ca^{2+} transients observed upon SOCE stimulation is, if any, minimal.

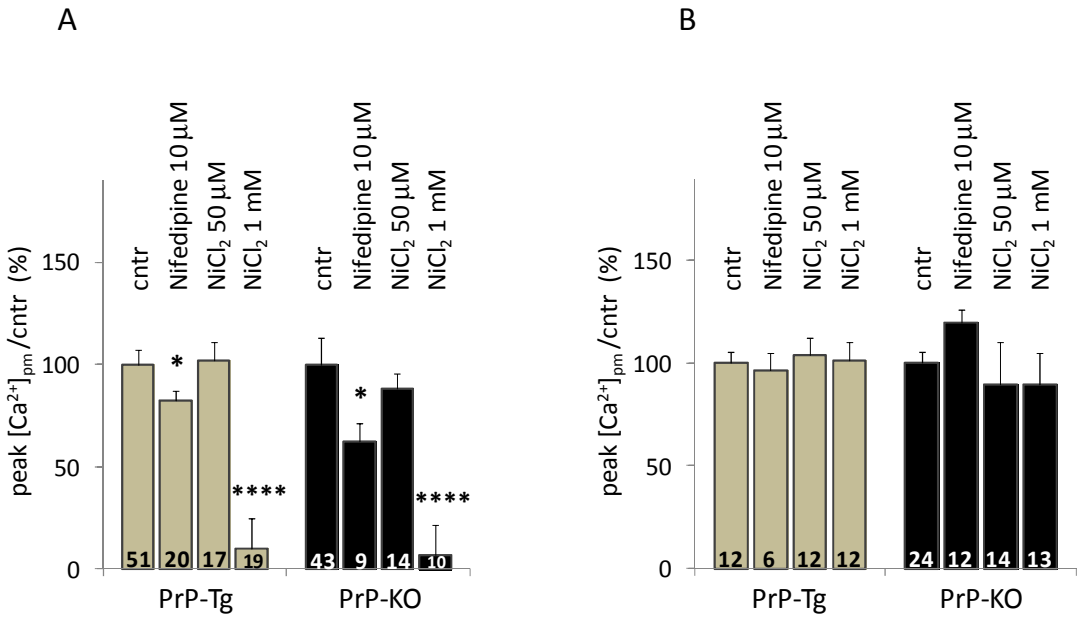

Figure 15. $[Ca^{2+}]_{pm}$ peaks elicited by VGCC (A) or SOCC (B) in the absence, or in the presence, of VGCC inhibitors. *(A), CGN were subjected to the strong depolarizing stimulus by 125 mM K^+, in the absence (cntr), or in the presence, of nifedipine (10 µM) or $NiCl_2$ (50 µM, 1mM). (B), The same inhibitors were absent (cntr), or present, when CGN were specifically treated to activate SOCE. Clearly, these molecules reduce $[Ca^{2+}]_{pm}$ when VGCC are specifically activated (A), but not when SOCE-activating protocol is applied (B). Normalized peak values: (A), 100 ± 2.7% in untreated PrP-Tg CGN; 82 ± 4.58% in PrP-Tg CGN with nifedipine; 102 ± 8.91% in PrP-Tg CGN with $NiCl_2$ 50 µM; 10 ± 14.91% in PrP-Tg CGN with $NiCl_2$ 1mM; 100 ± 12.82% in untreated PrP-KO CGN; 62 ± 8.62% in PrP-KO CGN with nifedipine; 88 ± 7.47% in PrP-KO CGN with $NiCl_2$ 50 µM; 6.6 ± 14.99% in PrP-KO CGN with $NiCl_2$ 1mM; (B), 100 ± 5.37% in untreated PrP-Tg CGN; 96.7 ± 8.23% in PrP-Tg CGN with nifedipine; 103.9 ± 8.28% in PrP-Tg CGN with $NiCl_2$ 50 µM; 101.5 ± 9.02% in PrP-Tg CGN with $NiCl_2$ 1mM; 100 ± 5.62% in untreated PrP-KO CGN; 120 ± 6.03% in PrP-KO CGN with nifedipine; 89.6 ± 20.8% in PrP-KO CGN with $NiCl_2$ 50 µM; 89.4 ± 15.7% in PrP-KOCGN with $NiCl_2$ 1 mM. *p<0.05; ****p<10^{-5} Student's t-test.*

4.1.3 Fyn is the link between PrP^C and SOCE

Multiple lines of evidence have linked PrP^C to Fyn (Mouillet-Richard *et al*., 2000; Santuccione *et al*., 2005), a member of the SFK expressed in neurons at high levels (Um *et al*., 2012). Depending on the used cell line, examples are the activation of Fyn following the antibody-mediated clustering of PrP^C at the cell surface (Pantera *et al*., 2004), and/or the binding of synthetic Aβ oligomers to PrP^C (Um *et al*., 2012).

In light of this data, we asked the question of whether Fyn signaling could be also involved in the regulation that PrP^C exerts on SOCE. To this end, we analyzed the phosphorylated, active state of Fyn in control and PrP-KO CGN under basal conditions

(i.e., in the presence of 1 mM $CaCl_2$). As reported in Fig. 16, WB analyses of phosphorylated Fyn (on Tyr 416) showed that PrP-KO CGN constitutively displayed higher levels of the active enzyme than control neurons. The same result was obtained by treating CGN with EGTA (100 µM), thus mimicking the conditions at which Ca^{2+} measurements were made (data not shown).

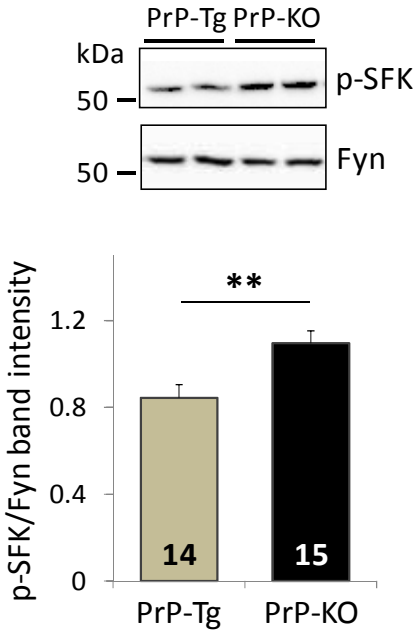

Figure 16. Fyn phosphorylation is higher in PrP-KO CGN than in PrP-Tg CGN under basal conditions. *CGN proteins were analyzed by WB (after 96h from plating) in the presence of $CaCl_2$ 1 mM. The upper panel reports a representative WB of p-SFK and of total Fyn (both run in duplicate) of PrP-Tg and PrP-KO CGN, while the lower panel reports the densitometric analysis of anti p-SFK immunosignal normalized to that of total Fyn. **p<0.01 Student's t-test.*

This result is further corroborated by the finding that total tyrosine-phosphorylated proteins were higher in PrP-KO neurons, both under basal conditions (i.e., in the presence of 1 mM $CaCl_2$) (Fig. 17), and in the presence of EGTA (100 µM) (data not shown).

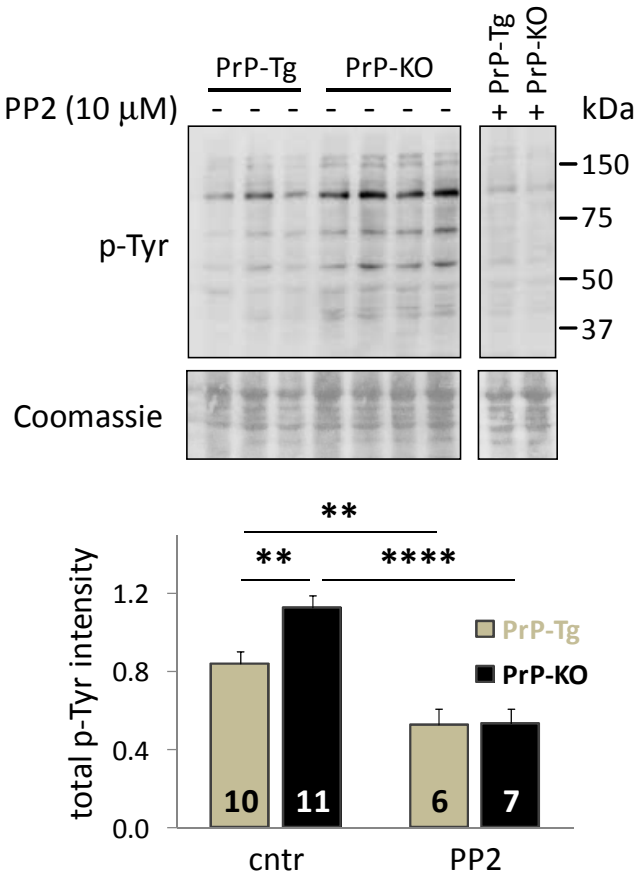

Figure 17. Tyr-phosphorylated proteins are higher in PrP-KO than in PrP-Tg CGN. *CGN, treated with or without the SFK inhibitor PP2 (10 μM), were subjected to WB analyses. The upper panels report a representative WB for p-Tyr of untreated (-) (top left), or PP2-treated (+) (top right), PrP-Tg and PrP-KO CGN, while the lower panel reports the densitometric analysis of p-Tyr immuno-signal of untreated (cntr) or PP2-treated (PP2) CGN, normalized to the density of the Coomassie blue staining. **p<0.01;****p<10^{-5} Student's t-test.*

Because of previous demonstrations showing that the pharmacological inhibition, or deletion, of tyrosine kinases reduces SOCE-induced Ca^{2+} transients in certain cell types (Zuo *et al*., 2011; Lee *et al*., 2006; Lopez *et al*., 2012), we examined if and how the specific inhibition of tyrosine kinases by PP2 was affecting SOCE. Fig. 18 shows that PP2 reduced the $[Ca^{2+}]_{pm}$ peak in both CGN types, and that it nullified the difference displayed by untreated PrP-KO and control neurons. These results strongly support the existence of an inverse relationship between the presence of PrP^C and Fyn activation, and that PrP^C restricts SOCE by downregulating the Fyn signaling pathway.

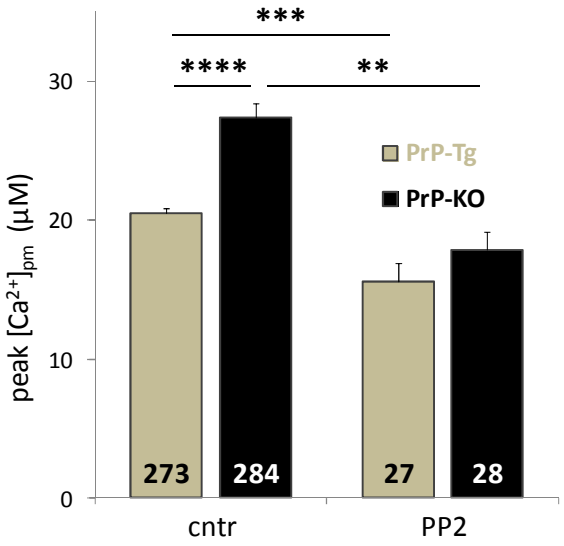

Figure 18. PrP^C controls SOCE by modulating Fyn activity. *After depleting neurons of Ca^{2+} to activate SOCE, CGN were perfused with $CaCl_2$ (1 mM) in the absence (cntr) or in the presence (PP2) of PP2 (10 µM). From the bar diagram, reporting the mean peak values of $[Ca^{2+}]_{pm}$ transients, it is evident that PP2 decreases $[Ca^{2+}]_{pm}$ peak, abrogating in this way the difference observed in untreated PrP-Tg and PrP-KO CGN. Peak values: 20.45 ± 0.41 µM in untreated PrP-Tg CGN; 15.60 ± 1.31 in PP2-treated PrP-Tg CGN; 27.33 ± 1.04 µM in untreated PrP-KO CGN; 17.84 ± 1.33 in PP2-treated PrP-KO CGN. **p<0.01; ***p<0.001; ****p<10^{-5} Student's t-test.*

4.1.4 Aβ$_{1-42}$ oligomers impair PrP^C-dependent control of SOCE

Following the notion that PrP^C binds soluble oligomeric Abeta, and that PrP^C-Abeta interaction may be crucial for AD-related neuronal impairment (Um and Strittmatter, 2013), we monitored PM Ca^{2+} transients to assess whether soluble Aβ$_{1-42}$ oligomers perturbed the control of PrP^C over SOCE.

To start, we qualitatively characterized the used Aβ$_{1-42}$ oligomers by WB before and after the aging process (1h, 37° C) which Aβ$_{1-42}$ fragments were subjected to. As shown in Fig. 19, already freshly dissolved Aβ$_{1-42}$ peptides (of approximately 5 kDa molecular mass in their monomeric form) migrated in different oligomerized forms, i.e., monomers, dimers, trimers and higher mass oligomers, and that the latter ones were efficiently increased in amounts by the aging process.

Fig. 20, reporting the effect on SOCE by soluble Aβ$_{1-42}$ oligomers added to CGN, shows that, compared to the untreated counterpart, they augmented PM Ca^{2+} peaks of PrP-Tg CGN to the same value detected in untreated PrP-KO CGN. Because no statistically significant effect was evident in Aβ$_{1-42}$-treated PrP-KO CGN, this result indicates that Aβ$_{1-42}$-induced dysregulation of SOCE was strictly PrP^C-dependent.

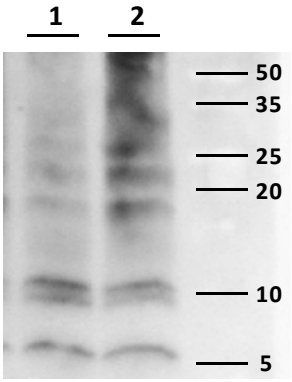

Figure 19. The "aging" of Aβ$_{1-42}$ increases the formation of high mass species. *A representative WB of chemically synthesized Aβ$_{1-42}$ subjected (lane 2), or not (lane 1), to the aging process (1 h, 37° C) indicates that aging process increases the presence of high mass species.*

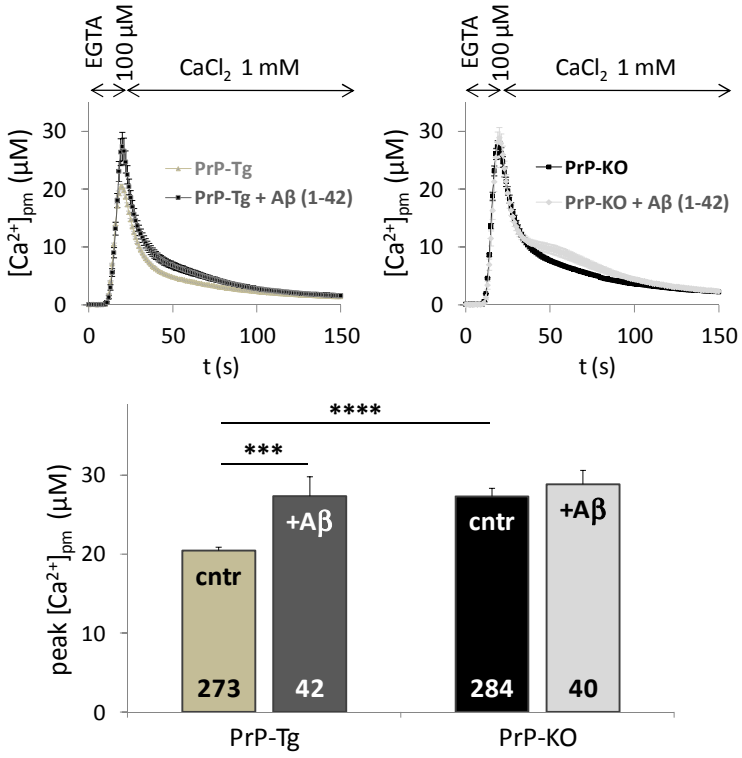

Figure 20. Soluble Aβ$_{1-42}$ oligomers alter the PrP^{C}-dependent control of SOCE. *After incubation in the absence (cntr) or in the presence (+Aβ) of soluble Aβ$_{1-42}$ oligomers (5 µM), CGN were treated to activate SOCE. Both the mean of the recorded traces (upper panels) and the bar diagrams (lower panel) reporting the mean $[Ca^{2+}]_{pm}$ peak values, indicate that treatment with soluble Aβ$_{1-42}$ oligomers increased $[Ca^{2+}]_{pm}$ peak values only in PrP-Tg CGN. Peak values: 20.45 ± 0.41 µM in untreated PrP-Tg CGN; 27.36 ± 2.45 in Aβ$_{1-42}$ treated PrP-Tg CGN; 27.33 ± 1.04 µM in untreated PrP-KO CGN; 28.84 ± 1.79 in Aβ$_{1-42}$ treated PrP-KO CGN. ***p<0.001;****p<10^{-5} Student's t-test.*

Importantly, we found that the capacity of $A\beta_{1-42}$ oligomers to disturb SOCE was paralleled by the effect on Fyn, given that they increased the level of active Fyn in PrP-Tg CGN, but left unaltered that of PrP-KO neurons (Fig. 21). It is therefore possible to conclude that oligomeric $A\beta_{1-42}$ increased SOCE by impairing the PrP^C-dependent downregulation of Fyn.

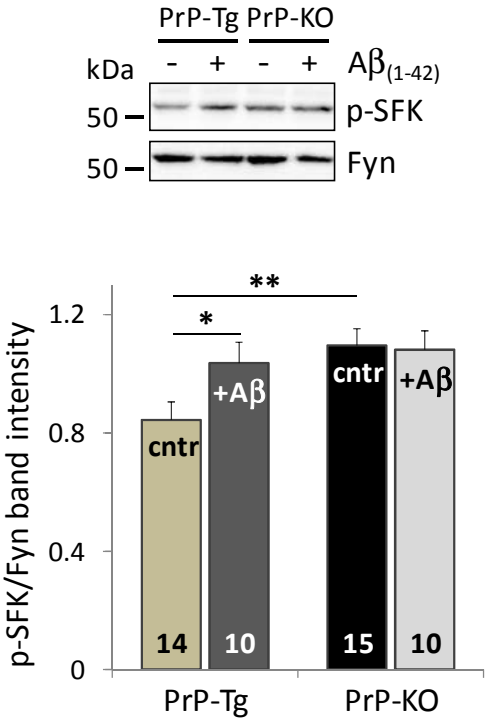

Figure 21. Soluble $A\beta_{1-42}$ oligomers enhance Fyn phosphorylation in a PrP^C-dependent way. *The upper panel reports a representative WB of p-SFK and of total Fyn of untreated (-), or $A\beta_{1-42}$-treated (+), PrP-Tg and PrP-KO CGN. The lower panel reports the densitometric analysis of the anti p-SFK immunosignal normalized to that of total Fyn. *p<0.05; **p<0.01 Student's t-test.*

5 CONCLUSIONS-PART 1

The conclusion that one can draw from this part of the work is that, by limiting Ca^{2+} influx through SOCE, PrP^C also limits the ion accumulation in the cytosol and in mitochondria. These results thus reinforce the notion of the pro-life behavior of PrP^C in neurons which are extremely sensible to Ca^{2+} dysomeostasis.

Our data have also shown that the regulation of SOCE by PrP^C occurs through Fyn tyrosine kinase, which can therefore represent the molecular intermediate of the PrP^C-SOCE linkage. In particular, our data suggest that PrP^C constitutively limits Fyn activity.

This function of PrP^C may have important consequences in neurodegeneration, especially with respect to the alleged action of the protein as a receptor for $A\beta_{1-42}$ oligomers (and other neurotoxic entities) for the transduction of their toxic message into neurons. One possibility is that $A\beta_{1-42}$-PrP^C docking directly activates Fyn, as already suggested. Alternatively, however, the demonstrated parallelism between $A\beta_{1-42}$-treated and PrP-KO neurons suggests that $A\beta_{1-42}$ oligomers alter/displace PrP^C, thus rendering PrP^C no longer able to control Fyn activity.

6 RESULTS –PART 2

6.1 PrP^C CONTROLS CALCIUM FLUXES THROUGH IONOTROPIC GLUTAMATE RECEPTORS

6.1.1 PrP^C reduces Ca^{2+} fluxes after stimulation of the NMDA and AMPA receptors

Because of the capacity of PrP^C to downregulate hippocampal NMDA-Rs (Khosravani *et al*., 2008), we analyzed whether this was true also in our experimental paradigms.

Fig. 22 reports Ca^{2+} fluxes detected by AEQpm (A), AEQcyt (B) and AEQmit (C), after addition of NMDA (50 µM) [and glycine (10 µM)], showing that the presence of PrP^C (grey) strongly diminished the rise of $[Ca^{2+}]_{pm}$ (by 100%) and of $[Ca^{2+}]_{cyt}$ (by 25%) compared to PrP-KO CGN (black). Instead, when monitoring $[Ca^{2+}]_{mit}$, an opposite picture emerged, i.e., PrP-Tg CGN accumulated ~ 20% more Ca^{2+} than PrP-KO neurons. A similar trend of Ca^{2+} fluxes was observed using AMPA as agonist (Fig. 23), in terms of lower and higher Ca^{2+} transients in PM-microdomains and mitochondria, respectively, displayed by PrP-Tg CGN compared to PrP-KO neurons. Likewise, although elicited Ca^{2+} peaks were of much smaller magnitude, these results were replicated using kainate to stimulate the third iGluR type (data not shown).

Two aspects of these results warrant consideration. The first one is the unprecedented observation that (at least in our cell model) the ablation of PrP^C enhances the activity not only of the NMDA-R but also of the other iGluRs. The second aspect of Fig. 22 in need of further consideration is why PrP-KO mitochondria accumulated less Ca^{2+} than PrP-Tg mitochondria, despite the higher external Ca^{2+} entry. To clarify this point, we carried out different types of experiments, reported in the following sections.

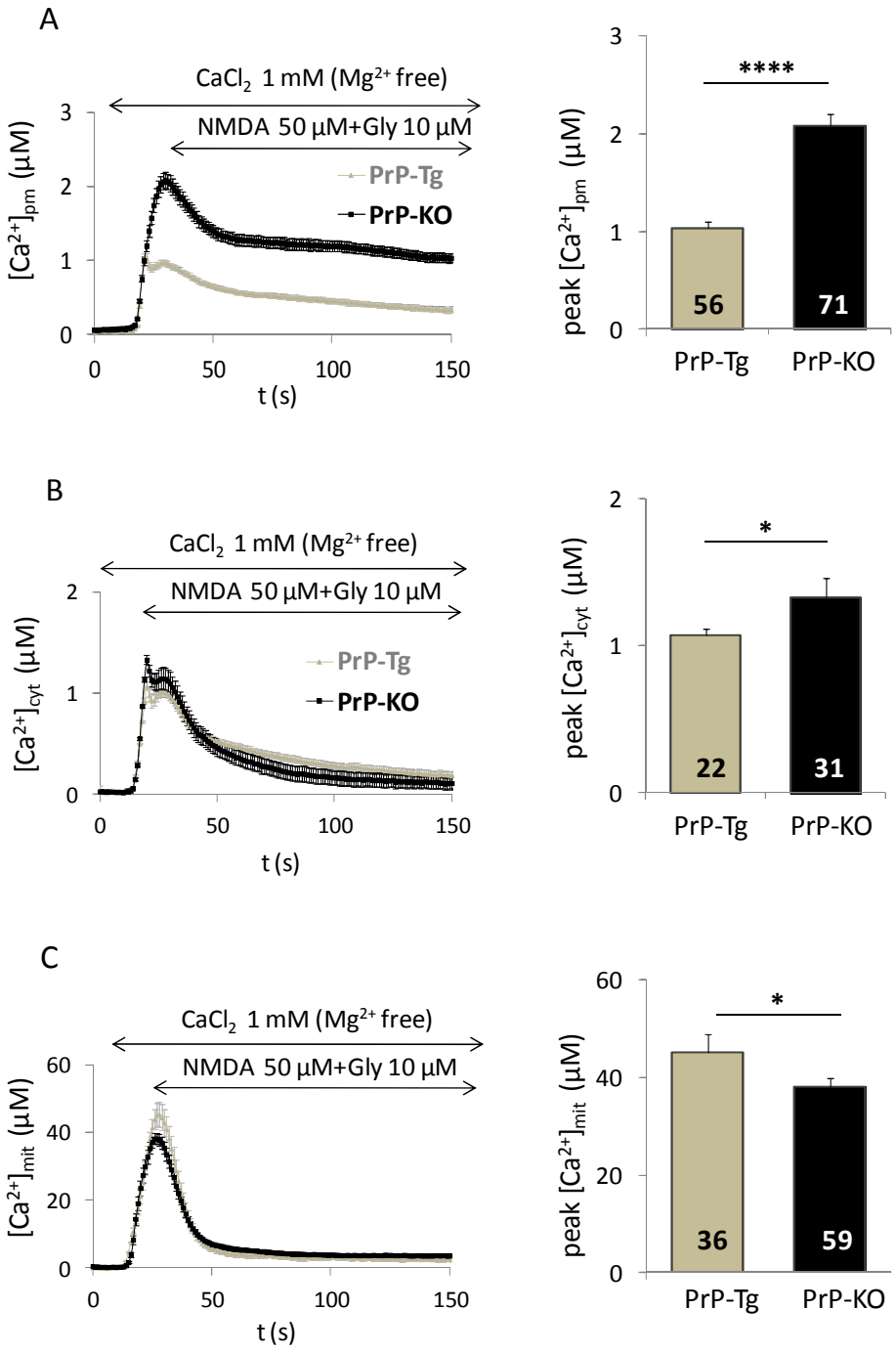

Figure 22. Ca^{2+} transients in CGN domains after stimulation of the NMDA-R. *Both the mean of the recorded traces (left panels), and the bar diagrams reporting the mean peak values of Ca^{2+} transients (right panels), indicate that PrP-KO (black) have higher Ca^{2+} fluxes than control PrP-Tg CGN (grey) near the PM (A) and in the cytosol (B). In the case of mitochondrial Ca^{2+} uptake (C), less Ca^{2+} is accumulated by PrP-KO CGN. Peak values: in PM micro-domains, 1.04 ± 0.07 µM in PrP-Tg CGN; 2.09 ± 0.11 µM in PrP-KO CGN; in the cytosol, 1.07 ± 0.04 µM in PrP-Tg CGN; 1.33 ± 0.01 µM in PrP-KO CGN; in mitochondria, 45.32 ± 3.09 µM in PrP-Tg CGN; 38.23 ± 1.61 µM in PrP-KO CGN. *p<0.05; ****p<10^{-5} Student's t-test.*

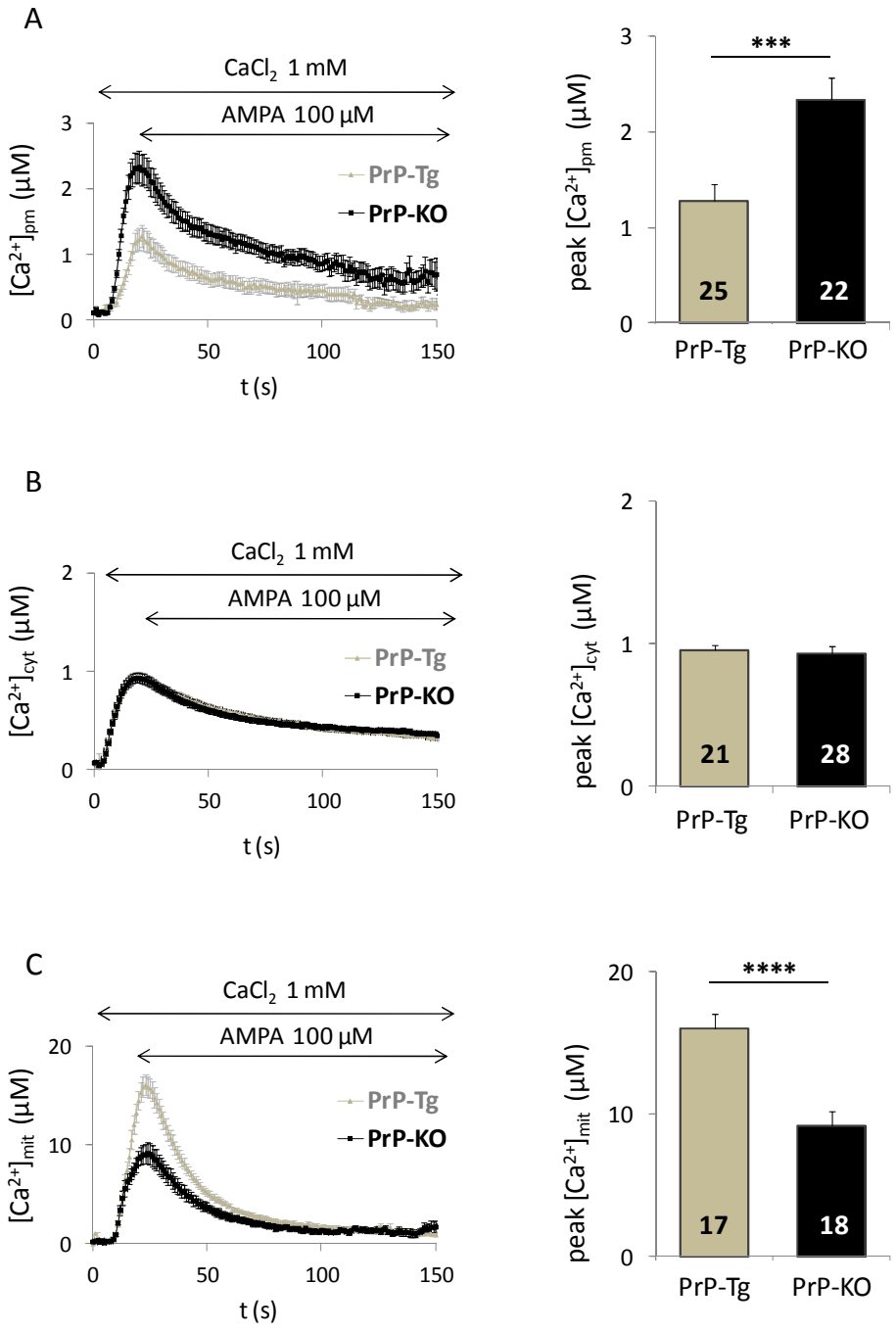

Figure 23. Ca^{2+} transients in CGN domains after stimulation of the AMPA-R. *In the presence of the AMPA agonist founded Ca^{2+} transients indicate that PrP-KO (black) have higher $[Ca^{2+}]_{pm}$, similar $[Ca^{2+}]_{cyt}$ and lower $[Ca^{2+}]_{mit}$ peaks compared to PrP-Tg CGN (grey). Peak values: in PM microdomains, 1.28 ± 0.17 µM in PrP-Tg CGN; 2.33 ± 0.24 µM in PrP-KO CGN; in the cytosol, 0.95 ± 0.24 µM in PrP-Tg CGN; 0.94 ± 0.24 µM in PrP-KO CGN; in mitochondria, 16.04 ± 1.02 µM in PrP-Tg CGN; 9.17 ± 1.04 µM in PrP-KO CGN. ***p<0.001; ****p<10^{-5} Student's t-test.*

6.1.2 *Biochemical, morphological and functional analyses of mitochondria from PrP-Tg and PrP-KO CGN*

First, we analyzed some mitochondrial parameters of the two CGN types, which showed that the number [assayed by WB (Fig. 24), immunofluorescence (Fig. 25), and electron microscopy (Fig. 26)], membrane potential [using the potentiomentric probe, TMRM (Fig. 27)], and expression of the Ca^{2+} uniport [MCU, (Fig. 28)], of mitochondria were independent of the presence of PrP^{C}.

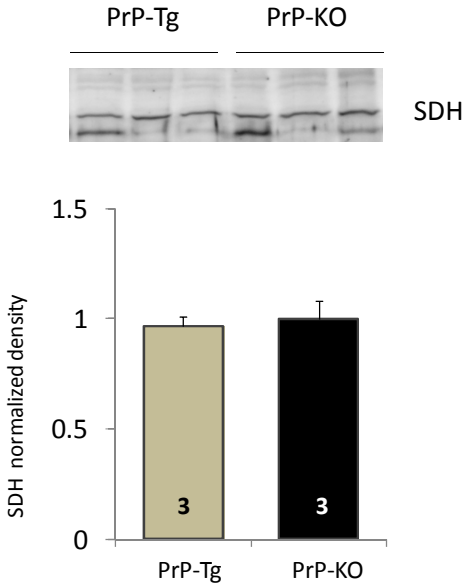

Figure 24. Expression of succinate dehydrogenase in PrP-Tg and PrP-KO CGN. *CGN proteins were analyzed by WB 96h after CGN plating, under basal conditions. The upper panel reports a representative WB of succinate dehydrogenase (SDH) (run in triplicate for each PrP genotypes) of PrP-Tg and PrP-KO CGN. The lower panel reports the densitometric analysis of the anti-SDH immunosignal normalized to that of total proteins stained with Ponceau red.*

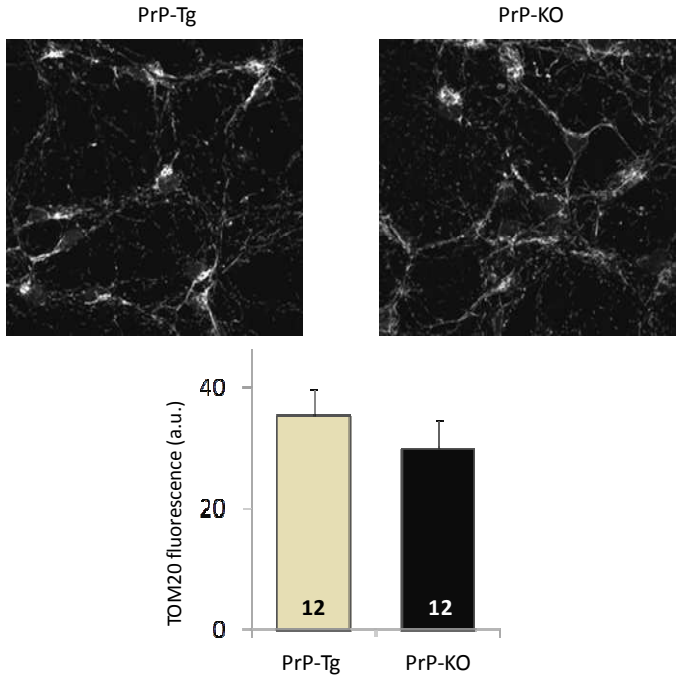

Figure 25. TOM20 fluorescence in PrP-Tg and PrP-KO. *The upper panels report images of TOM20 fluorescence of both CGN genotypes under basal conditions. The lower panel reports the quantification analysis of TOM20 fluorescence normalized to the corresponding selected area.*

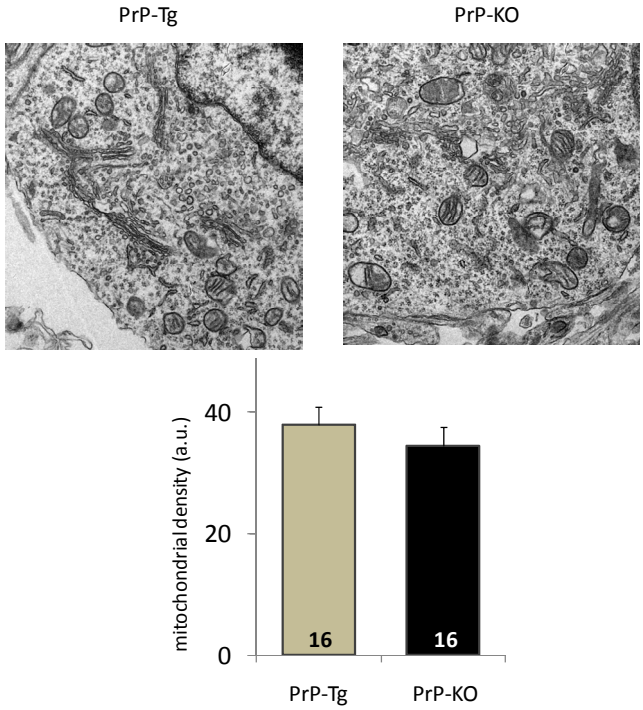

Figure 26. Electron microscopy-based analysis of the number of mitochondria of PrP-Tg and PrP-KO CGN. *Upper panels report electron microscopy images of both CGN genotypes under basal conditions, while lower panel reports the quantification analysis of the number of mitochondria normalized to the corresponding area.*

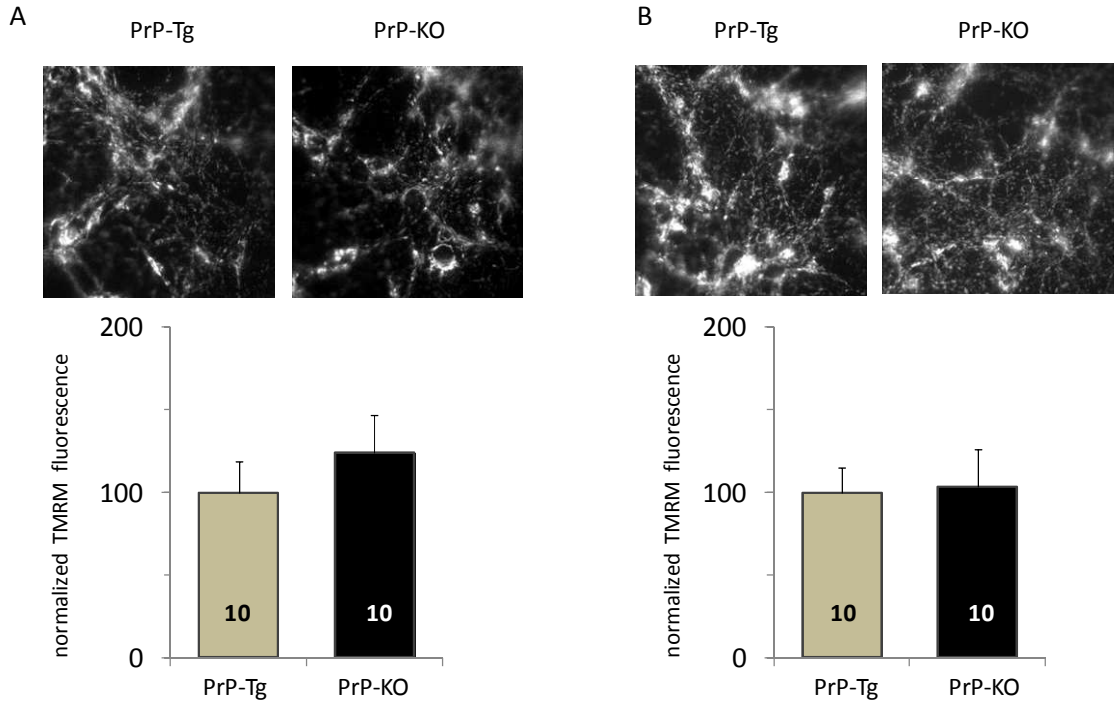

Figure 27. TMRM-based analysis of mitochondrial membrane potential in PrP-Tg and PrP-KO CGN. *Images of TMRM fluorescence of both CGN genotypes under basal conditions, in the presence (A) and in the absence of Mg^{2+} (B) (upper panels), to mimick the conditions in which AMPA-R and NMDA-R are respectively activated during Ca^{2+} measurements. Bar diagrams (low panels), reporting the mean normalized TMRM fluorescence, indicate that PrP-Tg and PrP-KO have the same mitochondrial membrane potential.*

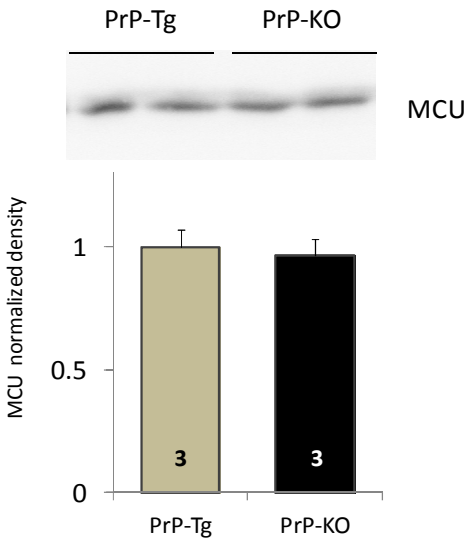

Figure 28. Expression of mitochondrial Ca^{2+} uniporter in PrP-Tg and PrP-KO CGN. *CGN proteins were analyzed by WB 96h after CGN plating, under basal conditions. The upper panel reports a representative WB of mitochondrial Ca^{2+} uniporter (MCU) (run in duplicate for each PrP genotypes) of PrP-Tg and PrP-KO CGN. The lower panel reports the densitometric analysis of the anti-MCU immunosignal normalized to that of total proteins stained with Coomassie blue.*

Instead, using electron microscopy, we observed that the mean distance of mitochondria from the PM was ~ 30% higher in PrP-KO CGN than in control neurons (Fig. 29). Retraction of PrP-KO mitochondria from the PM, the site of Ca^{2+} entry through iGluRs, could thus reasonably explain the results of Fig. 22C and 23C, i.e., that PrP-KO mitochondria were less "sensitive" than PrP-Tg mitochondria to the small Ca^{2+} quantity entering neurons after NMDA or AMPA (or kainate) addition.

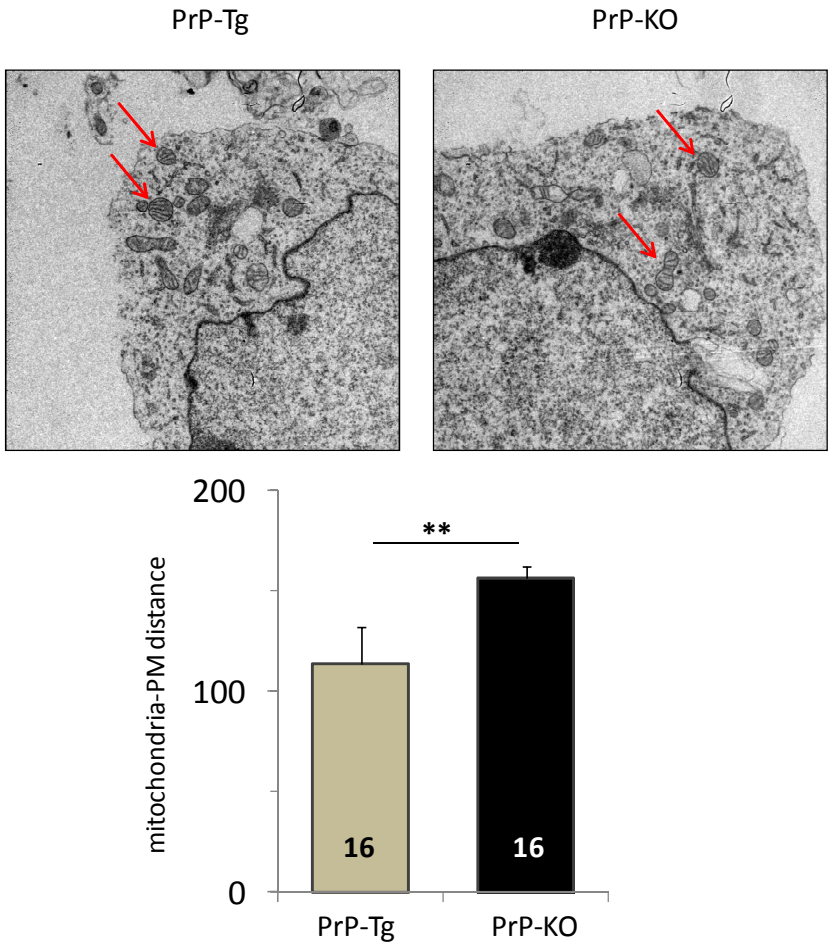

Figure 29. The mean distance of mitochondria from PM is higher in PrP-KO CGN. *Electron microscopy images (upper panel) and the bar diagram, reporting the mean normalized distance of mitochondria from the PM of the two CGN genotypes (lower panel), indicate that mitochondria of PrP-KO CGN (black) are more retracted from the PM than control neurons (grey). **p<0.01 Student's t-test.*

6.1.3 The decrease of Ca^{2+} entry by PrP^C after glutamate reduces CICR

Next, we stimulated CGN with glutamate that, being the physiologic agonist, would simultaneously activate all iGluRs and also mGluRs if present (Prezeau *et al*., 1994). As expected, following exposure to glutamate, PrP-KO CGN had more abundant Ca^{2+} transients (Fig. 30, black) at the PM and in the cytosol compared to control neurons (grey) (by 70% and 20%, respectively) (Figs. 30A and 30B). In both PrP genotypes, the mitochondrial Ca^{2+} uptake was increased with respect to the mere addition of NMDA (or AMPA), but – quite surprisingly – it was higher (by 40%) in PrP-KO CGN than in PrP-Tg neurons (Fig. 30C). The most sensible explanation for these findings entails that, following the stimulation of the IP_3-producing mGluR1 and mGluR5, the close apposition of ER and mitochondrial membranes (Rizzuto *et al*., 1998) allowed mitochondria to take up the Ca^{2+} released by IP_3-sensitive ER channels.

We tested this hypothesis by adding the mGluR1 and mGluR5 agonist, DHPG, which, however, produced only a minor mitochondrial Ca^{2+} uptake (Fig. 31). This result is in line with WB and semi-quantitative RT-PCR approaches showing that in CGN mGluR5 was present in extremely low amounts (data not shown). Conversely, mGluR1 was detected in our model cells, although data of Fig. 31 suggest that it was not fully operative under the employed conditions. Taken together, these findings indicate that the activity of IP_3-producing mGluRs is unlikely to contribute to glutamate-induced Ca^{2+} uptake by CGN mitochondria.

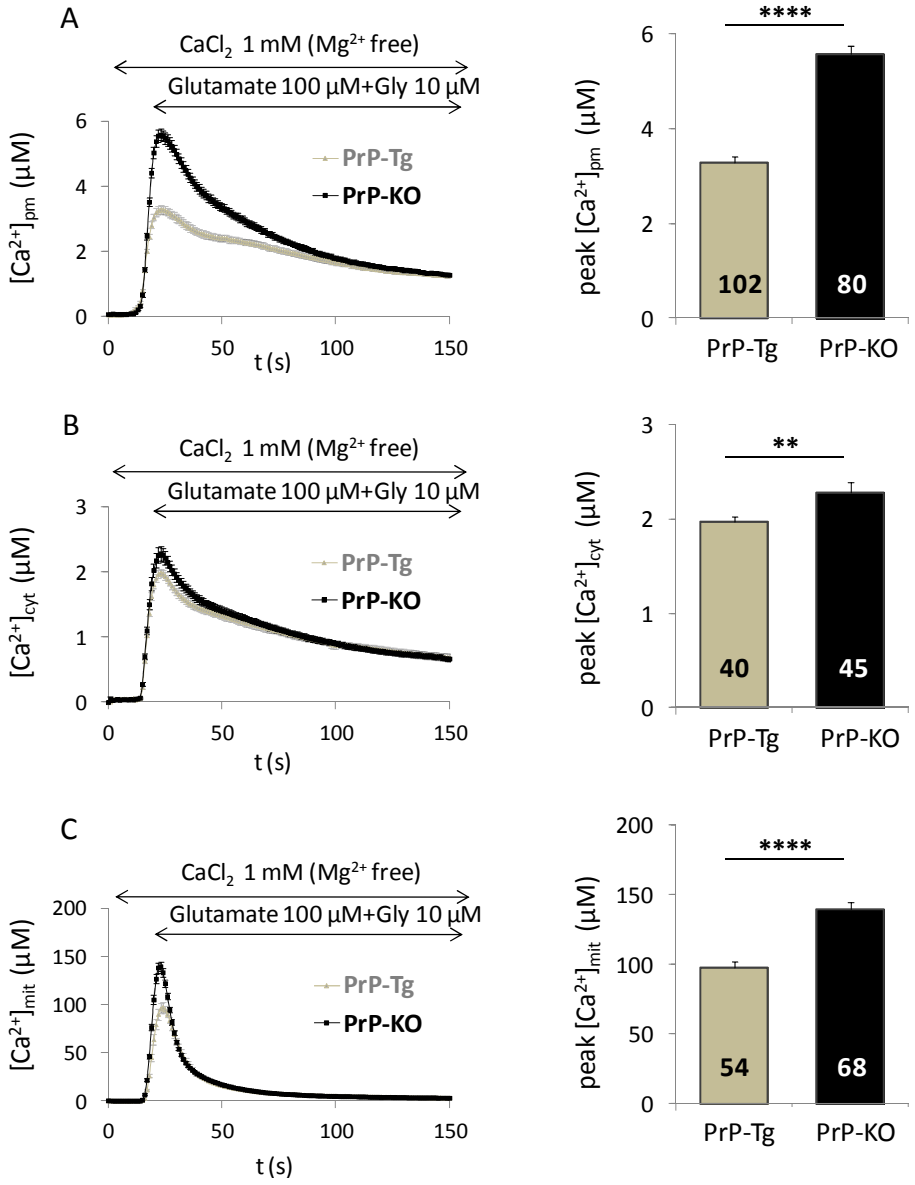

Figure 30. Ca^{2+} transients in CGN domains after glutamate addition. *Both the mean of the recorded traces (left panels), and the bar diagrams reporting the mean peak values of Ca^{2+} transients (right panels), indicate that PrP-KO (black) have higher Ca^{2+} fluxes than control PrP-Tg CGN (grey) near the PM (A), in the cytosol (B), and in the mitochondrial matrix (C). Peak values: in PM micro-domains, 3.29 ± 0.12 µM in PrP-Tg CGN; 5.59 ± 0.18 µM in PrP-KO CGN; in the cytosol, 1.99 ± 0.06 µM in PrP-Tg CGN; 2.28 ± 0.11 µM in PrP-KO CGN; in mitochondria, 97.51 ± 4.88 µM in PrP-Tg CGN; 139.93 ± 4.95 µM in PrP-KO CGN. **p<0.01 ; ****p<10^{-5} Student's t-test.*

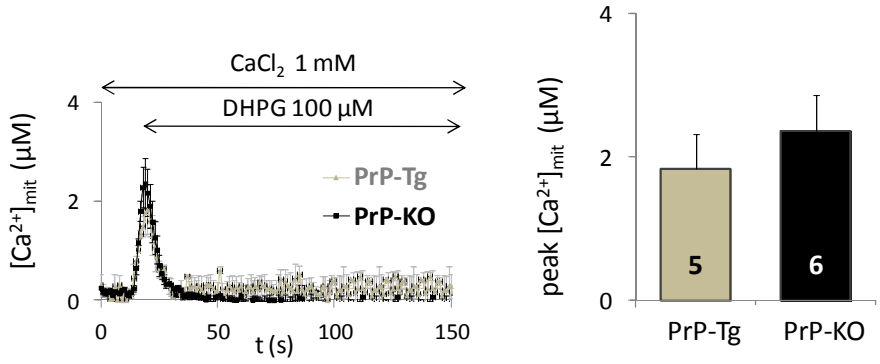

Figure 31. Ca^{2+} transients in mitochondria of CGN after treatment with mGluR1-5 agonist DHPG. *Both the mean of the recorded traces (left panel), and the bar diagram reporting the mean peak values of Ca^{2+} transients (right panel), indicate that DHPG induces only a small and similar response (compared to the values obtained with glutamate) in the two CGN genotypes. Peaks values: 1.83 ± 0.49 µM in PrP-Tg CGN; 2.36 ± 0.51 µM in PrP-KO CGN.*

We finally explored whether the CICR process [mediated by the RyR-channel present in CGN (data not shown)] could have been responsible for (part of) the observed mitochondrial Ca^{2+} accumulation. To this end, glutamate-induced $[Ca^{2+}]_{mit}$ was tested in the presence of a ryanodine concentration (50 µM) known to inhibit RyRs (Sutko *et al*., 1997). Fig. 32 shows that ryanodine produced a drastic reduction of the $[Ca^{2+}]_{mit}$ transient almost solely in PrP-KO CGN.

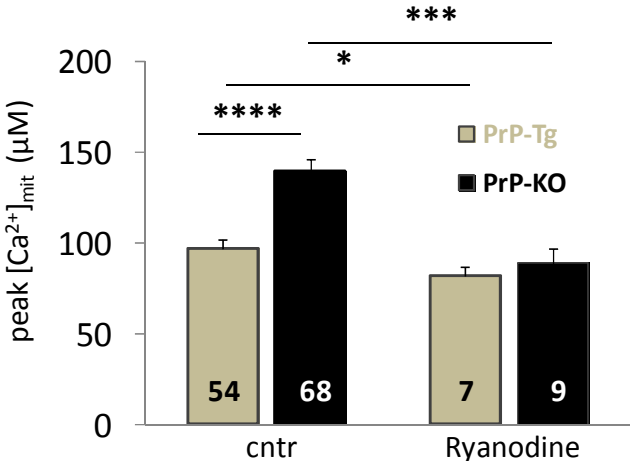

Figure 32. PrP^C indirectly reduces CICR. *CGN were perfused with a Mg^{2+}-free solution containing $CaCl_2$ (1 mM), glutamate (100 µM) [plus glycine (10 µM)], in the absence (cntr) or the presence (Ryanodine) of ryanodine (50µM). From the bar diagram, reporting the mean peak values of $[Ca^{2+}]_{mit}$ transients, it is evident that treatment with ryanodine decreases $[Ca^{2+}]_{mit}$ peak, abrogating the difference observed in untreated PrP-Tg and PrP-KO CGN. Peak values: 97.51 ± 4.88 µM in untreated PrP-Tg CGN; 82 ± 6.75 µM in ryanodine-treated PrP-Tg CGN; 139.93 ± 4.95 µM in untreated PrP-KO CGN; 89.09 ± 7.71 µM in ryanodine-treated PrP-KO CGN. *p<0.05 ***p<0.001 ; ****p<10^{-5} Student's t-test.*

This suggests that glutamate triggers CICR in PrP-KO neurons thanks to the substantial Ca^{2+} amount (~5.5 µM) entering through all iGluRs, and that the quantity of Ca^{2+} entering PrP-Tg CGN under these conditions (~3 µM) [or neurons of both PrP genotypes after stimulation of a single iGluR (~1-2 µM, Figs. 22, 23)] was insufficient to effectively elicit CICR.

The soundness of this conclusion is proved by the simultaneous exposure of CGN to the three iGluR agonists. With this protocol we observed that $[Ca^{2+}]_{pm}$ transients were comparable to those elicited by glutamate (Fig. 33A), and thus capable to trigger a higher mitochondrial Ca^{2+} uptake in PrP-KO than in PrP-Tg CGN (Fig. 33B).

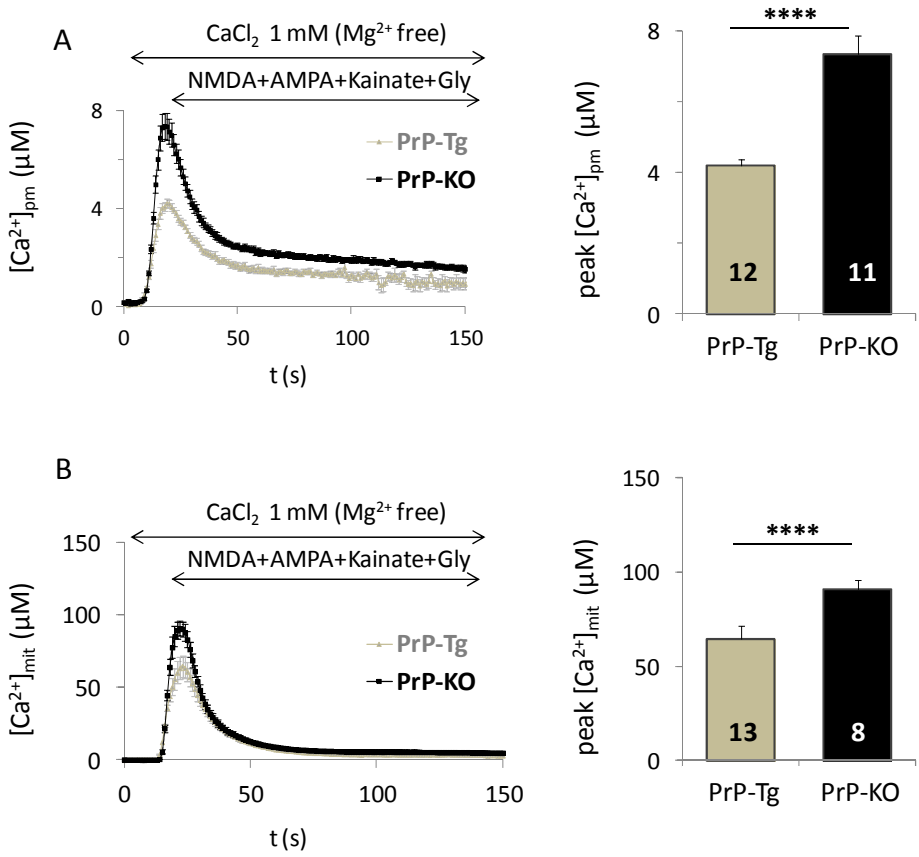

Figure 33. Ca^{2+} transients in CGN domains after stimulation of all iGluRs. *Both the mean of the recorded traces (left panels), and the bar diagrams reporting the mean peak values of Ca^{2+} transients (right panels), indicate that PrP-KO (black) have higher $[Ca^{2+}]_{pm}$ and $[Ca^{2+}]_{mit}$ peaks compared to PrP-Tg CGN (grey) after addition of NMDA (50 µM) [plus glicyne (10 µM)], AMPA (100 µM), kainate (30 µM). Peak values: in PM microdomains, 4.21 ± 0.18 µM in PrP-Tg CGN; 7.36 ± 0.53 µM in PrP-KO CGN; in mitochondria, 64.63 ± 6.82 µM in PrP-Tg CGN; 90.77 ± 5.13 µM in PrP-KO CGN. ****$p<10^{-5}$ Student's t-test.*

6.1.4 *Aβ$_{1-42}$ oligomers impair mitochondrial Ca^{2+} uptake in CGN treated with NMDA or glutamate in a PrP^{C}-dependent way*

When CGN were exposed to soluble Aβ$_{1-42}$ oligomers, the stimulation with glutamate (or NMDA) resulted in a significant decrease of $[Ca^{2+}]_{mit}$ in PrP-Tg CGN, but not in PrP-KO neurons (Figs. 34 and 35). However, differently from what observed in the case of SOCE, no alteration was found in sub-PM or cytosolic Ca^{2+} transients compared to untreated neurons, irrespective of the PrP genotype (data not shown).

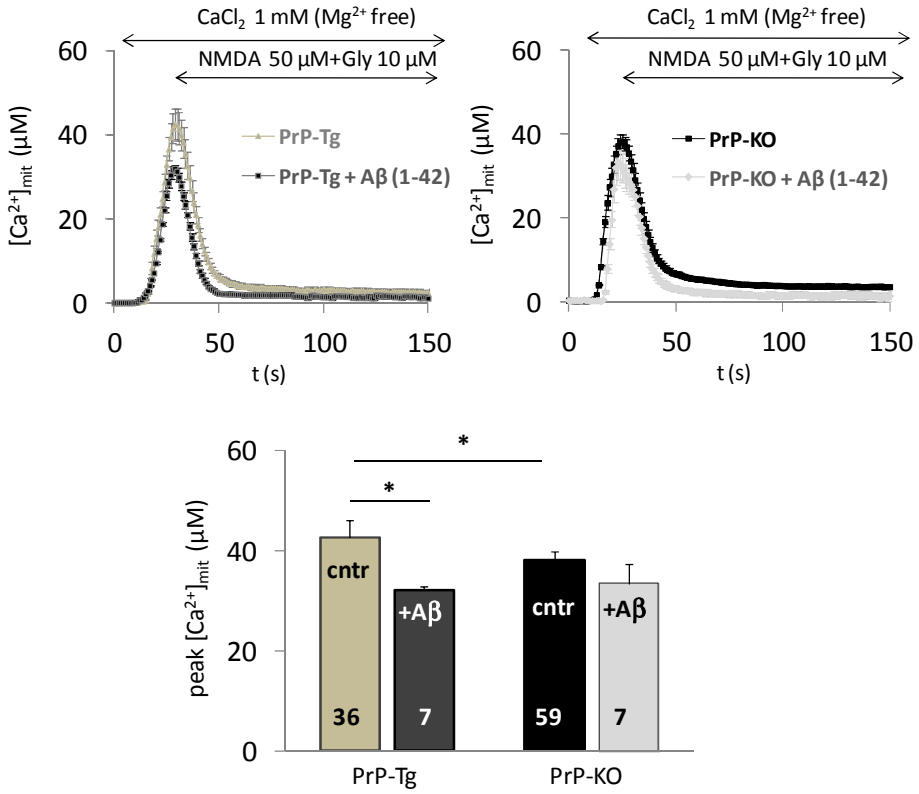

Figure 34. Aβ$_{1-42}$ oligomers alter mitochondrial Ca^{2+} accumulation after NMDA-R stimulation, in a PrP^{C}-dependent way. *CGN were perfused with a Mg^{2+}-free solution containing $CaCl_2$ (1 mM), NMDA (50 µM) [plus glycine (10 µM)] in in the absence (cntr) or in the presence (+Aβ) of soluble Aβ$_{1-42}$ oligomers (5 µM). Both the mean of the recorded traces (upper panels) and the bar diagrams (lower panel), reporting the mean $[Ca^{2+}]_{mit}$ peak values, indicate that treatment with soluble Aβ$_{1-42}$ oligomers reduces $[Ca^{2+}]_{mit}$ peak values only in PrP-Tg CGN. Peak values: 38.23 ± 1.61 µM in untreated PrP-KO CGN; 33.46 ± 4.01 in Aβ$_{1-42}$-treated PrP-KO CGN; 45.32 ± 3.09 µM in untreated PrP-Tg CGN; 32.03 ± 0.95 in Aβ$_{1-42}$ -treated PrP-Tg CGN). *p<0.05 Student's t-test.*

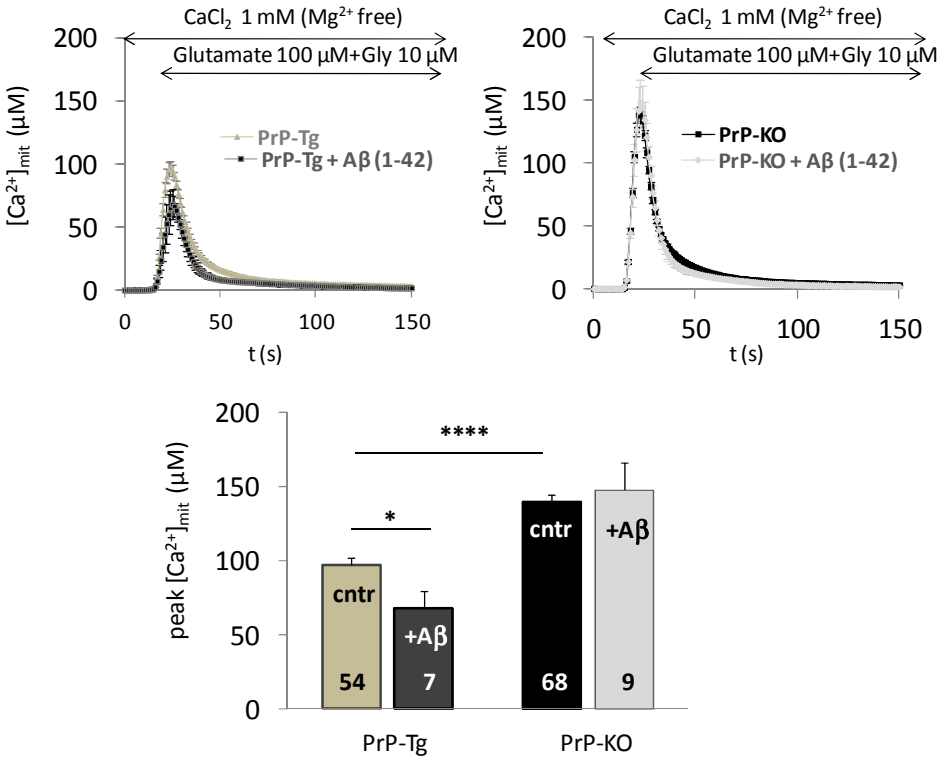

Figure 35. Aβ$_{1-42}$ oligomers alter mitochondrial Ca^{2+} accumulation after glutamate addition, in a PrP^C-dependent way. *CGN were perfused with a Mg^{2+}-free solution containing $CaCl_2$ (1 mM), glutamate (100 µM) and glycine (10 µM), in the absence (cntr) or in the presence (+Aβ) of soluble Aβ$_{1-42}$ oligomers (5 µM). Both the mean of the recorded traces (upper panels) and the bar diagrams (lower panel), reporting the mean $[Ca^{2+}]_{mit}$. Peak values: 97.51 ± 4.88 µM in untreated PrP-Tg CGN; 65.32 ± 13.90 in Aβ$_{1-42}$ -treated PrP-Tg CGN; 139.92 ± 4.96 µM in untreated PrP-KO CGN; 147.90 ± 18.41 in Aβ$_{1-42}$-treated PrP-KO CGN. *p<0.05;****p<10^{-5} Student's t-test.*

These results indicate that Aβ$_{1-42}$ oligomers influence mitochondrial Ca^{2+} uptake following iGluRs stimulation in a PrP^C-dependent way, but the mechanism of this action clearly differs from that proposed to explain the Aβ$_{1-42}$ effect on SOCE (i.e., a Fyn-dependent increase of Ca^{2+} entry from the extra-cellular space), and needs further investigation.

7 CONCLUSIONS –PART 2

The results of this second part of the thesis allow us to conclude that PrP^C is intimately involved in limiting the Ca^{2+} quantity entering into neurons, because it is capable to downregulate the activity of all three iGluRs in addition to SOCE. By controlling many transmembrane routes of Ca^{2+} entry, this aspect adds further importance to PrP^C as safeguard protein against neuronal excitability, which is further supported by the finding that PrP^C can also restrict mitochondrial Ca^{2+} uptake by indirectly controlling CICR through the limitation of iGluR-mediated Ca^{2+} entry.

Equally interesting is the finding that mitochondria of PrP-KO CGN are retracted from the PM, implying that PrP^C could be implicated in the control of mitochondrial movements. This may have important consequences for neurons and deserves further investigation, since an impaired trafficking of mitochondria could be prodromal to neuronal dysfunctions and, possibly, to neurodegenerative processes.

We found that soluble $A\beta_{1\text{-}42}$ was affecting Ca^{2+} fluxes also when CGN were stimulated by glutamate (or iGluRs agonist), and that this effect was dependent on the presence of PrP^C. This observation reinforces the notion that Aβ oligomers convey their neurotoxic message by binding to PrP^C and suggest that this may occur through the (PrP^C-dependent) alteration of neuronal Ca^{2+} handling. The mechanistic details of such an $A\beta_{1\text{-}42}$-PrP^C-glutamate triangle, however, remain to be elucidated.

8 GENERAL DISCUSSION AND FUTURE PERSPECTIVES

The work presented in this Ph.D. thesis has provided novel findings that further support the neuroprotective role of PrP^C against dangerous Ca^{2+} overload. This conclusion was achieved by combining the use of primary isogenic CGN expressing, or not, PrP^C, with Ca^{2+} probes allowing detection of compartmentalized Ca^{2+} oscillations, and with a few biochemical and morphological investigations.

The most important phenomenological result of the study refers to the capacity of PrP^C to reduce Ca^{2+} entry into neurons through different types of Ca^{2+} channels (SOCC and iGluRs), and – consequently – the accumulation of Ca^{2+} by mitochondria. This data highlights the ample spectrum of pathways governed (directly or indirectly) by PrP^C to protecting neurons against uncontrolled Ca^{2+} signals that may undermine neuronal functions and plasticity, and promote neuronal death, particularly in neurodegenerative disorders.

Mechanistically, we were able to correlate the PrP-dependent downregulation of SOCE to the control of Fyn activation. Fyn, a member of the SFK family, has long been suspected to act as downstream effector of PrP^C in regulating key processes, ranging from embryogenesis and neuritogenesis, to, at large, neuroprotective signaling (Mouillet-Richard *et al*., 2000; Graner *et al*., 2000; Chiarini *et al*., 2002;). To note, however, that, contrary to these past observations, for the first time to our knowledge we have provided evidence that PrP^C downregulates Fyn under basal conditions, highlighting in this way that the control of Fyn is part of the physiological function of PrP^C. In light of the renowned implication of Fyn in regulating NMDA-R activity (Khor and Sepurg, 1996; Tezuka *et al*., 1999; Xu *et al*., 2006), it is fair to speculate that Fyn could also be the intermediate between PrP^C and NMDA-Rs. Some preliminary data of the effect of SFK inhibitors on NMDA-mediated Ca^{2+} entry are in favour of this possibility although more detailed experiments are needed to establish the underlying mechanism. This will include immunocytochemistry and/or biochemical tools aiming at clarifying whether the NR2B subunit of the receptor is the one phosphorylated by Fyn in a PrP^C-dependent way – as already shown in the presence of Abeta oligomers (Um *et al*., 2012) – and if the degree of Fyn activation is correlatable with the residency of the NMDA-R at the PM under our experimental conditions.

As to the influence of PrP^C on mitochondrial Ca^{2+} uptake, data obtained with glutamate, or by stimulating specific iGluRs, have disclosed that it is accomplished by at least two ways, i.e., the attenuation of Ca^{2+} entry from the extracellular matrix, and the control of CICR. The two processes are known to be closely interconnected, in that

CICR can amplify PM Ca^{2+} signal, but the novel aspect provided by this work is that PrP^C is apparently at the top of the entire mechanism and that, by firstly limiting extracellular Ca^{2+} entry, it ultimately finely controls the quantity of Ca^{2+} taken up by mitochondria. This is extremely important for the cell life, since mitochondrial Ca^{2+} overload may initiate apoptosis. Mitochondria accumulate a substantial Ca^{2+} quantity also after SOCE. Under these conditions, however, ER Ca^{2+} stores are empty and mitochondria would then take up Ca^{2+} only from the cytosol. The higher amount detected in PrP-KO mitochondria could be explained not only by the larger Ca^{2+} influx through SOCC but also by the lower quantities of SERCA (and PMCA) pumps in these neurons (Lazzari *et al*., 2011), both of which increase $[Ca^{2+}]_{cyt}$.

However, to fully understand the control of PrP^C over mitochondrial Ca^{2+} accumulation, one needs to consider another unexpected result emerged from camparing control and PrP-KO CGN by electron microscopy of, i.e., that PrP^C "keeps in place" mitochondria close to the PM. Although previous studies have correlated PrP^C to different aspects of mitochondrial physiology (Miele *et al*., 2002, Paterson *et al*., 2007), none of them has tackled the issue of if and how PrP^C impinges on mitochondrial distribution. Our finding suggests that the physiological function of PrP^C includes the correct trafficking of mitochondria, although also in this case further investigations are needed to analyze in detail the underlying mechanism.

In conclusion, our results indicate that PrP^C is constitutively implicated in crucial physiological aspects, such as Fyn activation and Ca^{2+} homeostasis, opening the possibility that their PrP^C-mediated dysregulation impact profoundly into the life of neurons. This is likely to occur in prion disorders, in which functional PrP^C is continuously recruited into prions, but may be particularly relevant also for those disease-related species, like Aβ oligomers, which exploit PrP^C as surface binding partner for the downstream transduction of their toxicity. In AD, both Ca^{2+} dyshomeostasis (Green and LaFerla, 2008), and aberrant Fyn signaling (Lambert *et al*., 1998) were proposed to mediate the deleterious effects of oligomeric Aβ. Accordingly, it was shown that Fyn is activated after Aβ docking to PrP^C in hippocampal neurons, and that in these cells it forms super-molecular complexes with PrP^C (Larson *et al*., 2012; Um *et al*., 2012) by the intervention of mGluR5 in connecting Fyn and PrP^C on the opposite sides of the PM (Um *et al*., 2013). Clearly, the undetectable expression of mGluR5 in CGN suggests that in these neurons a different mechanism is involved.

We also provided further evidence that PrP^C may act as receptor for soluble $A\beta_{1\text{-}42}$ oligomers, since the treatment of PrP-Tg CGN with these peptide disrupt the PrP^C-Fyn-SOCE triangle, and more in general, the PrP^C-dependent control of Ca^{2+}

homeostasis. Considering the influence of PrP^C on Fyn, our findings partly resemble Fyn activation by PrP^C cross-linking (Mouillet-Richard *et al.*, 2000) or PrP^C-NCAM clustering (Santuccione *et al.*, 2005), but disclose a different underlying mechanism, whereby the interaction of PrP^C with extracellular ligands releases the basal attenuation by PrP^C of Fyn rather than the ligand-PrP^C complex directly promoting Fyn activation. Accordingly, one initial step of oligomeric $A\beta_{1-42}$ toxicity could involve PrP^C displacement from the role of sentinel against neuronal Ca^{2+} overloads. Additional studies are needed to clarify whether this effect is consequent to a structural modification of PrP^C, or a dislodgment from natural proteinaceous partners, or a modification of the membrane lipid architecture surrounding the protein.

Whichever the reason, a documented consequence of oligomeric $A\beta_{1-42}$ in CGN is increased SOCE, altered mitochondrial Ca^{2+} uptake upon SOCE or after stimulation with glutamate or NMDA, unrestricted Fyn activity, and higher amounts of p-Tyr proteins. However, because PrP-KO mice show no gross phenotype, nor overt signs of neurodegeneration, the alterations reported in this work cannot be sufficient to account for AD pathology. Nonetheless, they could act as necessary events that, combined with other PrP^C-dependent and/or PrP^C-independent insults, could eventually contribute to AD-related neuronal damage.

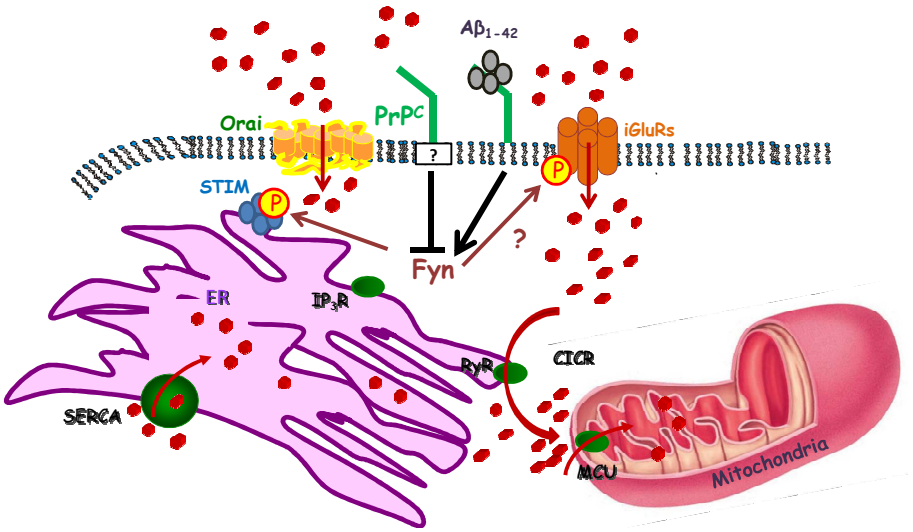

Figure 36. A possible mechanism by which PrP^C controls Ca^{2+} homeostasis in CGN. *The prime action of PrP^C is the downregulation of Fyn activity through a putative ligand. The consequent lower phosphorylation of STIM (bleu circles) (which in turn affects Orai), and probably of iGluRs, reduces Ca^{2+} entry (red circles) and the Ca^{2+} accumulation by mitochondria directly (in the case of SOCE) and through CICR (in the case of iGluRs). $A\beta_{1-42}$ (grey circles), by binding PrP^C, abrogates the control exerted by PrP^C on Fyn, which phosphorylates and activates SOCC, leading to an increased Ca^{2+} entry into the cell. Possibly this mechanism could be true also for iGluRs but needs to be confirmed by other experiments.*

9 REFERENCES

Aguzzi A, Baumann F, Bremer J. The prion's elusive reason for being. Annu Rev Neurosci. 2008; 31: 439-77.

Aguzzi A, Heikenwalder M. Pathogenesis of prion diseases: current status and future outlook. Nat Rev Microbiol. 2006; 4: 765-75.

Anandatheerthavarada HK, Biswas G, Robin MA, Avadhani NG. Mitochondrial trageting and a novel transmembrane arrest of Alzheimer's amyloid precursor protein impairs mitochondrial function in neuronal cells. J Biol Chem. 2003; 161: 41-54.

Avdulov NA, Chochina SV, Igbavboa U, Warden CS, Vassieliev AV, Wood WG. Lipid binding to amyloid beta peptide aggregates: preferential binding of cholesterol as compared with phosphatysilcholine and fatty acids. J Neurochem. 1997; 69: 1746-52.

Balducci C, Beeg M, Stravalaci M, Bastone A, Sclip A, Biasini E, Tapella L, Colombo L, Manzoni C, Borsello T, Chiesa R, Gobbi M, Salmona M, Forloni G. Syntethic amyloid-beta oligomers impair long-term memory independently of cellular prion protein Proc. Nat. Acad. Sci. 2010; 2295-3000.

Berridge MJ. Neuronal calcium signaling. Neuron. 1998; 21: 13-26.

Berridge MJ, Lipp P & Bootman MD. The versatility and universality of calcium signalling. Nat Rev Mol Cell Biol. 2000; 1: 11-21.

Berridge MJ, Bootman MD & Roderick HL. Calcium signalling: dynamics, homeostasis and remodelling. Nat Rev Mol Cell Biol. 2003; 4: 517-29.

Berridge MJ. Calcium regulation of neuronal rhythms, memory and Alzheimer's disease. Journ Physiol. 2014; 592: 281-93.

Borchelt DR, Koliatsos VE, Pardo CA, Price DL. Rapid anterograde axonal transport of the cellular prion glycoprotein in the peripheral and central nervous system. J Biol Chem. 1994; 269: 14711-14.

Brini M, Marsault R, Bastianutto C, Alvarez J, Pozzan T, Rizzuto R. Transfected Aequorin in the Measurement of Cytosolic Ca^{2+} Concentration ($[Ca^{2+}]_c$). J Biol Chem. 1995; 270: 9896-903.

Brown DR, Qin K, Herms JW, Madlung A, Manson J, Strome R, Fraser PE, Kruck T, von Bohlen A, Schulz-Schaeffer W, Giese A, Westaway D, Kretzschmar H. The cellular prion protein binds copper in vivo. Nature. 1997; 390: 684-87.

Brown DR, Besinger A. Prion protein expression and superoxide dismutase activity. Biochem J. 1998; 334:423-429.

Brown DR, Nicholas RS, Canevari L. Lack of prion protein expression results in a neuronal phenotype sensitive to stress. J Neurosci Res. 2002; 67: 211–224.

Bruce ME and Fraser H. Scrapie strain variation and its implications. Curr Top Microbiol. Immunol. 1991; 172:125-38.

Butterfield DA, Drake J, Pocernich C, Castegna A. Evidence of oxidative damage in Alzheimer's disease brain: central role for amyloid β-peptide. Cell. 2001; 7:548-54.

Cahalan MD. How to STMulate calcium channels. Science. 2003; 330: 43-44.

Calella AM, Farinelli M, Nuvolone M, Mirante O, Moos R, falsig J, Mansuy IM, Aguzzi A. Prion protein and Abeta-releted synaptic toxicity impairment. EMBO Mol Med. 2010; 2: 306-14.

Candy SC, Brickley S, Farrant M. NMDA receptor subunits: diversity, development and disease. Curr Opin Neurobiol. 2001; 3: 327-35.

Casley CS, Lakics V, Lee HG, Broad LM, Day TA, Cluett T, Smith MA, O'Neill MJ, Kingston AE. Up-regulation of astrocyte metabotropic glutamate receptor 5 by amyloid β peptide. Brain Res. 2009; 1260: 65–67.

Catterall WA, reyes P, Snutch TP, Striessning J. Nomenclature and structure-function reletionships of voltage-gated Ca^{2+} channels. Pharmacol Rev. 2005; 57: 411-25.

Caughey B, Brown K, Raymond GJ, Katzenstein GE, Thresher W. Binding of the protease-sensitive form of PrP (prion protein) to sulfated glycosaminoglycan and congo red. J Virol. 1994; 68: 2135-2141.

Caughey B, Kocisko DA, Raymond JG, Lansbury PT. Aggregates of scrapie-associated prion protein iduce the cell-free conversion of protease-sensitive prion protein to the protease-resistant state. Chem Biol. 1995; 2: 807-17.

Chen S, Mangé A, Dong L, Lehmann S, Schachner M. Prion protein as trans-interacting partner for neurons is involved in neurite outgrowth and neuronal survival. Mol Cell Neurosci. 2003; 22: 227-33.

Chen S, Yadav SP, Surewicz WK. Interaction between human prion protein and amyloid beta (Abeta) oligomers: role of N-terminal residues. J Biol Chem. 2010; 285: 26377-83.

Chesebro B, Trifilo M, Race R, White KM, Teng C, LaCasse R, Raynond L, Favara C, Priola S, Caughey B, Masliah E, Oldstone M. Anchorless prion protein results in infectious amyloid disease without clinical scrapie. Science. 2005; 308: 1435-39.

Chiarini LB, freitas ARO, Zanata MS, Brentani RR, Martins VR, Linden R. Cellular prion protein transduces neuroprotective signals. EMBO Jour. 2002; 21: 3213-67.

Chrétien F, Dorandeu A, Adle-Biassette H, Ereau T, Wingertsmann L, Brion F, Gray F. A process of programmed cell death as a mechanisms of neuronal death in prion diseases. Clin Exp Pathol. 1999; 47: 181-191.

Chung E, Ji Y, Sun Y, Kascsak RJ, Kascsak RB, Mentha PD, Strittmatter SM, Wisniewski T. Anti PrPC monoclonal antibody infusion as a novel treatment for cognitive deficits in an Alzheimer's disease model mouse. BMC Neurosci. 2010; 11: 1-11.

Collinge J, Whittington MA, Sidle KC, Smith CJ, Palmer MS, Clarke AR, Jefferys JG. Prion protein is necessary for normal synaptic function. Nature 1994; 370: 295-97.

Collins MO, Hushi H, Brandom JM, Andreson CN, Blackstock WP, Choudhary JS, Grant SG. Molecular characterization and comparison of the components and multiprotein complexes in the postsynaptic proteome. J Neurochem. 20006; 1: 16-23.

Connor JA, Tseng H, Hockberger PE. Depolarization and transmitter-induced changes in intracellular Ca^{2+} of rat cerebellar granule cells in explants cultures. J Neuiorsci. 1987; 7: 1384-1400.

Cull-Candy SG and Lezskiewicz DN. Role of distinct NMDA receptor subtypes at central synapses. Sci STKE. 2004; 255: re16.

Curtis DR. Phillis JW, Watkins JC. The chemical excitation of spinal neurons by certain acidic amino acids. J Physiol. 1960; 150: 656-82.

Decout A, Labeur C, Goethals M, Brasseur R, Vandekerckhove J, Rosseneu M. Enhanced efficiency of a target fusogenic peptide. Biochim. Biophys. Acta. 1998; 1372: 102–116.

Devi L, Prabhu BM, Galati FD, Avadhani NG, Anandatheerthavarada HK. Accumulation of amyloid precursor protein in the mitochondrial import channels of human Alzheimer's disease brain is associated with mitochondrial dysfunction. J Neurosci. 2006; 26: 9057-68.

Dingledine R, Borges K, Bowie D, Traynelis SF. The glutamate receptor ion channels. Pharmacol rev. 1999; 51:7-61.

Dorandeu A, Wingertsmann L, Chrétien F, Delisle MB, Vital C, Parchi P, Montagna P, Lugaresi E, Ironside JW, Budka H, Gambetti P, Gray F. Neuronal apoptosis in fatal familial insomnia. Brain Pathol. 1998; 8: 531-37.

Duchen MR. Mitochondria and calcium: from cell signaling to cell death. J. of Physiol. 2000; 529: 57-68.

Dziadek MA, Johnstone LS. Biochemical properties and cellular localization of STIM proteins. Cell calcium. 2007; 42: 123-32.

Eckert A, Schindowski K, Leutner S, Luckhaus C, Touchet N, Czech C & Muller WE. Alzheimer's disease-like alterations in peripheral cells from presenilin-1 transgenic mice. Neurobiol Dis. 2001; 8, 331-42.

Edbauer D, Winkler E, Regula JT, Pesold B, Steiner H & Haass C. Reconstitution of gamma-secretase activity. Nat Cell Biol. 2003; 5: 486-88.

Eigen M. Prionics or the kinetic basis of prion diseases. Biophysical Chem. 1996; 63: 1-18.

El-Agnaf OMA, MAhil DSM, Patel BP, Austen MB. Oligomerization and toxicity of β-amyloid-42 imlicated in Alzheimer's disease. Biochem and Biophysic Res Comm. 2000; 3: 1003-7.

Ferraguti F, Shigemoto R. Metabotropic glutamate receptors. Cell Tissue Res. 2006; 326: 483-504.

Follenzi A, Naldini L. HIV-based vectors. Met in Mol Med. 2002; 69: 259-74.

Forloni G, Angeretti N, Chiesa R, Monzani E, Salmona M, Bugiani O, Tagliavini F. Neurotoxicity of a prion protein fragment. Nature. 1993; 362: 543-6.

Gauczynski S, Peyrin JM, Haïk S, Leucht C, Hundt C, Rieger R, Krasemann S, Deslys JP, Dormont D, Lasmézas CI, Weiss S. The 37-kDa/67-kDa laminin receptor acts as the cell-surface receptor for the cellular prion protein. EMBO J. 2001; 20: 5863-5875.

Gimbel DA, Nygaard HB, Coffey EE, Gunther EC, Lauren J, Gimbel Z, Strittmatter SM. Memory impairment in transgenic Alzheimer mice requires prion protein. J Neurosci. 2010; 30: 6367-74.

Graner E, Mercadante A, Zanata SM, Forlenza OV, Cabral ALB, Velga SS, Juliano MA, Roesler R, Walz R, Minetti A, Izquierdo I, Martins VR, Brentani RR. Cellular prion protein binds laminin and mediates neuritogenesis. Mol Brain Res. 2000; 76: 85-92.

Green KN, LaFerla FM. Linking calcium to Abeta and Alzheimer's disease. Neuron. 2008; 59:190-94.

Griffith JS. Self-replication and scrapie. Nature. 1967; 215(105):1043-4.

Guisado EP, Campbell DG, Deak M, Barrientos AA, Morrice N, Alvarez I, Alessi DR, Romero FJM. Phosphorylation of STIM1 at ERK1/2 target sites modulates store-operated calcium entry. J Cell Sci. 2010; 123: 3084-93.

Gwack Y, Srikhant S, Cruz-Guilloty F, Oh-hora M, Hogan PG, Rao A. Biochemical and functional characterization of Orai proteins. J Biol Chem. 2007; 282: 16232-43.

Hansen SM, Berezin V, Bock E. Signaling mechanisms of neurite outgrowth induced by the cell adhesion molecules NCAM and N-cadherin. Cell Mol Life Sci. 2008; 65: 3809-3821.

Haraguchi T, Fisher S, Olofsson S, Endo T, Groth D, Tarentino A, Borchelt DR, Teplow D, Hood L, Burlingame A, Lycke E, Kobata A, Prusiner SB. Asparagine-linked glycosylation of the scrapie and cellular prion proteins. Arch Biochem . 1989; 274: 1–13.

Hayashi T. Effects of sodium glutamate on the nervous system. K Journ of med. 1954; 4: 183-92.

Herms JW, Korte S, Gall S, Schneider I, Dunker, Kretzschmar HA. Altered intracellular calcium homeostasis in cerebellar granule cells of prion protein-deficient mice. J Neurochem. 2000; 75: 1487-92.

Hundt C, Peyrin JM, Haïk S, Gauczynski S, Leucht C, Rieger R, Riley ML, Deslys JP, Dormont D, Lasmézas CI, Weiss S. Identification of interaction domains of the prion protein with its 37-kDa/67-kDa laminin receptor. EMBO J. 2001; 20: 5876-86.

Inoue S. In situ Abeta pores in AD brain are cylindrical assembly of Abeta protofilaments. Amyloid. 2008; 15: 223-33.

Jeffrey M, Halliday WG, Bell J, Johnston AR, Macleod NK, Ingham C, sayers AR, Brown DA, fraser JR. Synapse loss associated with abnormal PrP precedes neuronal degeneration in the scrapie-infected murine hippocampus. Neuropathol Appl Neurobiol. 2000; 26: 41-54.

Johnson, Ascher. Voltage dependent block by intracellular Mg^{2+} of N-methyl-D-aspartate-activated channels. Biophys J. 1990; 57: 1085-90.

Kahachaturian. The role of calcium regulation in brain aging: reexamination of a hypothesis. Ag Clin and Exp Res. 1989; 1: 17-34.

Kanaani J, Prusiner SB, Diacovo J, Baekkeskov S, Legname G. Recombinant prion protein induces rapid polarization and development of synapses in embryonic rat hippocampal neurons in vitro. J Neurochem. 2005; 95: 1373-86.

Kendall JM, Newby GS, Ghalaut V, Dormer RL, Cambell AK. Engineering the Ca2+ activated photoprotein aequorin with reduced affinity for calcium. Biochem and Biophys Res Comm. 1992; 2: 1091-97.

Kessels HW, Nguyen LN, Nabavi S, Malinow R. The prion protein is a receptor for amyloid-beta. Nature. 2010; 466: 1-2.

Khor G, Sepurg PH. Subtype-specific regulation of recombinant NMDA receptor-channels by protein tyrosine kinases of the src family. J Physiol. 1996; 492: 445-52.

Khosravani H, Zhang Y, Tsutsui S, Hameed S, Altier C, Hamid J, Chen L, Villemaire M,Ali Z, Jirik FR, Zamponi GW. Prion protein attenuates excitotoxicity by inhibiting NMDA receptors NMDA receptors. J Gen Physiol. 2008; 181: 551.

Kirstensson K, Feuerstein B, Taraboulos A, Hyun WC, Prusiner SB, DeArmond SJ. Scrapie prions alter receptor-mediated calcium responses in cultured cells. Neurology. 1993; 2335-41.

Klein WL. Aβ toxicity in Alzheimer's disease: globular oligomers (ADDLs) as new vaccine and drug targets. Neurochem Int. 2002; 5:345-52.

Knapp AG, Schmidt KF and Dowling JE. Dopamine modulates the kinetics of ion channels gated by excitatory amino acids in retinal horizontal cells. Proc Natl Acad Sci. 1990; 87:767–71.

Kocisko DA, Come JH, Priola SA, Chesebro B, raymon GJ, Lansbury PT, Caughey B. Cell-free formation of protease-resistant prion protein. 1994; 370: 471-4.

Kohl R, Antoine M, Reimers K, Kiefer P. FGF3 attached to a phosholipid membrane anchor gains a high transforming capacity. Implications of microdomains for FGF3 cell transformation. J Biol Chem. 2002; 277: 32760–67.

Kojima A, Konishi M, Akizawa T. Prion fragment peptides are digested with membrane type matrix metalloproteinases and acquire enzyme resistance through Ca^{2+} binding. Biomol. 2014; 4: 510-26.

Korte S, Vassallo N, Kramer ML,. Kretzschmar HA, Herms J. Modulation of L-type voltage-gated calcium channels by recombinant prion protein. J Neurochem. 2003; 87:1037-1042.

Laine J, Marc ME, Sy MS, Axelrad H. Cellular and subcellular morphological localization of normal prion protein in rodent cerebellum. Eur J Neurosci. 2001; 14: 47–56.

Lalonde J, Saia G, Gill G. Store-operated calcium entry promotes the degradation of the transcription factor Sp4 at resting conditions. Science. 2014; 328: p. ra51.

Lambert MP, Barlow AK, Chromy BA, Edwards C, Freed R, Liosatos M, Morgan TE, Rozovsky I, Trommer B, Viola KL, Wals P, Zhang C, Finch CE, Krafft GA, Klein WL. Diffusible, nonfibrillar ligands derived from Abeta1-42 are potent central nervous system neurotoxins. Proc Natl Acad Sci. 1998; 95:6448-53.

Larson M, Sherman MA, Amar F, Nuvolone M, Schneider JA, Bennett DA, Aguzzi A, Lesné SE. The Complex PrP^{C} -Fyn Couples Human Oligomeric Aβ with Pathological Tau Changes in Alzheimer's Disease. J Neurosci. 2012; 32:16857-851.

Lashuel HA, Hartley DM, Petre BM, Wall JS, Simon MN, Walz T, Lansbury PT. Mixtures of wild type and pathogenic (E22G) form of Aβ40 in vitro accumulate protofibrils, including amyloid pores. J Mol Med. 2003; 4: 795-808.

Lashuel HA, Hartley DM, Petre BM, Walz T, Lansbury PT. Neurodegenerative disease: Amyloid pores from pathological mutations. Nature. 2002; 418: 291.

Laurén J, Gimbel DA, Nygaard HB, Gilbert JW, Strittmatter SM. Cellular prion protein mediates impairment of synaptic plasticity by amyloid-β oligomers. Nature. 2009; 457: 1128-1132.

Lawson VA, Collins SJ, Masters CL, Hill AF. Prion protein glycosylation. J Neurochem. 2005; 93: 793–801.

Lazzari C, Peggion C, Stella R, Massimino ML, Lim D, Bertoli A, Sorgato MC. Cellular prion protein is implicated in the regulation of local Ca^{2+} movements in cerebellar granule neurons. J Neurochem. 2011; 116: 881-890.

Lee IY, Westway D, Smit AFA, Wank K, Seto J, Chen L, Acharya C, Ankener M, Baskin D, Cooper C, Yao H, Prusiner SB, Hood LE. Complete genomic sequence and analysis of the prion protein gene region from three mammalian species. Genome Res. 1998; 8: 1022-37.

Lee KM, Son SW, Babnigg G, Villereal ML. Tyrosine phosphatase and cytochrome P450 activity are critical in regulating store-operated calcium channels in human fibroblasts. Exp Mol Med. 2006; 38:703–17.

Li J, Browning SP, Mahal SP, Oelschlegel AM, Weissmann C. Darwinian evolution of prions in cell culture. Science. 2010; 327: 869-72.

Li S. Hong S, Shepardosn E, Walsh DM, Shankar GM, Selkoe D. Soluble oligomers of Amyloid β protein facilitate hippocampal long-term depression by disrupting neuronal glutamate. Neuron. 2009; 62: 788-801.

Lim D, Fedrizzi L, Tartari M, Zuccato C, Cattaneo E, Brini M, Carafoli E. Calcium homeostasis and mitochondrial dysfunction in striatal neurons of Huntington disease. J Biol Chem. 2008; 283: 5780-89.

Lin HAI, Bhatia R, Lal R. Amyloid β protein forms ion channels: implications for Alzheimer's disease pathophysiology. Faseb J. 2001; 13: 2433-44.

Linden R, Martins VR, Prado MA, Cammarota M, Izquierdo I, Brentani RR. Physiology of the prion protein. Physiol Rev. 2008; 88: 673-728.

Liou J, Kim ML, Heo D, Jones JT, Myers JW, Ferrel JE, Meyer T. STIM is a Ca^{2+} sensor essential For Ca^{2+}-store depletion-triggered Ca^{2+} influx. Curr Biol. 2005; 15: 1235-41.

Lopes MH, Hajj GN, Muras AG, Mancini GL, Castro RM, Ribeiro KC, Brentani RR, Linden R, Martins VR. Interaction of cellular prion and stress-inducible protein 1 promotes neuritogenesis and neuroprotection by distinct signaling pathways. J Neurosci. 2005; 25: 11330-11339.

Lopez E, Jardin I, Berna-Erro A, Bermejo N, Salido GM, Sage SO, Rsado JA, Redondo PC. STIM1 tyrosine-phosphorylation is required for STIM1-Orai1 association in human platelets. Cell Sign. 2012; 1315-22.

Lu YM, Roder JC, Davidow J and Salter MW. Src activation in the induction of long-term potentiation in CA1 hippocampal neurons. Science. 1998; 279: 1363–67.

Mallucci GR, rattè S, Asante EA, Linehan J, Gowland I, Jeffrey JGR, Collinge J. Post natal knock-out of prion protein alters hippocampal CA1 properties, but does not result in neurodegeneration. EMBO J. 2002; 202-10.

Manczak M, Anekonda TS, Henson E, Park BS, Quinn J, Reddy PH. Mitochondria are a direct site of Aβ accumulation in Alzheimer's disease neurons: implications for free radical generation and oxidative damage in disease progression. Hum mol gen. 2006; 15: 1437-49.

Marsault R, Murgia M, Pozzan T, Rizzuto R. Domains of high Ca^{2+} beneath the plasma membrane of living A7r5 cells. EMBO J. 1997;16: 1575-81.

Mattson MP. Cellular action of beta-amyloid precursor protein and its insoluble and fibrillogenic derivatives. Physiol Rev. 1997; 77: 1081-32.

Mattson MP. Pathways towards and away from Alzheimer's disease. Nature. 2004; 430: 631-9.

Miele G, Jeffrey M, Turnbull D, Manson J, Clinton M. Ablation of cellular prion protein expression affects mitochondrial numbers and morphology. Biochem Biophys Res Comm. 2002; 291: 372-77.

Montero M, Brini M, Marsault R, Alvarez J, Sitial R, Pozzan T, Rizzuto R. Monitoring dynamic changes in free Ca^{2+} concentration in the endoplasmic reticulum of intact cells. EMBO J. 1995; 14: 5467-75.

Mouillet-Richard S, Ermonval M, Chebassier C, Laplanche JL, Lehmann S, Launay JM, Kellermann O. Signal transduction through prion protein. Science, 2000; 289: 1925-28.

Mouillet-Richard S, Ermonval M, Chebassier C, Laplanche JL, Lehmann S, Launay JM, Kellermann O. Signal trsnduction through prion protein. Science. 2000; 289: 1925.

Moya KL, Sales N, Hassig R, Creminon C, Grassi J, Di Giamberardino L. Immunolocalization of the cellular prion protein in normal brain. Microsc Res. 2000; Tech 50: 58–65.

Niciu MJ, Keldmendi B, Sanacora G. Overview of glutamatergic neurotransmission in the nervous system. Pharmacol Biochem and Behav. 2012; 656-64.

Olsen JV, gnad BB, Macek GF, Kunar C, Mortensen P, Mann M. Global in vivo, and site-specific phospshorylation dynamics in signaling networks. Cell. 2006; 127: 635-48.

Pan KM, Baldwin M, Nguyen, Gasset M, Serban A, Groth D, Mehlhorn I, Huang Z, Fletterick RJ, Cohen FE. Conversion of alpha-helices into beta sheet features in the formation of scrapie prion protein. Proc. Natl. Acad. Sci. USA 1993; 90: 10962-66.

Pan T, Wong BS, Liu T, Li R, Petersen RB, Sy MS. Cell-surface prion protein interacts with glycosaminoglycans. Biochem J. 2002; 368: 81-90.

Pantera B, Bini C, Cirri P, Paoli P, Camici G, Manao G, Caselli A. PrP^C activation induces neurite outgrowth and differentiation in PC12 cells: role for caveolin-1 in the signal transduction pathway. J Neurochem 2004; 110: 194-207.

Park CY, Shchengloviton A, Dolmetsch R. The CRAC channel activator STIM1 binds and inhibits L-type voltage gated calcium channels. Science. 2010; 330: 101-5.

Paterson AW, Curtis JC, Nacleod NK. Complex I specific increase in superoxide formation and respiration rate by PrP-null mouse brain mitochondria. J Neurochem. 2007; 105: 177-91.

Peggion C, Bertoli A, Sorgato MC. Possible role for Ca^{2+} in the pathophysiology of the prion protein?. Biofactors. 2011; 37: 241-49.

Plant LD, Webster NJ, Boyle JP, Ramsden M, Freir DB, Peers C, et al. Amyloid beta peptide as a physiological modulator of neuronal 'A'-type K^+ current. Neurobiol Aging 2006; 27:1673-83.

Powell AD, Toescu EC, Collinge J, Jeffery JS. Alterations in Ca^{2+}-buffering in prion-null mice: association with reduced after hyperpolarization in CA1 hippocampal. J Neurosci. 2008; 28: 3877-86.

Pradines E, Loubet D, Mouillet-Richard S, Manivet P, Launay JM, Kellermann O, Schneider B. Cellular prion protein coupling to TACE-dependent TNF-alpha shedding controls neurotransmitter catabolism in neuronal cells. J Neurochem. 2009; 110: 912-23.

Prezeau L, Carrette B, Helpap K, Kerry J, Pin P, Bockaert J. Pharmacological characterization of metabotropic glutamate receptors in several types of brain cells in primary cultures. Mol Pharmacol. 1994; 45: 470-77.

Prusiner SB. Prions: novel infectious pathogens. Adv Virus Res. 1984; 29: 1-56.

Putney JW Jr, Bird GS. The inositol phosphate-calcium signaling system in non excitable cells. Endocr Rev 1993; 14:610-31.

Ramsden M, Plant LD, Webster NJ, Vaughan PF, Henderson Z, Pearson HA. Differential effects of unaggregated and aggregated amyloid beta protein (1–40) on K^+ channel currents in primary cultures of rat cerebellar granule and cortical neurones. J Neurochem 2001; 79:699-712.

Rangel A, Burgaya F, Gavin R, Soriano E, Aguzzi A, del rio J. Enhanced susceptibility of Prnp-deficient mice to kainate-induced seizures, neuronal apoptosis, and death. Role of AMPA/kainate receptors. J Neurosci Res. 2007; 12: 2741-55.

Re L, Rossini F, Re F, Bordicchia M, Mercanti A, Fernandez OSL, Barocci S. Prion protein potentiates acetylcoline release at the neuromuscular junction. Pharmacol Res. 2006; 53: 62-68.

Resenberger UK, Harmeier A, Woomer AC, Goodman JL, Muller V, Krishnan R, Vabulas RM, Kretzschmar HA, Harti FU, Multhaup G, Winklhofer KF, Taztel J. The cellular prion protein mediates neurotoxic signaling of β-sheet-rich conformers independent of prion replication. EMBO J. 2011; 18,30: 2057-70.

Rieger R, Edenhofer F, Lasmezas CI, Weiss S. The human 37-kDa laminin receptor precursor interacts with the prion protein in eukaryotic cells. Nat Med. 1997; 3: 1383-1388.

Riek R, Hornemann S, Wider G, Billeter M, Glockshuber R, Wüthrich K. NMR structure of the mouse prion protein domain PrP(121-321). Nature. 1996; 382: 180-82.

Rizzuto R, Pinton P, Carrington W, Fay FS, Fogarty KE, Lifshitz LM, Tuft AR, Pozzan T. Close contacts with the endoplasmic reticulum as determinants of mitochondrial Ca^{2+} responses. Science. 1998; 280: 1763-66.

Rizzuto R, Simpson AWM, Brini M, Pozzan T. Rapid changes of mitochondrial Ca^{2+} revealed by specifically targeted recombinant aequorin. Nature. 1992; 358:325-27.

Rothman SM, Thurston JH, Hauhart RE. Delayed neurotoxicity of excitatory amino acids in vitro. Neurosci. 1987; 471-80.

Roucou X, Gains M, LeBlanc AC. Neuroprotective functions of prion protein. J Neurosci res. 2004; 75: 153-61.

Rovira C, Arbez N, Mariani J. Aβ (25-35) and Aβ (1-40) act on different calcium channels in CA1 hippocampal neurons. Biochem and Biophys Res. 2002; 5: 1317-22.

Safar J, Roller PP, Gajduesek DC, Gibbs CJ Jr. Thermal stability and conformational transitions of scrapie amyloid (prion) protein correlate with infectivity. Protein Sci. 1993; 2: 2206-16.

Sakaguchi S, Katamine S, Nishida N, Moriuchi R, Shigematsu K, Sugimoto T, Nakatani A, Kataoka Y, Houtani T, Shirabe S, Okada H, Hasegawa S, Miyamoto T, Noda T. Loss of cerebellar Purkinje cells in aged mice homozygous for a disrupted PrP gene. Nature 1996; 380: 528–31.

Santuccione A, Sytnyk V, Leshchyns'ka I, Schachner M. Prion protein recruits its neuronal receptor NCAM to lipid rafts to activate p59fyn and to enhance neurite outgrowth. J Cell Biol. 2005; 169: 341-54.

Schneider B, Mutel V, Pietri M, Ermoval M, Mouillet-Richard S, Kellermann O. NADPH oxidase and extracellular regulated kinases1/2 are targets of prions protein signalling in neuronal and nonneuronal cells. Proc Natl Acad Sci U S A. 2003; 100: 13326-31.

Scott M, Groth D, Foster D, Torchia M, Yang SL, DeArmond SJ, Prusiner SB. Propagation of prions with artificaial properties in transgenic mice expressing chimeric PrP genes. Cell. 1993; 73: 979-88.

Selkoe DJ. The genetics and molecular pathology of Alzheimer's disease: roles of amyloid and the presenilins. Neurol Clin. 2000; 18: 903-22.

Shankar GM, Li S, Mahta TH, Munoz MA, Shepardson NE, Smith I, Brett FM, Farrel mA, Rowan MJ, Lemere CA, Regan CM, Walsh DM, Sabatini BL, Selkoe JD. Amyloid-β protein dimmers isolated directly from Alzheimer’s brains impair synaptic plasticity and memory. Nat Med. 2008; 14: 837-42.

Shyu WC, Lin SZ, Chiang MF, Ding DC, Li KW, Chen SF, Yang HI, Li H. Overexpression of PrPC by Adenovirus-mediated gene targeting reduces ischemic injury in a stroke rat model. J Neurosci. 2005; 2:8967-77.

Simons K, Ikonen E. Functional rafts in cell membranes. Nature. 1997; 387: 569-572.

Simons K, Toomre D. Lipid rafts and signal transduction. Nat Rev Mol Cell Biol. 2000; 1: 31–39.

Singh A, Kong Q, Luo X, Petersen RB, Meyerson H, Singh N. Prion protein (PrP) knock-out mice show altered iron metabolism: a functional role for PrP in iron uptake and transport. Plos one. 2009; 4: e6115.

Sivanesan S, Tan A, Rajadas J. Pathogenesis of Abeta oligomers in synaptic failure. Curr Alzh Res. 2013; 10: 316-23.

Sorgato MC, Bertoli A. From cell protection to death: May Ca^{2+} signals explain the chameleonic attributes of the mammalian prion protein?. Biochem Biophis Res Commun. 2009; 379: 171-4.

Sparkes RS, Simon M, Cohn VH, Fournier RE, Lem J, Klisak I, Heinzmann C, Blatt C, Lucero M, Mohandas T. Assignment of the human and mouse prion protein genes to homologous chromosomes. Proc Natl Acad Sci U S A. 1986; 83: 7358-62.

Spudich A, Frigg R, Kilic E, Kilic U, Oesch B, Raeber A, Bassetti CL, Hermann DM. Aggravation of ischemic brain injury by prion protein deficiency: role of ERK-1/-2 and STAT-1. Neurobiol Dis. 2005; 20: 442-9.

Stahl N, Baldwin MA, Burlingame AL, Prusiner SB. Identification of glycoinositol phospholipid linked and truncated forms of scrapie prion protein. Biochemistry. 1990; 29:2279-84.

Stuermer CA, Langhorst MF, Wiechers MF, Legler DF, Von Hanwehr SH, Guse AH, Plattner H. PrPc capping in T cells promotes its association with the lipid raft proteins reggie-1 and reggie-2 and leads to signal transduction. FASEB J. 2004; 18: 1731-33.

Stutzmann GE. Calcium dysregulation, IP3 signaling and Alzheimer's disease. The Neurosc. 2005; 11: 110-15.

Sutko JL, Airey JA,Welch W, Ruest L. The pharmacology of ryanodine and releted compounds. Pharmacol Rev. 1997; 49: 53-98.

Syntichacki P, Tavernarakis N. The biochemistry of neuronal necrosis: roque biology? Nature Rev Neurosci. 2003; 4: 672-84.

Telling GC, Scott M, Gabizon R, Torchia M, Cohen FE, DeArmon SJ, Prusiner SB. Prion propagation in mice xpressing human and chimeric PrP transgenes implicates the interaction of cellular PrP with another protein. Cell. 1995; 79-90.

Terzi E, Holzemann G, Seeling J. Inetraction of Alzheimer beta amyloid peptide (1-40) with lipid membranes. Biochem. 1997; 36: 14845-52.

Tezuka T, Umemon H, Akiyama T, Nakanisghi S, Yamamoto T. PSD-95 promotes Fyn-mediated tyrosine pohosphorylation of the N-methil-D-aspartate receptor subunit NR2A. PNAS. 1999; 96: 435-40.

Toni M, Spisni E, Griffoni C, Santi S, Riccio M, Lenaz P, Tomasi V. Cellular prion protein and caveolin-1 interaction in a neuronal cell line precedes Fyn/ERK 1/2 signal transduction. J Biomed and Biotec. 2006; 1-13.

Um JW, Nygaard HB, Heiss JK, Kostylev MA, Stagi M, Vortmeyer A, Wisniewski T, Gunther EC, Stritmatter SM. Alzheimer amyloid-β oligomer bound to postsynaptic prion protein activates Fyn to impair neurons. Nat Neurosci 2012; 15: 1227-35.

Um JW, Kaufman AC, Kostylev M, Heiss JK, Stagi M, Takahashi H,. Kerrisk ME, Vortmeyer, Thomas Wisniewski A, Koleske AJ, Gunther EC, Nygaard HB, Strittmatter SM. Metabotropic glutamate receptor 5 is a coreceptor for Alzheimer Aβ oligomer bound to cellular prion protein. Neuron. 2013; 79:887-902.

Um JW, Strittmatter SM Amyloid-β induced signaling by cellular prion protein and Fyn kinase in Alzheimer disease. Prion. 2013; 7: 37-41.

Walsh DM, Selkoe DJ. Aβ oligomers-a decade of discovery. J Neurochem. 2007; 5: 1172-84.

Walz R, Amaral OB, Rockenbach IC, Roester R, Izquierdo I, Cavalheiro EA, Martins VR, Brentani R. Increased sensitivity to seizures in mice lacking cellular prion protein. Epilepsia. 1999; 12: 1679-82.

Wang LY, Dudek EM, Browning MD and MacDonald JF Modulation of AMPA/kainate receptors in cultured murine hippocampal neurones by protein kinase C. J Physiol. 1994a; 475:431–37.

Wang LY, Orser BA, Brautigan DL and MacDonald JF Regulation of NMDA receptors in cultured hippocampal neurons by protein phosphatases 1 and 2A. Nature. 1994b; 369:230–32.

Wang Y, Deng X, Gill DL. Calcium signaling by STIM and Orai: intimate coupling details revealed. Science. 2010; 148: pe42.

Weise J, Crome O, Sandau R, Schulz-Schaeffer W, Bähr M, Zerr I. Upregulation of cellular prion protein (PrPC) after focal cerebral ischemia and influence of lesion severity. Neurosci Lett. 2004; 372: 146-150.

Weise J, Sandau R, Schwarting S, Crome O, Wrede A, Schulz-Schaeffer W, Zerr I, Bähr M. Deletion of cellular prion protein results in reduced Akt activation, enhanced postischemic caspase-3 activation, and exacerbation of ischemic brain injury. Stroke. 2006; 37: 1296-1300.

Williams RT, Manji SS, Hanckock MS, Van Stekelenburg L, Eid JP, Senior PV, Kazenwadel JS, Shandala T, Saint R, Smith PJ, Dziadek MA. Identification and characterization of the STIM (stromal interaction molecule) gene family: coding for a novel class of transmembrane proteins. Biochem J. 2001; 357: 673-85.

Wissenbach U, Philipp SE, Gross SA, Flockerzi V. Primary structure, chromosomal localization and expression in immune cells of the murine ORAI and STIM genes. Cell Calcium. 2007; 42: 439-46.

Wong K, Qju Y, Hyun W, Nixon R, Vancleff J, Salazar S, Prusiner SB, DeArmond SJ. Decreased receptor-mediated calcium response in prion-infected cells correlates with decreased membrane fluidity and IP3 release. Neurology. 1996; 47: 741-50.

Xu F, Plummer MR, Kakazawa T, Yamamoto T, Black IB, Wu K. Barin-derived neurotrophic factor rapidly increases NMDA receptor channel activity through Fyn-mediated phosphorylation. Brain Res. 2006; 1: 22-34.

Yu L, Edalij R, Harlan JE, Holztman JF, Lopez AP, Labkovski B, Hillen H, Barghorn S, Ebert U, Richardson PL, Miesbauer L, Solomon L, Bartley D, Walter K, Johnson R, hajduk PJ, Olejinickzac T. Structural characterization of a soluble amyloid β peptide oligomer. Biochem. 2009; 48: 1870-77.

Zahn R, Liu A, Luhrs T, Riek R, von Schroetter C, Lopez Garcia F, Billeter M, Calzolai L, Wider G, Wuthrich K. NMR solution structure of the human prion protein. Proc Natl Acad Sci USA 2000; 97: 145–150.

Zhang SL, Yu Y, Roos J, Kozak JA, Deerick TJ, Ellisman MH, Stauderman KA, Cahalan MD. STIM1 is a Ca^{2+} sensor that activates CRAC channels and migrates from the Ca^{2+} store to the plasma membrane. Nature. 2005; 437: 902-5.

Zhu X, Lee HG, Raina AK, Perry G, Smith MA. The role of mitogen-activated protein kinsase pathways in Alzheimer's disease. Neuro Sign. 2003; 11: 270-81.

Zuo WL, Du JY, Huang JH, Li S, Zhang G, Chen SL, Ruan YC, Cheng CHK. Tyrosine phosphorylation modulates store-operated calcium entry in cultured rat epididymal basal cells. J Cell Physiol. 2011; 226: 1069-73.

10 ACKNOWLEDGEMENTS

I would like to thank all the persons who in one way or the other have contributed to the accomplishment of this Ph.D. thesis, and who made most enjoyable this work to me. In particular, my thanks go to:

Maria Catia Sorgato, my Professor and Supervisor, for allowing me to carry out this research, for the attention and dedication with which I was followed and for teaching me how to proceed in research.

Dr. Alessandro Bertoli, whose contribution has been extremely important for my work; thank you for the continuous help and suggestions and for teaching me the precise method of analyses.

Dr. Marilina Massimino and Dr. Caterina Peggion, who shared their expertise in cell culturing, WB and light/electron microscopy approaches, for all the suggestions and for the pleasant moments spent together.

My fellow Ph.D. students Angela and Rosa, undergraduate students Francesca and Migena, and Paolo for the collaborations and the great time spent together inside and outside the lab.

Prof. Ernesto Carafoli and Dr. Marta Giacomello for their continuous advise, help and suggestions.